

https://dspace.org/

Interfacial phenomena between liquid electrolytes and semiconducting base metal sulfides

Fink, James Brewster

2015-03-11
http://hdl.handle.net/10539/17258

Downloaded from a DSpace repository. https://dspace.org/

INTERFACIAL PHENOMENA BETWEEN LIQUID ELECTROLYTES AND SEMICONDUCTING BASE METAL SULFIDES

James Brewster Fink

A Dissertation Submitted to the Faculty of Science
University of the Witwatersrand, Johannesburg
for the Degree of Master of Science

Johannesburg 1979

STATEMENT

All of the data presented herein have been obtained by the author except where so stated. The current-voltage curves were made in the Department of Chemistry at the University of Arizona, Tucson, Arizona, U.S.A., in 1976, under the guidance of Dr. George Wilson, The impedance measurements were made in the Department of Mineral and Process Chemistry at the National Institute for Metallurgy, Randburg, Transvaal, Republic of South Africa, in 1979, under the guidance of Dr. Roger Paul. All stated opinions and interpretations are the responsibility of the author. This work has not been submitted for a higher degree to any other university.

Signed: _____

James B. Fink July 1979

Oh, for the powers of super-
natural vision that we might
divine the secrets of the
earth beneath us!

-William H. Brown,
On the South African
Frontier, 1899.

ABSTRACT

Electrochemical measurements have been performed on naturally occurring base metal sulfides. The emphasis has been on members of the copper-iron-sulfur system. The purpose was to determine whether or not there is an observable phenomenological difference between the electrochemical responses of certain economic and non-economic sulfides.

The results of the research show copper sulfides, copper-iron-sulfides and iron sulfides do produce distinct signatures within the framework of the laboratory procedures followed.

An added bonus to the research was the observation that Warburg impedance probably does not play as strong a role in the induced polarization geophysical method as has been proposed for the past two decades.

TABLE OF CONTENTS

		Page
ABSTRACT		
1	INTRODUCTION	
1.1	Background	1
1.2	Purpose	3
1.3	Limitations	4
2	ELECTROCHEMISTRY	
2.1	Introduction	6
2.2	Cell terminology	6
2.3	Faraday's law	9
2.4	Tafel's law	10
2.5	Nernst equation	13
2.6	Electrified interface	15
2.7	Electrode polarisation	26
3	VOLTAMMETRY	
3.1	Solid electrodes	37
3.2	Basic equations	40
3.3	Purpose	42
3.4	Procedure	43
3.5	Results	44
3.5.1	Pyrite	44
3.5.2	Marcasite	47
3.5.3	Pyrrhotite	47
3.5.4	Chalcopyrite	52
3.5.5	Chalcocite	54
3.6	Summary	56
4	IMPEDANCE MEASUREMENTS	
4.1	Introduction	57
4.2	Faradaic impedance	57
4.2.1	Faradaic conduction	58
4.2.2	Nonfaradaic conduction	59
4.3	Warburg impedance	59
4.4	Purpose	61
4.5	Procedure	77
4.6	Results	80
4.6.1	Pyrite	85
4.6.2	Chalcopyrite	95
4.6.3	Chalcopyrite and pyrite	100
4.6.4	Chalcocite	106
4.7	Summary	109
5	CONCLUSIONS	
5.1	General	110
5.2	Results	111
5.3	Epilogue	118
APPENDIX A	Electrode Preparation	
A.1	Electrode design	119
A.2	Sample selection and sizing	119

		Page
A.3	Casting	121
A.4	Sawing and sealing	121
A.5	Polishing	123
A.6	Wax impregnation	123
A.7	Surface area determination	123
A.8	Ohmic contact	124
APPENDIX B	Semiconductivity Determinations	
B.1	Seebeck thermoelectric effects	125
B.2	Purpose	125
B.3	Results	125
APPENDIX C	Reference Electrodes	
C.1	Three requirements	127
C.2	Calomel electrode	128
C.3	Limitations	128
C.4	Half-cell potential	128
APPENDIX D	Cell Design	
D.1	Cell geometry	130
D.2	Luggin capillary	130
D.3	Impedance cell	131
BIBLIOGRAPHY		133

LIST OF FIGURES

Figure No.		Page
2.1	Schematic representation of an electrochemical cell designed for experimental observation of interfacial phenomena.	8
2.2	Typical Tafel plot where η is potential in volts, i is current density in amps per square cm.	12
2.3	Density of states (abscissa) versus energy (ordinate) for three types of solids.	17
2.4	A diagrammatic depiction of the distribution of cations, anions and water molecules at a hypothetical interface. The lower figure is a plot of the relative potential across the interface.	22
2.5	Comparison of ideal parabola with observed electrocapillary measurements.	24
2.6	Schematic current-voltage curves for a cell with identical irreversible electrodes. A,B,C and D represent instantaneous initial values after increasing times of current flow, η_Ω is the ohmic polarisation curve and $\alpha+\beta+\gamma$ is the total polarisation at current density i.	27
2.7	The concentration of oxidant normalised to the equilibrium value plotted against the distance from the electrode surface in reaction layer thicknesses where t represents various elepsed times of electrolysis.	35
3.1	Triangular waveform used for cyclicvoltammetry (CV).	38
3.2	Multiple composite of the pyrite composite curves.	45
3.3	Current-voltage curves for pyrite in .25M NaCl with pH's ranging from 2 to 10.	48
3.4	Plot of anodic and cathodic limiting potentials as a function of pH. Data from Fig. 3.3.	49

Figure No.		Page
3.5	Composite of the marcasite current-voltage curves. Area is given as the average area.	50
3.6	Composite of the pyrrhotite current-voltage curves. Area is given as the average area.	51
3.7	Composite of the chalcopyrite current-voltage curves. Area is given as the average area.	53
3.8	Composite of the chalcocite current-voltage curves. Area is given as the average area.	55
4.1	Relationship between magnitude and phase in the complex plane.	62
4.2	Complex plane plot of an ideal resistance.	63
4.3	Complex plane plot of an ideal capacitance.	65
4.4	Complex plane plot of an ideal resistance and capacitance in series.	66
4.5	Complex plane plot of a parallel RC circuit. The frequency occurring at the top of the semicircle is the resonant frequency for that circuit. The diameter of the circle is equal to R_{ct}.	68
4.6	Complex plane plot of a resistor in series with a parallel RC circuit. The semicircle of Fig. 4.5 is simply translated to the right by an amount equal to R_s.	69
4.7	Complex plane plot of the Warburg impedance when C_{dl}, R_{ct} and R_s equal zero.	70
4.8	Complex plane plot of a resistor in series with the Warburg impedance.	73
4.9	Complex plane plot of a Randles' circuit where R_{ct} and C_{dl} are very small relative to the Warburg impedance.	74
4.10	Complex plane plot of a Randles' circuit where R_{ct} and C_{dl} are very	76

Figure No.		Page
	small relative to the Warburg impedance and the ac diffusion layer interacts with the Warburg diffusion layer.	
4.11	Complex plane plot of a Randles' circuit where R_{ct} and the Warburg impedance are held at unity and C_{dl} is varied.	78
4.12	Complex plane plot for the reduction of ferric ions to ferrous on a gold rotating disk electrode (from Armstrong et al, 1976).	79
4.13	Current-time plot (on left) showing adjustment of current to a 50 mV increase in anodic potential from +350 to +400 mV. Plot on right is of CV measurements made after the current had stabilized. The slope of the CV plots indicates the slope of the current voltage curve at the indicated potential. The plots are for several cycles and show no noticeable hysterisis effects.	83
4.14	Current-voltage plot of equilibrium currents for various potentials in the stability range for pyrite.	84
4.15	Complex plane plot of anodic impedance spectra for pyrite.	86
4.16	Complex plane plot of cathodic impedance spectra for pyrite.	88
4.17	Complex plane plot of cathodic impedances for py-u-01.	91
4.18	Complex plane plot of cathodic impedances at 0.1 Hz for py-u-01.	92
4.19	Complex plane plot of pyrite impedances measured by Angoran (1975).	93
4.20	Complex plane plot of pyrite impedances measured by Angoran (1975).	94
4.21	Complex plane plot of anodic impedance spectra for chalcopyrite.	96
4.22	Complex plane plot of the high frequency portion of the anodic impedance spectra for chalcopyrite shown in Fig. 4.21. (note scales).	97

Figure No.		Page
4.23	Complex plane plot of cathodic impedance spectra for chalcopyrite.	99
4.24	Complex plane plot of chalcopyrite impedances measured by Angoran (1975).	101
4.25	Complex plane plot of chalcopyrite impedances measured by Angoran (1975).	102
4.26	Complex plane plot of rest potential impedance spectrum for chalcopyrite. Note expanded scale.	103
4.27	Complex plane plot of anodic impedance spectra for pyrite and chalcopyrite. Note inductive responses.	105
4.28	Complex plane plot of a rest potential impedance spectrum for chalcocite.	107
4.29	Complex plane plot of anodic impedance spectra for chalcocite.	108
A.1	Schematic cross-sectional view of a typical electrode used in this research.	120

LIST OF TABLES

Table		Page
B.1	THERMOELECTRIC (SEEBECK) DETERMINATION OF CARRIER TYPE	126

1 INTRODUCTION

1.1 Background

The impetus of the research described herein is of a geophysical nature, but the problems encountered and the methods employed are entirely electrochemical. This sort of interdisciplinary work is becoming more common in many fields as the problems once considered to be in the fringe area of one discipline have actually been found to lie well within the recently expanded scope of another. Such is the case for the induced polarisation (IP) phenomenon.

Sumner (1976) gives a comprehensive treatment of the IP technique, discussing the electrochemical implications and their historical significance. There has been a great deal of laboratory research performed in pursuit of the precise fundamental causes of the IP effect. Generally, these studies have been scaled down field methods performed on natural or synthetic rock samples and very few carried out were specifically electrochemically oriented to investigate the actual sulfide/electrolyte interface. Of these latter few, the most noteworthy are those reported by Madden, et al, in a series of four reports for the United States Atomic Energy Commission published during 1957 through 1959. These reports are the first to discuss the relationships of various interfacial phenomena with a geophysical connotation. Their results have been adopted as the ultimate

authority for IP researchers and have been referenced extensively throughout the geophysical literature. Other investigations specifically involving interfacial phenomena are three recent publications appearing in Geophysics. The first, authored by Angoran and Madden (1977), described their research into the chemical basis of IP. The other two, authored by Klein and Shuey (1978), involved the non-linear aspects of the sulfide/electrolyte interface, but were not oriented towards IP. Hence, Madden's influence predominates in the interpretation of both the early and later IP oriented work. According to Madden and Marshall (1959), their measurements indicated that the rate limiting process controlling the impedance response was ionic diffusion occurring in the electrolyte adjacent to the sulfide. They also indicated that the magnitude of the impedance was relatively independent of sulfide type and of the salt concentration of the electrolyte. They ascribed their results to a solution diffusion Warburg impedance.

However, claims made by Zonge (1972) and Katsube and Collett (1973) indicated the possibility of mineral discrimination through impedance measurements made on rock samples. This means the impedance must be dependent on the sulfide type. This conclusion was clearly at variance with the conclusions of Madden and Marshall.

Pursuant to the possibility that the sulfide associated metal ion in solution may be involved in the IP phenomenon, Angoran, (1976) under Madden's direction, performed a relatively comprehensive suite of impedance measurements to investigate the chemical basis of IP. The end result tended

to reaffirm Madden's previous conclusion that the solution diffusion Warburg impedance was the dominant factor in producing the IP phenomenon. This has resulted in somewhat of an impasse between the proponents and opponents of mineral discrimination using impedance methods.

1.2 Purpose

It was the purpose of this research to make impedance measurements similar to those made by Madden et al (1957-1959) and Angoran (1976) but varying different electrochemical parameters and applying a different interpretational approach. It was hoped the results would contribute towards answering the mineral discrimination question.

Since Hansuld (1961) and Sato (1960) had demonstrated a wide stability field for some sulfides, current-voltage measurements were performed to determine where, in the current-voltage plane at standard pH's, the most representative impedance measurements should be made. Impedance measurements were then made in the normal range of stabilities to determine the spectral dependence of bias potential, a step not performed by Madden and Marshall. The data were then plotted and interpreted using complex plane analysis. The data were not fitted with a single preconceived equivalent circuit model. However, they were qualitatively interpreted by curve comparison using a variety of fundamental spectral types, each derived from a different equivalent circuit model.

The ultimate goal of the impedance measurements was to determine whether or not there were diagnostic phenomena

observable in the spectra such that iron sulfides could be distinguished from copper or copper-iron sulfides. Within the limitations of the technique applied and the electrochemical cell employed, this goal was achieved.

1.3 Limitations

Any research of this type generally suffers from severe incompletion. The amount of time, materials and effort necessary to carry this research to completion is far beyond that available to a student in a graduate degree program. As a result, the work has been spread over several years and some of the measurements made at large time intervals. Collectively, the steps produce a logical sequence from a general approach to a specific result.

Accordingly, the preliminary measurements (current-voltage curves) served as a focusing tool to determine how and where the impedance measurements should be made. Consequently, they are given a rather cursory discussion. This was not because of the lack of information content but rather to limit the discussion to the parameters relevant to the impedance measurements. Sulfide mineral dissolution reactions are dealt with extensively in the metallurgical literature, consequently the possible chemical reactions occurring during the measurements have not been presented. Again, the emphasis of this research was in the area where the sulfide was at equilibrium and not undergoing any net reaction.

Not all mineral types involved in the IP phenomenom were studied. The results obtained from the ones that were

studied, however, clearly illustrate the necessity for a great deal more research to be done in this area. Regardless of its limitations, the present research: a. covers the most critical aspects pertinent to the objective, b. arrives at new conclusions, and c. points the direction for further investigation.

2 ELECTROCHEMICAL TERMINOLOGY

The research performed is electrochemically oriented but the end result is related to geophysical applications. Consequently, much of the terminology used is foreign to the geophysicist. This chapter is included to explain many of the basic concepts and terms used in electrochemistry. By including a separate chapter of this sort, lengthy digressions to explain simple terms can be avoided later.

2.1. Ionics and Electrodics

The field of electrochemistry can be subdivided into two prominent categories; ionics and electrodics (Bockris and Reddy, 1974). Ionics is concerned primarily with electrochemical phenomena occurring entirely in bulk solution, whereas electrodics is concerned with the electrochemical phenomena observable at the interface between electronic conductors and ionic conductors. Any phenomena occurring entirely within an electronic conductor are the subject of solid-state physics. The research performed herein is primarily that of electrodics but ionics and solid-state physics are resourced necessarily to effect completeness.

2.2. Cell Terminology

Many electrochemical phenomena can be produced and observed with a two electrode cell, but to confine interest to a single electrode a third or reference electrode is essential. Hence, measurements are generally performed with a three electrode cell. A pair of electrodes is necessary to

apply a stimulus (input) and a pair is required to measure the response (output). One electrode is common and is typically called the working electrode. It is the working electrode that receives most of the attention in electrochemical measurements. The two remaining electrodes are called the counter electrode (the other half of the input pair) and the reference electrode (the other half of the output pair). A schematic representation of a typical observational cell is shown in Fig.2.1.

A system consisting of two electrodes in an electrolyte under conditions of electrolysis is called an electrolytic cell. The terms "electrolysis"or "electrolytic" imply the system accepts energy from its surroundings in order to bring about chemical transformations. This is different from a galvanic cell in that galvanic implies the system is either in a currentless state or supplies electrical work to its surroundings. In fact, a given system may possess both functions, depending on the value of the external voltage.

If at a given electrode the result of an electrochemical reaction is the transfer of a negative charge from the metallic phase into the solution, the resulting current is called cathodic. The ions in solution that receive the negative charge are said to be electronated, or to undergo reduction. In the opposite case, when ions donate charge to the metallic phase, the current is called anodic and the ions are said to be de-electronated, or to undergo oxidation (Bockris and Reddy, 1974). The corresponding electrodes are called the cathode and the anode. Chemical reactions in

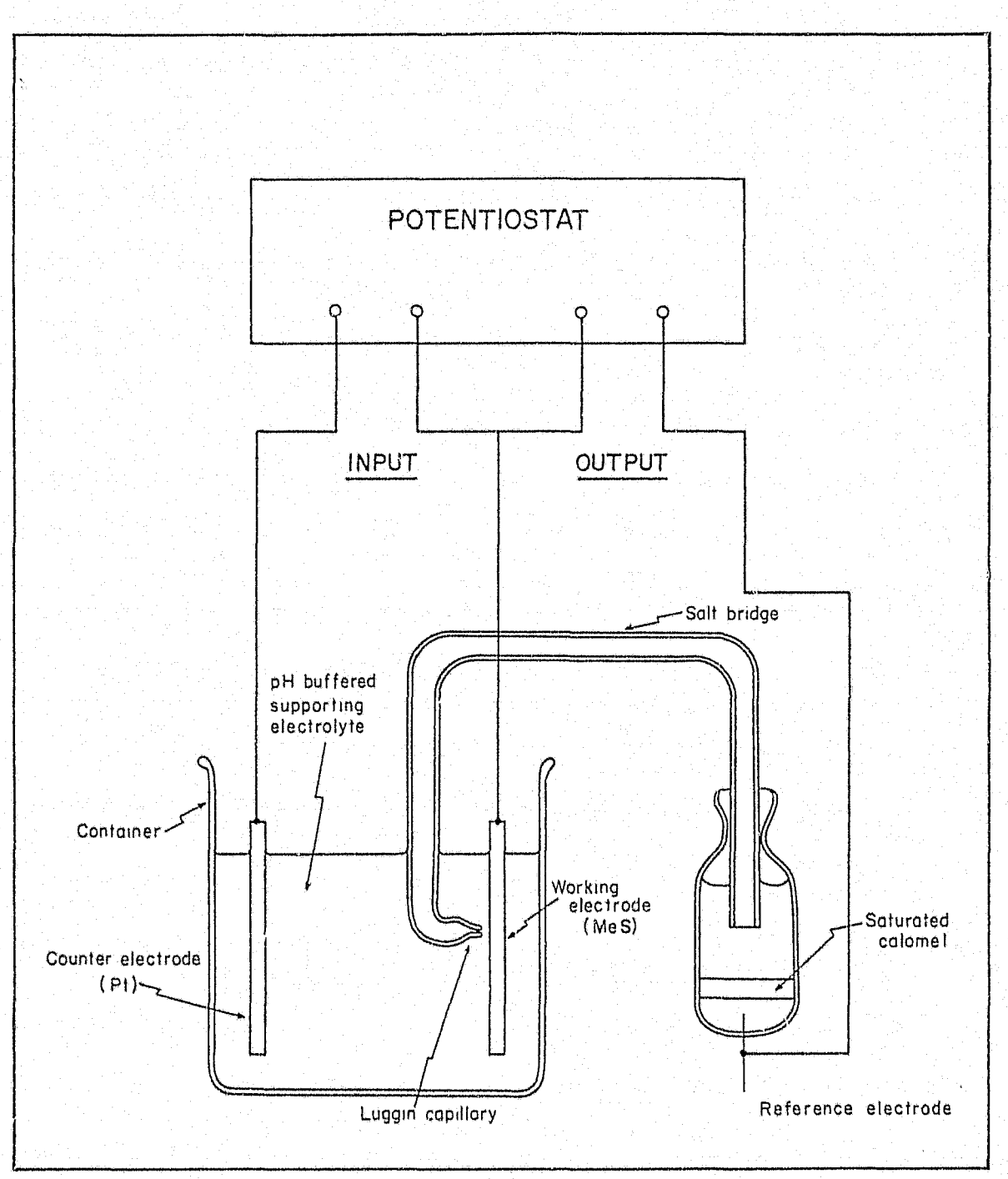


Fig. 2.1. Schematic representation of an electrochemical cell designed for experimental observation of interfacial phenomena.

which electrons are transferred to or from an electrode are called electron or charge transfer reactions. A reversible charge transfer reaction is one having a large value for the exchange current density and involves two separate but related symmetric electrode reactions. In this research the anodic current will conventionally be taken as positive.

If electrical current flows through the electrode-electrolyte interface, changes occur in the system associated with the processes that make the current flow possible. These processes are of both a chemical and physical nature and are called collectively the electrode process. The substances involved in an electrode reaction are called electroactive. The main electrochemical process in this ensemble of steps forming the electrode process is the immediate exchange of charge between the electrode and an electroactive species in solution. They may be either soluble or insoluble in the solutions or present in the electrode material. Usually, counter electrodes are made of relatively inert material and working electrodes can be either inert or active.

2.3 Faraday's Laws

The concept of electrical current in electrochemistry must be treated carefully. The total current flowing through a cell is much less important than the current density at an electrode. The relationship is simple,

$$i = \frac{I}{A} \qquad 2.1.$$

where I equals the total current in amps, A equals the electrode surface area in square centimeters, and i equals the current density in amps per square centimetre.

A current i passing through a cell for time t causes an electrochemical conversion M (in grams) at an electrode which is proportional to the charge i t (Faraday's first law) and to the equivalent mass g of converted substance (Faraday's second law). Faraday's laws are therefore expressed by

$$M = \frac{git}{F} \qquad 2.2$$

where F is the amount of electricity required for the conversion of one equivalent weight and is called the Faraday. One Faraday equals approximately 96 500 Coulombs per equivalent weight. The equation

$$F = e_o N \qquad 2.3$$

describes the relationship between the Avogadro number N, the elementary charge of an electron e_o and one Faraday. Thus, one Faraday is the total charge of one mole of electrons.

2.4 Tafel's Law

Typically, electrochemical investigations involve one of three current density ranges. Qualitatively, these can be classified as low current, intermediate current or large current measurements. The justification for this type of classification is evident from Tafel's law.

In 1905 Tafel established his classic relationship,

i.e. the potential difference across an electrode/electrolyte interface at which an electrochemical reaction is occurring changes linearly with the logarithm of the current density, i, or $E = a \pm b \ln i$ 2.4

where a and b are independent of E, or in exponential form

$$i = \exp(a/b)\exp(\pm E/b) \qquad 2.5$$

The Tafel equation is actually an approximation of the Butler-Volmer equation (Bockris and Reddy, 1973) and is valid only for a very limited current and potential range. The Butler-Volmer equation states that

$$i = i_o \left[\exp\left(\frac{-\beta F\eta}{RT}\right) - \exp\left(\frac{(1-\beta)F\eta}{RT}\right) \right] \qquad 2.6$$

where η is defined as the overvoltage, or $\eta = E - Eeq$ (where Eeq is the equilibrium potential for the reaction in concern), and β is a symmetry factor. For small values of η,

$$\exp\left(\frac{-\beta F\eta}{RT}\right) \quad \text{and} \quad \exp\left(\frac{(1-\beta)F\eta}{RT}\right)$$

can be replaced by

$$1 - \frac{\beta F\eta}{RT} \quad \text{and} \quad 1 - \frac{(1-\beta)F\eta}{RT}$$

respectively. Substituting these values shows

$$i = i_o \frac{F\eta}{RT} \qquad 2.7$$

Thus, over a limited range of potential, i varies linearly with current. In actual measurements it can be seen that this is only a first-order approximation. The actual shape of the current-voltage curves is controlled by several polarisation or overvoltage phenomena (see section on electrode polarisation). The type of polarisation phenomena to be observed generally dictates the current density level and the measurement technique. Electrochemical data are usually plotted with the conventions as noted on Fig.2.2 and are characteristically called current-voltage

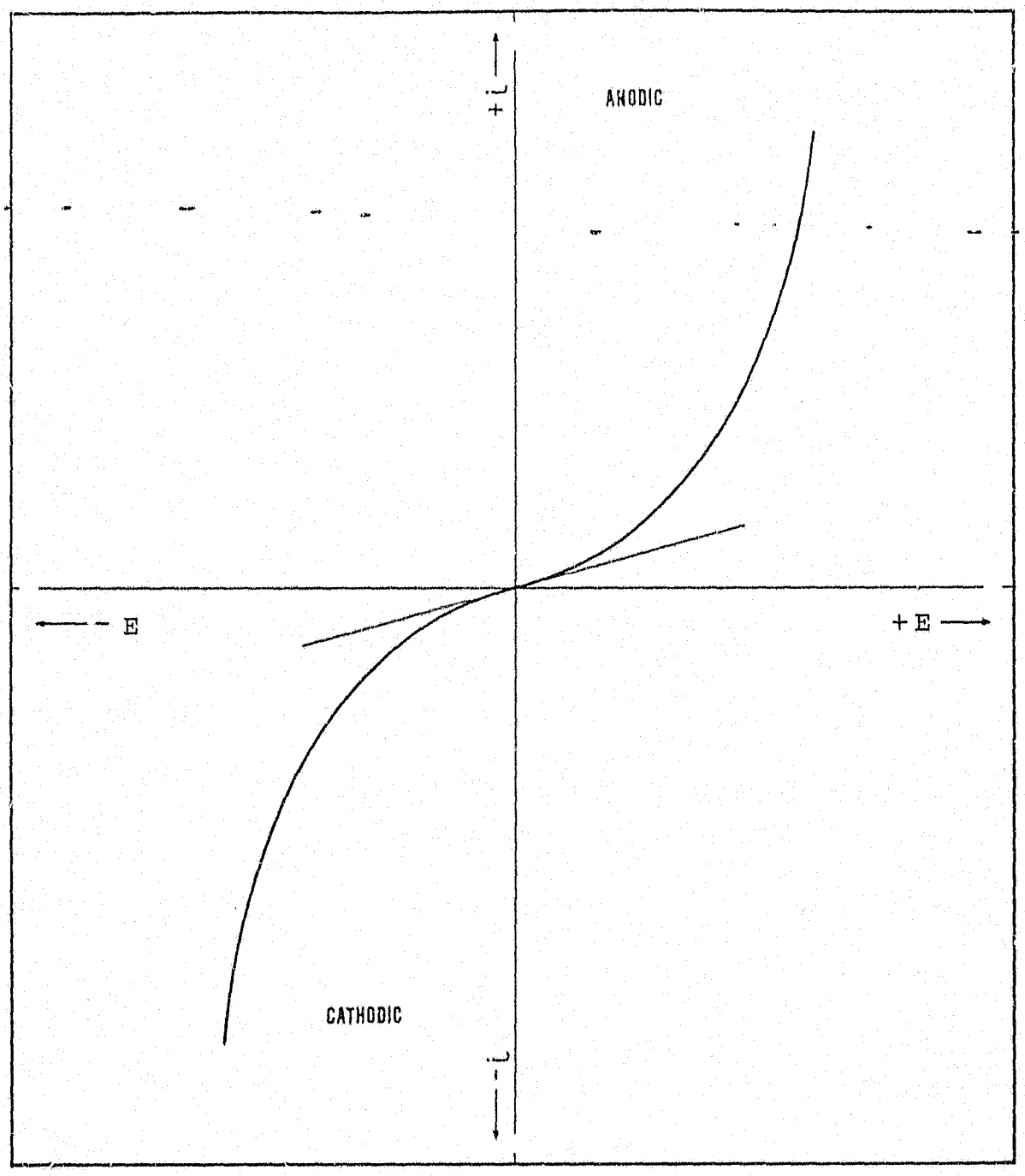


Fig. 2.2. Typical current-voltage plot where E is potential in volts, i is current density in amps per square cm.

curves. The term Tafel plot is used for generalized system descriptions and seldom for polarisation investigations.

2.5 Nernst Equation

Theoretically, the Gibbs free energy G, of a system is one of its most useful properties. This is a composite of properties of state of the system and basically is a combination of enthalpy content H, and entropy S, or

$$G = H - TS \qquad 2.8$$

where T is the absolute temperature. If all substances are present in their standard states,

$$G^{o} = H^{o} - TS^{o} \qquad 2.9$$

The free energy per mole of a substance is called its chemical potential ξ . The chemical potential of a substance is its partial molar free energy, and serves as a basis for the proper definition of activity a, (Pecsok and Shields, 1968);

$$G/\text{mole} = \overline{G} = \xi = \overline{G}^{o} + RT \ln a \qquad 2.10$$

where R is the universal gas constant.

The free energy of a system is the summation of the free energy of its components. Whenever there is a possibility of a chemical reaction within a system, the total free energy must decrease or the reaction will not occur. Thus, the driving force of a chemical reaction is measured by dG, the change in free energy, which is the difference between the free energy of the products and that of the

reactants.

At standard temperature and pressure,

$$dG = dH - T\,dS = dG^{o} + R\,T\,\ln a_{p} - R\,T\,\ln a_{r} \qquad 2.11$$

where a_p equals the activity of the products and a_r equals the activity of the reactants. Reactions will take place spontaneously only if $dG < 0$. If $dG > 0$, there will be a tendency for the reverse reaction to take place, and if $dG = 0$, the reaction is at equilibrium.

The change in free energy is also a measure of the maximum amount of electrical work that can be obtained from the cell if it is operated reversibly:

$$dG = -W \quad (@STP) \qquad 2.12$$

The electrical work, W, is the product of the charge times for potential difference through which it is transferred. For a charge of one F and for n moles of electrons transferred, the work must be;

$$dG = -W = -n\,F\,E_{cell} \qquad 2.13$$

where E_{cell} represents a potential difference between two electrodes of a cell and dG is the change in free energy of that cell reaction. Combining equations 2.11 and 2.13.

$$-n\,F\,E_{cell} = dG^{o} + R\,T\,\ln a_{p} - R\,T\,\ln a_{r} \qquad 2.14$$

and rearranging the terms:

$$E_{cell} = \frac{-dG^{o}}{nF} - \frac{RT}{nF}\ln\frac{a_{p}}{a_{r}} \qquad 2.15$$

gives the general form of the Nernst equation. The term $-dG^{o}/nF$ is more commonly called the standard potential and is the measured potential of an electrode relative to the standard hydrogen electrode (SHE) when all participating species are in their standard states. Using the symbol E^{o} for standard potential, substituting the numerical values for the constants and converting to base 10 logarithms, the common form of the Nernst equation is

$$E = E^{o} - \frac{0.059}{n} \log \frac{a_p}{a_r} \qquad 2.16$$

2.6 Electrified Interface

2.6.1 Space Charge

The electrical properties of any solid material are dependent on the particles forming the material and the forces operating on the particles. Since the surface of a material is a structural boundary to the particles, certainly the particles near the surface feel somewhat different forces than do the particles within the bulk. A gradual change in internal forces is observed as the surface is approached from within, which results in a net electrostatic charge on the surface. This charge is called the space charge and is exhibited to some degree in all solid materials. Space charge has three defining parameters: 1.the potential difference between an equilibrium point in the bulk of the material and that of the surface $(d\Phi/dx)$, 2.the absolute value of the surface potential of the material, i.e. E_F or Fermi energy, and 3.the thickness of Debye length, L_D, of the space charge. The Debye length in turn dictates

the gradient of the potential across the space charge.

In materials that are good electrical conductors, i.e. metals, the space charge is a function of available conduction electrons. Hence, $d\Phi/dx$ is quite small and E_F is relatively large. A characteristic value for the Debye length in metals is about 0.5×10^{-7} mm (Mehl and Hale, 1976). This situation of a very compact space charge is the solid state analog of the situation occurring in an electrolysis cell in which the concentration gradient is very small due to the abundance of conducting ions in a saturated solution.

In materials that are poor electrical conductors, i.e. insulators, there are no electrons available for conduction under normal circumstances and the resultant space charge spans the entire material. Hence, $d\Phi/dx$ is quite large and E_F is relatively small. In this particular case, the gradient of the space charge is linear across the material.

In semiconductors and semimetals, the quantity of conduction electrons or holes is limited and dictates the electrical properties of the material. The relationship between the Fermi energy and the conduction and valence bands for metals, semimetals and semiconductors can be seen in Fig.2.3. The Debye length for a semiconductor with intrinsic conductivity is given by

$$L_D = \{(\varepsilon_1 k T) / (4 \pi e^2 n_i)\}^{\frac{1}{2}} \qquad 2.17$$

where ε_1 is the dielectric constant of the semiconducting material, k is Boltzmann's constant, T is the absolute temperature, e is the charge of an electron and n_i is the concentration of electrons in a semiconductor with intrinsic

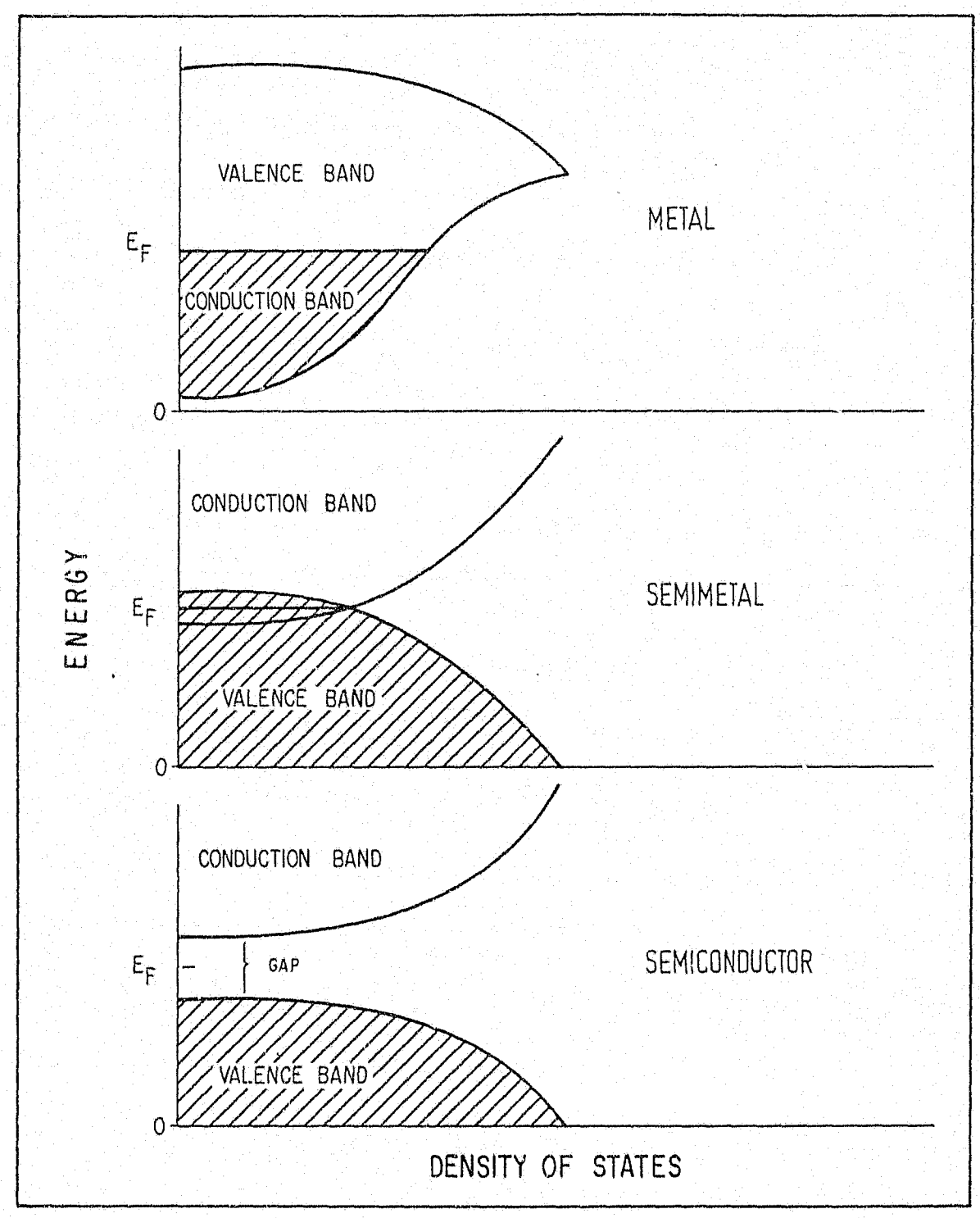


Fig. 2.3. Density of states (abscissa) versus energy (ordinate) for three types of solids.

conductivity (Myamlin and Pleskov, 1967). Also in semiconductors, the space charge can be of either polarity depending on whether the semiconductor is an n-type or p-type. Both types are encountered in naturally occurring sulfides. $d\Phi/dx$ is analogous to the Zeta potential of the diffuse layer in solution and the potential gradients for both the space charge and diffuse layer vary exponentially.

The resultant effect of the space charge, regardless of material or origin, is the presence of a net electrostatic charge at the surface of the material. This net charge is such that any nearby oppositely charged mobile ion is attracted and any nearby mobile polar molecule is preferentially oriented and attracted. Depending on the magnitude of the space charge, the attracted particles adhere, or are absorbed, in various manners.

2.6.2 Adsorption

Adsorption occurs in various modes. The most common in aqueous systems is solvation or hydration. Solvation is simply the electrostatic attraction and adherence of water molecules to either an ion in solution or a solid immersed in solution. It is well known that a water molecule has a dipole moment due to the asymmetry of the molecular structure. It is this dipole moment that enables a water molecule to be both oriented and attracted electrostatically. Since, by definition, water is ubiquitous in aqueous solution, it is invariably involved in the structure of the solution phase of the solid/solution, or electrode/electrolyte, interface. Its specific role will be explained in

the discussions of the inner and outer Helmholtz planes. Two types of adsorption mechanisms are generally considered in the electrode/electrolyte situation, i.e. physical adsorption and chemical adsorption.

Physical adsorption is the combination of weak electrostatic attraction and chemical adherence of an ion or molecule to a surface. The ion or molecule can be adsorbed in two manners : 1.simple adsorption or 2. specific adsorption. Simple adsorption involves the attraction of a solvated ion or molecule, i.e. with a layer of sheath of adsorbed water molecules. This solvated ion shows a weaker net charge and hence weaker attraction than an unsolvated ion due to the partial involvement of the charge in adsorbing water molecules. Also the solvated ion or molecule cannot get as close to the adsorbate because of the sheath of water molecules and is consequently even more weakly adsorbed.

Specific adsorption on the other hand involves the direct adsorption of an unsolvated ion or molecule and is consequently stronger than simple adsorption. Both simple and specific adsorption are weak, involving not more than a few kilocalories per mole. The type of bonding is by van der Waals forces and as a result, ions can be adsorbed on like charged surfaces. There is no activation energy necessary and several layers may form on some surfaces.

Chemical adsorption or chemisorption is much stronger. Generally, if molecules are involved, dissocation occurs and ionic or covalent bonds are formed. The heat of adsorption is greater than 15 kcal per mole(Bockris and Reddy,1973) indi-

cating an endothermic reaction which can be induced electrically. Ordinarily, chemisorption will not occur at standard temperature and pressure (STP) due to kinetic limitations and if it does occur, it is irreversible. Typically, chemisorption is the first stage of oxidation of most metals. Physical adsorption often takes place after chemisorption ceases.

2.6.3 Inner Helmholtz Plane

The inner Helmholtz plane (IHP) consists of a plane found by the locus of the charge centroids for a layer of ions specifically adsorbed on a planer surface. This is illustrated in Fig.2.4. It should be noted that electrode surfaces are generally drawn as planes although on a molecular or atomic scale they obviously are quite irregular. However, to best illustrate the situation on the solution side of an interface the planer representation will suffice.

Under no external influence, i.e. no applied potential, the IHP is predominantly populated by oriented water molecules, but the presence of the water in no way affects the description or location of the IHP, as it is, by definition, formed only by the specific or contact adsorbed ions. The potential drop across this region is assumed to be linear. Due to the charge separation, a capacitance effect is observed. This capacitance is called IHP capacitance and has a minimum dimensionless dielectric constant, k_{IHP}, of about 6 (Bockris and Reddy, 1973) due to the ordering of the water molecules. For comparison, the k_{water} at STP is about 79. Other layers of charge separation exist but none have

as low a dielectric constant as the IHP. This, in effect, places the IHP in a rather influential situation.

2.6.4 Outer Helmholtz Plane

The outer Helmholtz plane (OHP) consists of the locus of the charge centroids for the solvated ions at their position of closest approach to a surface. This is also illustrated in Fig.2.4. The OHP is also the point at which the potential gradient changes from being linear across the adsorbed ions to exponential in the diffuse layer. The dielectric constant, K_{OHP} is about 36 (Bockris, ibid). Commonly the IHP and OHP are collectively referred to as the compact layer or compact double layer.

2.6.5 Diffuse Layer

The diffuse layer consists of a gradual concentration change from the OHP to the bulk solution. The potential due to the concentration gradient is considered to be exponential. It is expressed as

$$c_x = c_o \exp(-\nu x) \qquad 2.18$$

where c_o equals the concentration at the layer of solvated ions, x is the distance relative to the layer of solvated ions and ν is the effective diameter of the solvated ion. The diffuse layer thickness seldom exceeds 1×10^{-5}mm and is strongly concentration and potential dependent. In fact, it appears that all of the capacitances that can be ascribed to the interfacial region are potential dependent. The diffuse layer is also shown in Fig.2.4.

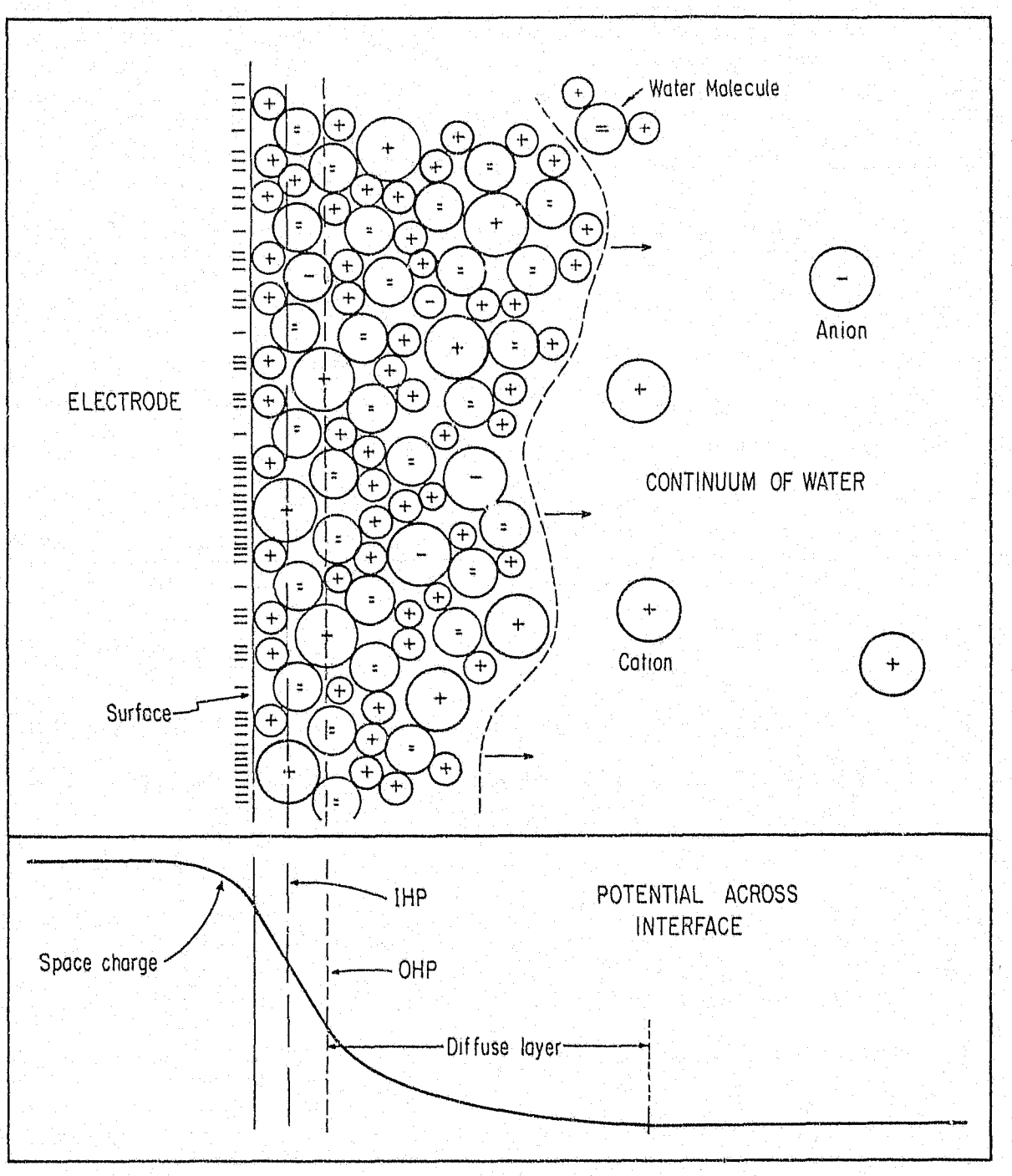


Fig. 2.4. A diagrammatic depiction of the distribution of cations, anions and water molecules at a hypothetical interface. The lower figure is a plot of the relative potential across the interface.

2.6.6 Double-layer Capacitance

In 1853 when Helmholtz originally formulated the concept of charged surfaces and the corresponding solution effects, he alluded to a double layer to describe the two balancing layers of charge he assumed existed at interfaces. This double layer consisted of a layer of negative charges (electrons) on the metal side of the interface and a layer of positive charges (ions) on the solution side. Since that time, the term double layer has been applied to virtually every combination of layers encountered across the entire interfacial region and has subsequently become somewhat ambiguous in meaning. The term double-layer as used in this research will be the combination of the IHP and OHP as one layer and the diffuse layer as the other.

The charge on the electrode (q_m) is equal and opposite to the sum of the charges in the IHP (q_{IHP}) OHP (q_{OHP}) and the diffuse layer (q_d). Thus,

$$q_m = -(q_{IHP}+q_{OHP}+q_d) = - q_{soln} \qquad 2.19$$

At a point called the electrocapillary maximum (ECM), q_m equals zero as does $-q_s$. This explains the term point of zero charge or PZC. From Fig.2.5 it can be seen that the change in the surface tension versus change in potential will give the electrical charge on the system. This result is called the Lippmann equation,

$$d\gamma/dE' = -q_m \qquad 2.20$$

where γ equals surface tension in milliNewtons per m and the potential E' is for a constant composition. In turn,

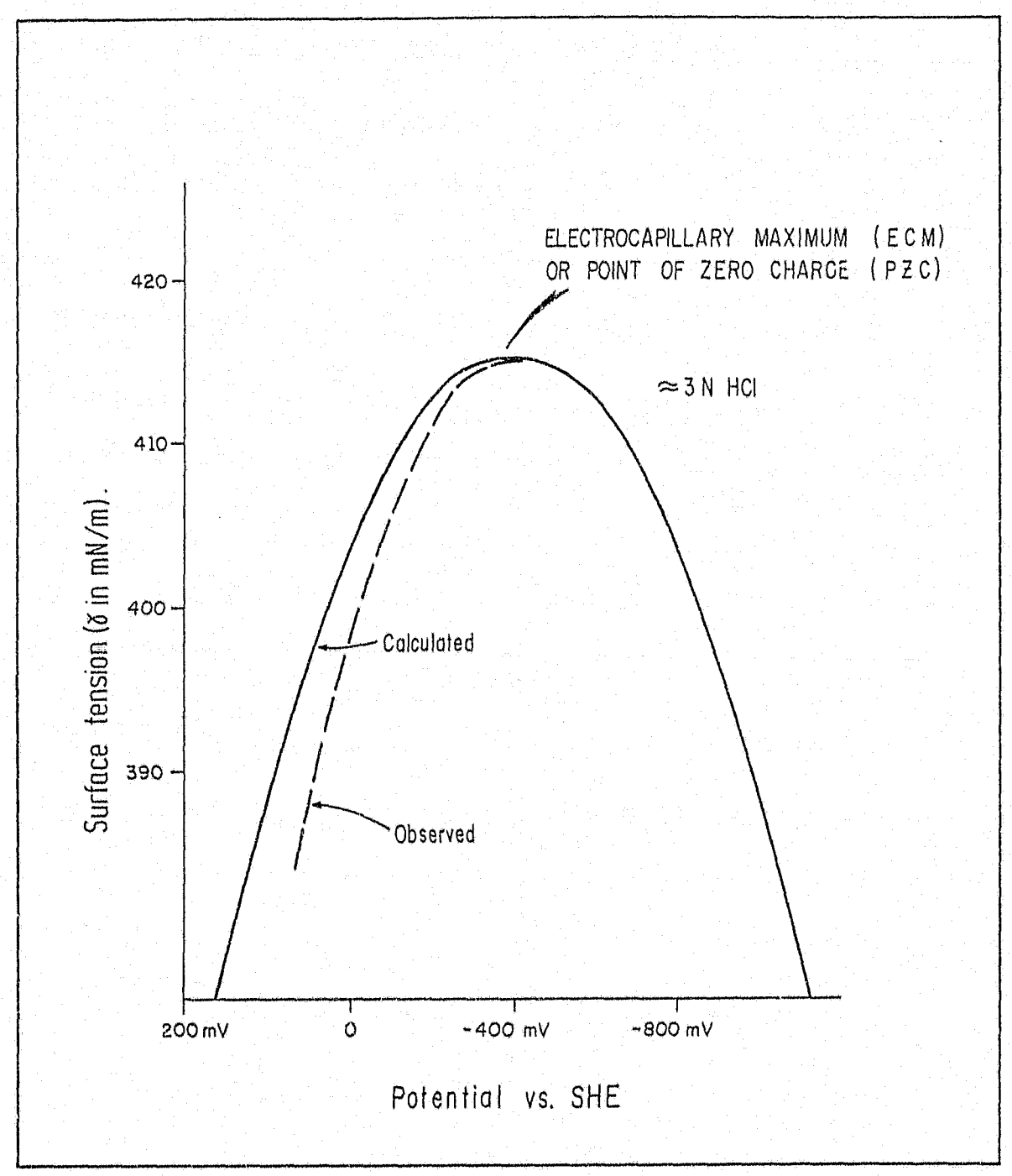


Fig. 2.5. Comparison of ideal parabola with observed electrocapillary measurements on a mercury electrode.

the surface excess is given by

$$\Gamma(\pm) = -\frac{\pm}{RT}(d\gamma/d \ln a_{\pm}) \text{ constant } E'_{\pm} \qquad 2.21$$

Since each layer of charge separation has its own capacitance, the reciprocal of the total capacitance for the interfacial region is simply the sum of the reciprocals of each capacitance,

$$\frac{1}{C_{total}} = \frac{1}{C_{space}} + \frac{1}{C_{IHP}} + \frac{1}{C_{OHP}} + \frac{1}{C_{diff}} \qquad 2.22$$

Obviously, the lowest capacitance will dictate the net capacitance and the first order capacitive effects. This is precisely the role of the IHP and is readily apparent in the electrocapillary measurements. The functions of the other capacitances serve to modify this first-order effect but never to dominate it. These modifying effects include the capacitance jump and lack of parabolic symmetry about the pzc. The calculated capacity for the electrode surface to OHP region is 16 to 17 $\mu F/cm^2$ and is fairly independent of the radius of the ions involved but is potential dependent (Bockris and Reddy, 1973).

An ideally polarized electrode is one at which no charge transfer takes place across the interface regardless of potential. Naturally, such electrodes exist in theory alone but differences of up to ten orders of magnitude between threshold values of charge transfer have been observed (Bockris and Reddy, 1973).

Electrocapillary curves display a definite asymmetry. The curves can be very nearly parabolic but large deviations have been observed for positive potentials, which

reflect a sensitivity to anions in solution- and moderate deviations have been observed for negative potentials, reflecting a sensitivity to cations. The asymmetry also implies that the differential capacity on one side of the ECM is different from the other side. In turn, this necessitates having a potential dependent capacitance as previously mentioned. This fact must be kept in mind when referring to the equation for total capacitance.

2.7 Electrode Polarisation

An electrochemical cell through which a finite current is passing has a potential different from its zero current or equilibrium value. This difference is ordinarily called overvoltage, overpotential or polarisation and is given the symbol η. In this research the term polarisation will be used exclusively. It is observed experimentally using a three electrode system, measuring the potential of the working electrode with respect to a reference electrode. It is defined as the difference in potential when the electrode is at equilibrium and when it is sustaining a net anodic or cathodic reaction :

$$\eta = E_{reaction} - E_{equilibrium} \qquad 2.23$$

Theoretically, η may be composed of five quantities: ohmic polarisation η_Ω, diffusion polarisation η_d, reaction polarisation η_r, charge transfer polarisation η_{ct}, and crystallization polarisation η_x (Vetter, 1967).

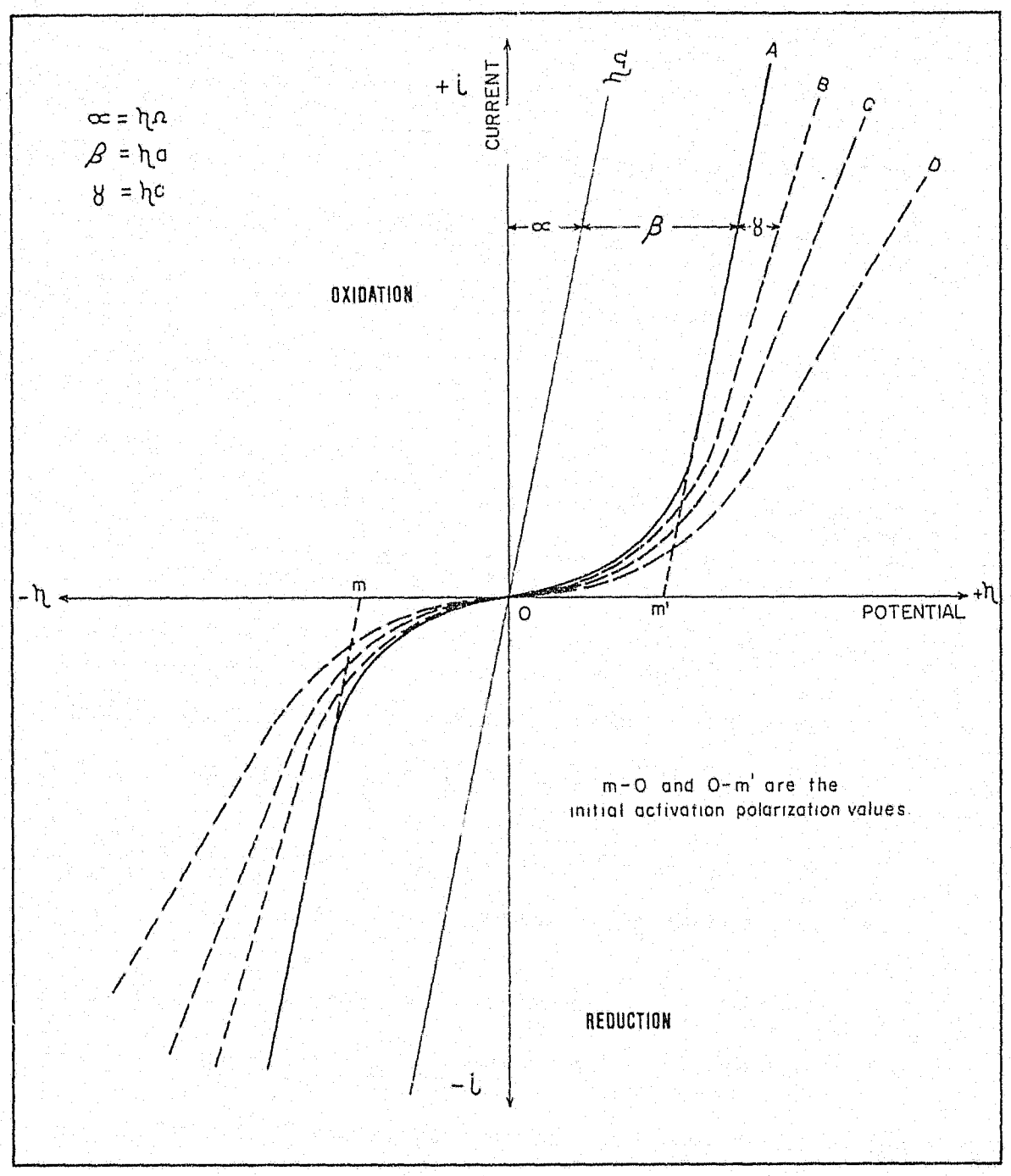


Fig. 2.6. Schematic current-voltage curves for a cell with identical irreversible electrodes. A, B, C and D represent instantaneous initial values after increasing times of current flow, η_Ω is the ohmic polarisation curve and $\alpha+\beta+\gamma$ is the total polarisation at current density i.

Therefore,

$$\eta_{total} = \sum \eta_{(\Omega,d,r,ct,x)} \qquad 2.24$$

Commonly, the sum of the diffusion polarisation η_d and the reaction polarisation η_r is called the concentration polarisation η_c. Likewise, charge transfer polarisation η_{ct} and crystallization polarisation η_x are collectively called the activation polarisation η_a. This grouping results in the often encountered representation of total polarisation by three types; ohmic, concentration and activation. In this form, these parameters are experimentally observable and can be represented graphically in their respective relationships in the current-voltage plane. This is shown in Fig.2.6. It appears essential to the understanding of this research to clarify the differences between the various types of polarisation as well as why they are grouped.

When current is applied to a cell, ohmic polarisation appears instantaneously, activation polarisation ordinarily requires some milliseconds; and concentration polarisation is built up more slowly (Lyons, 1967). Ohmic polarisation is directly proportional to current (hence the name); concentration polarisation increased exponentially with current; and there is a rapid initial rise and then a more gentle increase of activation polarisation with increasing current (Lyons,1967). When the current is interrupted, these polarisations disappear in the same order and fashion preserving a type of symmetry.

2.7.1 Ohmic Polarisation

Ohmic polarisation, or iR drop, results from the attempt to measure the potential of any working electrode in a cell of finite resistance. It is a function of the conductivity of the solution; the conductivity of the electrode material exerts no influence on the type nor on the rate of electrochemical processes and is not involved in the net potential difference as shown in equation 2.23. It is purely the potential difference between the reference electrode and the working electrode and it can be minimized by placing the reference electrode extremely close to the working electrode. Techniques for iR drop compensation or elimination have been proposed but not considered for this research as ohmic polarisation does not play a critical role in the interfacial phenomena sought.

2.7.2 Concentration Polarisation

Concentration polarisation η_c, exists in principle at every working electrode (Adams, 1969). With sustained electrolysis, concentrations at the electrode surface differ from that in the bulk of the solution and the electrode potential must differ from its value with no current flow. Concentration polarisation is the basis of voltammetry. A current-voltage curve is primarily the measurement of concentration polarisation effects at an electrode. The rate limiting process in concentration polarisation is the speed and relative efficiency by which ions in solution can shuttle to and from areas of low ionic or bulk concentration to the electrode interface where charge transfer

is taking place. This process is known as diffusion polarisation. When ions can be supplied to an interface at a rate greater then they can be consumed by the reaction taking place, the rate limiting process is called reaction polarisation. This is a purely chemical phenomenon, and accordingly, the rate constant is independent of electrode potential.

2.7.3 Activation Polarisation

Activation polarisation η_a, involves either the conversion of an electrochemically inert bulk species into an active form or a change of state of an active form. Whereas the concentration polarisation is primarily a function of transporting ions to and from the interface, activation polarisation is the needed potential to force a species to undergo charge transfer at the interface. This is a non-trivial phenomenon often involving multiple species. If, after an ion undergoes charge transfer, it combines with the surface of the electrode to increase the mass of the electrode, it is said to plate out. The overpotential required to force plating is called the crystallization polarisation. While such a relatively large potential is necessary to create the solid state bonds, it is assumed that crystallization polarisation is of negligible importance in the present research as it only occurs at or very near limiting electrode potentials.

2.7.4 Mass Transfer

When a potential is applied to an electrolytic cell, the

electroactive species undergoing oxidation must be moved from an equilibrium point in the solution to the negatively polarised electrode interface, undergo charge transfer, and the resultant form be moved back to the bulk solution. The same situation applies for the species undergoing reduction at the opposing electrode. The rate limiting process is a function of current density. For low current densities the charge transfer process will likely be rate limiting whereas at high current densitites the movement of species or mass transfer will likely be rate limiting. If the rate determining process is mass transfer then the reaction may be reversible or irreversible (Adams, 1969). Under special conditions such as stirring or agitation where the electroactive species are supplied to the interface in large quantities compared to or greater than the charge transfer rate, the system is charge transfer controlled. Sometimes an intermediate step or chemical transformation occurs at an even slower rate than charge transfer or mass transfer. For these situations, the reactions are said to be kinetically controlled. The three mass transfer modes normally encountered are 1. migration, 2. convection, and 3. diffusion.

Migration is caused by a potential gradient existing in the body of the solution. The electric field creates a current in the solution by forcing negative ions to flow one way and positive ions the opposite direction. Neutral species are unaffected. The rate of movement of a charged particle depends on the magnitude of its charge, size, and

electroactive species undergoing oxidation must be moved from an equilibrium point in the solution to the negatively polarised electrode interface, undergo charge transfer, and the resultant form be moved back to the bulk solution. The same situation applies for the species undergoing reduction at the opposing electrode. The rate limiting process is a function of current density. For low current densities the charge transfer process will likely be rate limiting whereas at high current densitites the movement of species or mass transfer will likely be rate limiting. If the rate determining process is mass transfer then the reaction may be reversible or irreversible (Adams, 1969). Under special conditions such as stirring or agitation where the electroactive species are supplied to the interface in large quantities compared to or greater than the charge transfer rate, the system is charge transfer controlled. Sometimes an intermediate step or chemical transformation occurs at an even slower rate than charge transfer or mass transfer. For these situations, the reactions are said to be kinetically controlled. The three mass transfer modes normally encountered are 1. migration, 2. convection, and 3. diffusion.

Migration is caused by a potential gradient existing in the body of the solution. The electric field creates a current in the solution by forcing negative ions to flow one way and positive ions the opposite direction. Neutral species are unaffected. The rate of movement of a charged particle depends on the magnitude of its charge, size, and

degree of solvation. When large amounts of supporting electrolyte are involved the resultant iR drop in the solution is so small that the effect on the ions is minimized and can therefore be neglected.

Convection can be either thermally or mechanically induced. Convection is essentially agitation or stirring of a solution in such a manner as to create a flow of electrolyte past the electrode surface. It can also develop when density variations appear near the electrode surface.

Diffusion exists whenever concentration differences are established and it plays a part in every practical electrode reaction once electrolysis is initiated. Diffusion is similar to heat flow, hence it can be treated readily by theoretical analysis. The situation prevailing in the cell employed for this research can be best described as linear diffusion to a planar electrode.

Following a derivation by Adams (1969), a redox reaction is given as $Ox + ne^- \leftrightarrow Red$. Ignoring the effects of migration and convection, three observations can be made from experiments made at controlled potential: 1. the current is proportional to the concentration of the oxidant in bulk solution, 2. the current is also proportional to the area of the electrode, and 3. the current decreases monotonically with increasing time of electrolysis.

Fick's first law relates diffusion rate to concentration as

$$dN/dt = -D_o A \frac{dC_o}{dx} \qquad 2.24$$

where N equals the number of moles of a substance diffusing past a given cross-sectional area of A in cm^2 in a time dt, D_o is the diffusion coefficient with dimensions m^2s^{-1}, C_o is the concentration of the oxidant in bulk solution and x is the linear distance perpendicular to the face of the electrode increasing in the direction of the solution.

The flux (ζ moles $cm^{-2}s^{-1}$) of material diffusing per unit time and through unit area is obtained simply by normalizing Fick's first law to the electrode area. Hence,

$$\zeta = \frac{dN}{A\,dt} = -D_o \frac{dC_o}{dx} \qquad 2.25$$

Clearly, the change in C_o with time, between two planes at distances x and x + dx, is the difference between the number of moles of Ox entering at plane x + dx and leaving at plane x. Therefore,

$$\frac{dC_o}{dt} = \frac{\zeta(x + dx) - \zeta(x)}{dx} \qquad 2.26$$

From the definition of a limit, it can be seen that

$$\frac{\zeta(x + dx) - \zeta(x)}{dx} = \frac{d\zeta}{dx} \qquad 2.27$$

as dx goes to zero. Thus,

$$\frac{dC_o}{dt} = \frac{d\zeta}{dx} \qquad 2.28$$

Substituting the definition of flux leaves

$$\frac{d\zeta}{dx} = D_o \frac{d^2C_o}{dx^2} \qquad 2.29$$

and in turn, substituting the limiting condition for the

concentration, gives

$$\frac{dC_o}{dt} = D_o \frac{d^2 C_o}{dx^2} \qquad 2.30$$

which is Fick's second law, the fundamental equation for linear diffusion.

Applying suitable boundary values and using transform techniques the concentration can be shown (Delahay, 1954) to be the derivative of the error function of the form

$$\mathrm{erf}(\lambda) = \frac{2}{\pi^{\frac{1}{2}}} \exp(-\partial^2) d\partial \qquad 2.31$$

The result is

$$\frac{dC(x,t)}{dx} = \frac{C_o}{(D_o t)} \exp(-x^2/4 D_o t) \qquad 2.32$$

The solution to the error function can be found in tables and varies from zero to one.

Using the resultant equation, concentration/distance profiles for selected values of the time of electrolysis can be calculated. Some sample values are shown in Fig. 2.7 where the ordinate is the amount of consumed oxidant normalized to the equilibrium value and is plotted against distance from the electrode face on the abscissa. To obtain the amount of reduced species, it is only necessary to calculate the error function complement

$$\mathrm{erfc}(\lambda) = 1 - \mathrm{erf}(\lambda) \qquad 2.33$$

The instantaneous current i_t will be directly proportional to the flux at $x = 0$,

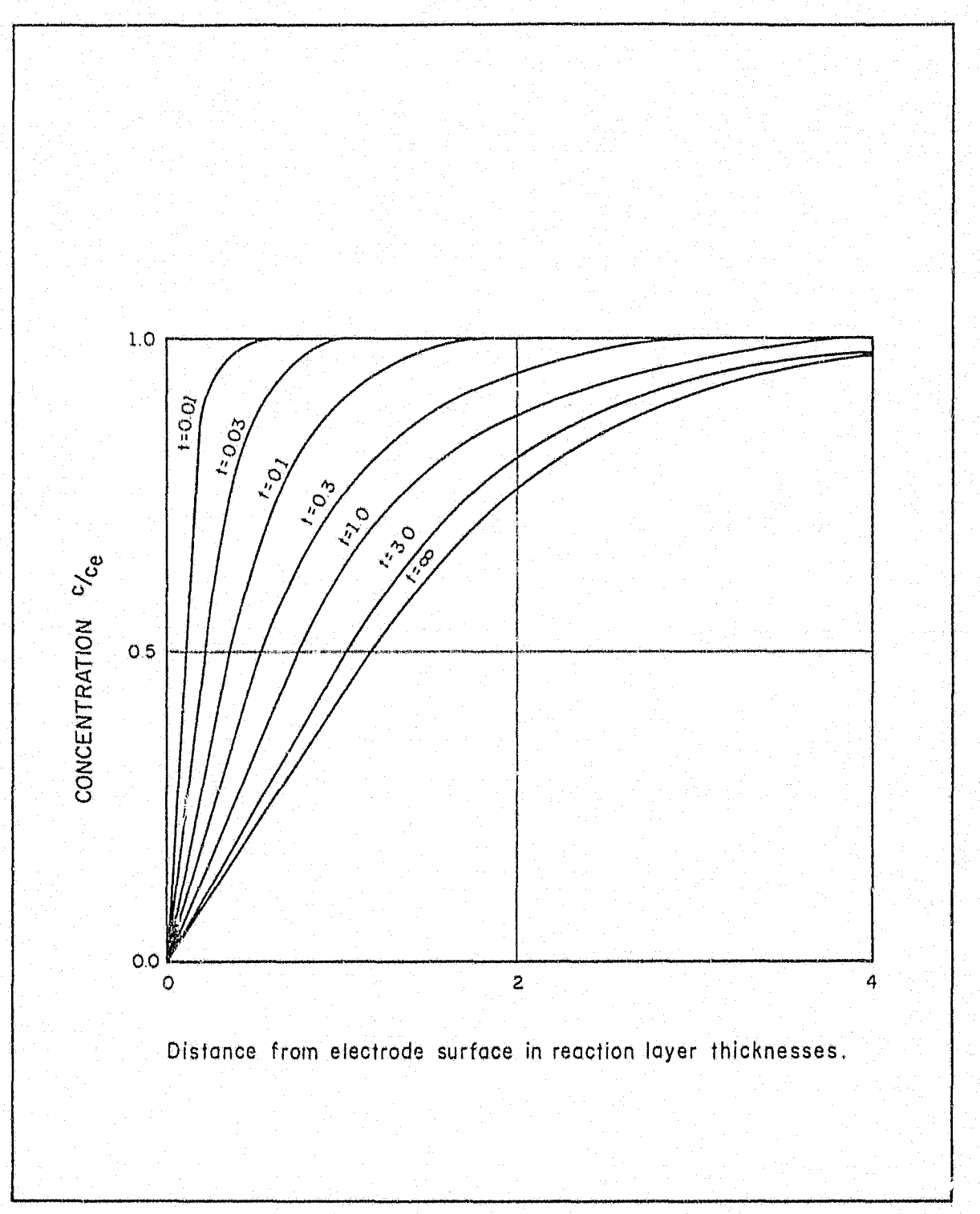


Fig. 2.7. The concentration of oxidant normalized to the equilibrium value plotted against the distance from the electrode surface in reaction layer thicknesses where t represents various elapsed times of electrolysis. Due to convection, the reaction layer thickness is finite for very large t.

$$i_t = nFA\lambda(o,t) = nFAD_o \left.\frac{dC_o(o,t)}{dx}\right|_{o,t} \qquad 2.34$$

By differentiating equation 2.34 and evaluating at x=0, one gets

$$\frac{dC(t)}{dx} = \frac{C_o}{(D_o \pi t)^{\frac{1}{2}}} \qquad 2.35$$

Substituting into the instantaneous current equation gives

$$i_t = nFAD_o^{\frac{1}{2}} C_o (\pi t)^{-\frac{1}{2}} \qquad 2.36$$

which is known as the Cottrell equation.

This result demonstrates that the current is directly proportional to bulk concentration and the area of the ele[illegible] and that current decreases inversely with the squa[illegible]t of time. Also, Cottrell's equation can be writt[illegible]

$$A = (i_t t^{\frac{1}{2}} \pi^{\frac{1}{2}})(nFC_o D_o^{\frac{1}{2}})^{-1} \qquad 2.37$$

giving the electrochemical area. This equation is quite useful when using imperfect electrodes such as naturally occurring sulfides if the other parameters can be determined.

$$i_t = nFA\lambda(o,t) = nFAD_o \frac{dC_o(o,t)}{dx}\bigg|_{o,t} \qquad 2.34$$

By differentiating equation 2.34 and evaluating at x=0, one gets

$$\frac{dC(t)}{dx} = \frac{C_o}{(D_o \pi t)^{\frac{1}{2}}} \qquad 2.35$$

Substituting into the instantaneous current equation gives

$$i_t = nFAD_o^{\frac{1}{2}} C_o (\pi t)^{-\frac{1}{2}} \qquad 2.36$$

which is known as the Cottrell equation.

This result demonstrates that the current is directly proportional to bulk concentration and the area of the electrode and that current decreases inversely with the square root of time. Also, Cottrell's equation can be written

$$A = (i_t t^{\frac{1}{2}} \pi^{\frac{1}{2}})(nFC_o D_o^{\frac{1}{2}})^{-1} \qquad 2.37$$

giving the electrochemical area. This equation is quite useful when using imperfect electrodes such as naturally occurring sulfides if the other parameters can be determined.

3 VOLTAMMETRY

3.1 Solid Electrode Voltammetry

A simple means of classifying electrochemical reactions, and at the same time obtaining a measure of their rates, is the use of current-voltage curves at a given electrode. At solid electrodes probably the best approaches to obtain current-voltage curves are single sweep linear potentiometry (SSLP) and cyclic voltammetry (CV). SSLP was performed on all the electrodes made for this study. Only the composited results are presented. These composites were arrived at through a stacking procedure used to produce a representative current-voltage curve for each particular sulfide type.

In CV the potential applied to an electrode is changed linearly with time in a repetitive manner as shown in Fig. 3.1. The current is measured as a function of potential or time. If only a single anodic or cathodic sweep is performed, the technique is usually referred to as SSLP. In both techniques, the experiment is often conducted in unstirred solutions. Stirring and varying the sweep or cyclic rates are options that can be used to distinguish between certain types of reactions. Stirred, unstirred and multiple sweep rates were all employed in this research.

The basic feature of a current-voltage plot is the appearance of a change in current gradient or a current peak at a potential characteristic of the electrode reac-

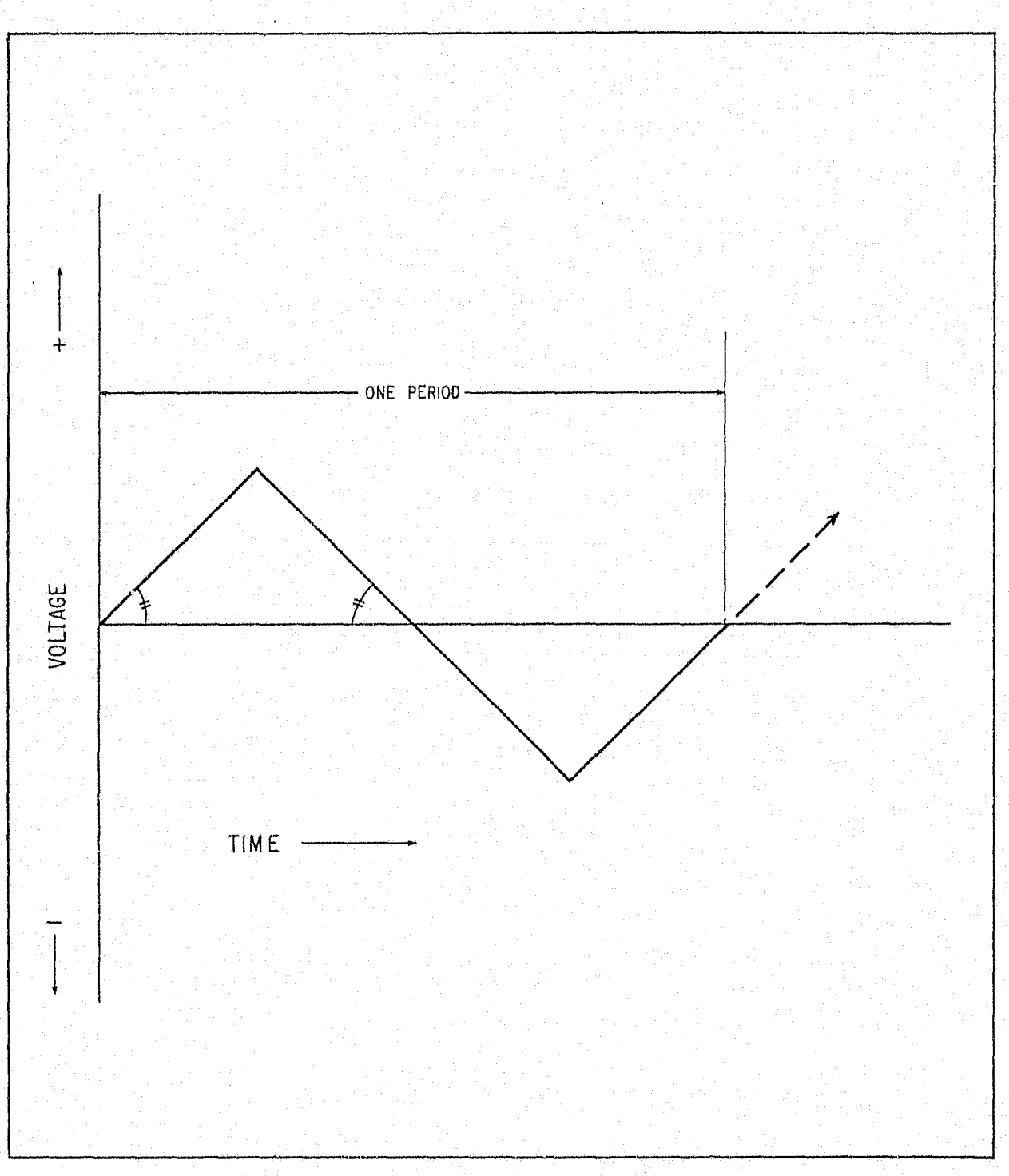


Fig. 3.1 Triangular waveform used for cyclic voltammetry (CV).

tion taking place. The position and shape of a given current change or peak depends on such factors as sweep rate, electrode material, solution composition and the concentration of reactants. Of the two techniques, only SSLP can provide accurate kinetic parameters, since the equations derived apply only in that there are no concentration gradients in solution just before the sweep is started. Cycling the potential several times creates complex concentration gradients near the electrode surface and the boundary-layer problem has not been solved (Gileadi et al, 1975). Thus, CV is better suited to the identification of steps in the overall reaction and of new species which appear in solution during electrolysis as a result of combined electrochemical and chemical steps. Nevertheless, an approximate value of the rate constant can be derived from the separation of the anodic and cathodic peak potentials at a given sweep rate for irreversible reactions.

The mechanisms derived from CV alone are relevant only to the specific experimental conditions chosen, and may not be applicable to steady-state electrolysis of the same systems in well stirred solutions. Kinetic parameters can be evaluated correctly only if the mechanism or reaction is known and the equations relevant to this mechanism are employed. In spite of these limitations, CV has been widely employed for the study of organic electrode reactions and it is particularly valuable for the qualitative detection of intermediates formed in complex reaction sequences. Numerous calculations of the shape of the current-voltage curves for various assumed mechanisms have been published

and compared with the experimentally observed curves. Only two phenomena were considered relevant to the data obtained in this research. The foremost of the two is that of the limiting potentials in both the anodic and cathodic directions. These potentials define the linear or quasi-linear central region of the current-voltage curve in which the impedance measurements were made. The second phenomenon was that of reaction rate limited potential dependent currents occurring within the linear region.

3.2 Basic Equations

The basic equations of SSLP relate the peak current density, i_p , and the corresponding potential, E_p , to the electrochemical specific rate constant, k_s , at the standard potential E^o , the Tafel slope b , the concentration in solution C^o and the sweep rate $v = dE/dt$. For a simple cathodic charge transfer process under reversible conditions, where both reactant and product are soluble, i_p in amp/cm^2 at 25^{o}C is given by

$$\left|i_p\right| = 2.72\times10^5 n^{3/2} D^{\frac{1}{2}} C^o v^{\frac{1}{2}} \qquad 3.1$$

where D is in cm^2/s , C^o in mole/cm^3 and v in volt/s . E_p is related to the polarographic half-wave potential $E_{\frac{1}{2}}$ by

$$E_p = E_{\frac{1}{2}} - 1.109\frac{RT}{nF} \qquad 3.2$$

Note that E_p is quite close to $E_{\frac{1}{2}}$, which itself is related to the standard electrode potential by the equation

$$E_{\frac{1}{2}} = E^o - \frac{RT}{nF}\ln(f_r/f_o)(D_o/D_r)^{\frac{1}{2}} \qquad 3.3$$

where the subscripts refer to the oxidized and reduced species and f stands for the activity coefficient.

When the rate of the reverse reaction is negligible throughout the potential region studied, the following equations apply

$$\left|i_p\right| = 3.01\times10^5 n\left(\frac{2.3RT}{bF}\right)^{\frac{1}{2}} D^{\frac{1}{2}} C^{o} v^{\frac{1}{2}} \qquad 3.4$$

where all units are as in equation 3.1 and b is in volts. The peak potential is given under these conditions by

$$E_p = E_{\frac{1}{2}} - b\left(0.52-\tfrac{1}{2}\log\left(\frac{b}{D}\right)-\log k_s + \log v\right) \qquad 3.5$$

The variation of E_p with sweep rate is an indication of the departure of the system from equilibrium. The specific rate constant, k_s , at the standard potential and the Tafel slope can be calculated from a plot of E_p versus log v according to equation 3.5, provided the diffusion coefficient is known. The extrapolation of the Tafel slope to the potential axis will give the activation potential for that particular reaction.

As the sweep rate changes, the various reaction mechanisms often show a resonant interaction. The transformation from one type of behaviour to the other occurs at a characteristic sweep rate v_c which depends primarily on the value of k_s and, to a lesser degree, on D and b . At this sweep rate the values of E_p calculated from equations 3.2 and 3.5 are equal.

The equations given above apply quantitatively only to first-order charge transfer reactions with no kinetic or catalytic complications.

Aside from the quantitative parameters that can be obtained, there are many qualitative criteria that should be observed and understood. In CV, a type of response can be seen where products formed in the anodic process are reduced in the subsequent cathodic sweep forming a new peak. These peaks are typically steeper and greater than the corresponding anodic peaks due to the formation of insoluble products during the anodic process which accumulate at the electrode surface. The E_p (anodic) and E_p (cathodic) difference increases with increasing amount of deposit on the electrode surface.

It was during the impedance measuring phase of the research that the CV measurements were made. None of the reaction based phenomena were observed indicating a high degree of irreversibility.

3.3 Purpose

The express purpose of performing SSLP on the sulfides was to establish the potential limits (or reaction potentials) of the region of quasi-linearity on the current-voltage curve and simultaneously, through the use of a large number of samples, arrive at a representative current-voltage curve for each sulfide type. This quasi-linear region is bounded by hydrogen evolution on the cathodic side and electrode corrosion or dissolution on the anodic side. Some excellent work in this area has been done by Klein (1977) and Klein and Shuey (1978). Some of the work described herein is very similar to that of Klein's but with subtle differences.

Klein's work involved a range of pH's and a variety of

electrolytes whereas this work is, for the most part, confined to a neutral pH and a simple binary electrolyte. Klein's goal was to investigate the application of voltammetry to geophysical prospecting by evaluating the voltammetric responses of various sulfides. The goal of the present research was to establish an electrochemical framework within which impedance measurements could be made. Once this framework was established, impedance measurements were made at a variety of potentials within this framework to examine the potential dependence of the impedance spectra on interfacial properties. The impedance data are presented in the next chapter.

3.4 Procedure

The voltammetric data were collected using equipment made available in the Department of Chemistry at the University of Arizona, Tucson, Arizona, U.S.A. The work was performed during 1976 under the guidance of Dr. George Wilson of the Dept. of Chemistry.

The equipment used was a standard three electrode cell (described in Appendix D), a Princeton Applied Research 173 potentiostat and an X-Y recorder. The reference electrode used was a saturated calomel electrode (SCE) and is described in Appendix C. The working electrodes were made of pyrite, pyrrhotite, marcasite, chalcopyrite, bornite and chalcocite. The fabrication technique is described in Appendix A.

All measurements were made in a Britton-Robinson pH

buffered .25M NaCl supporting electrolyte at STP. The electrolyte was stirred (when desired) by a magnetic stirrer and was degassed with N_2. Generally, the SSLP measurements used a sweep or scan rate of 10 mV/s. The electrodes were polished, inserted in the electrolyte and allowed to reach equilibrium (determined by a net exchange current of less than 1 μA). The cell was then scanned in one polarity, the electrode removed and polished, solution changed and degassed, electrode reinserted and allowed to reach equilibrium. The cell was then scanned in the reverse polarity. This approach was used to avoid intermediate reactions due to the change of state of reaction products created during the previous scan and to aid in producing an optimal background polarisation curve. Typically, considerable deposits covered the electrode surfaces especially during anodic runs. These deposits were also observed and described by Klein and Shuey (1978). The hypothetical reactions and reaction products are not presented here as the curve shape and relevant parameters are the sought after information.

3.5 Results

3.5.1 Pyrite - FeS_2

Fig. 3.2 is a multiple composite of the pyrite current-voltage curves. It can be seen that the curve is composed of four linear segments; the anodic dissolution segment occurring at a potential of +650 mV, the cathodic discharge segment occurring at a potential of -1070 mV, the equilibrium segment between -250 mV and +400 mV, and the apparent rate limited segment between -250 mV and -1070 mV. Of

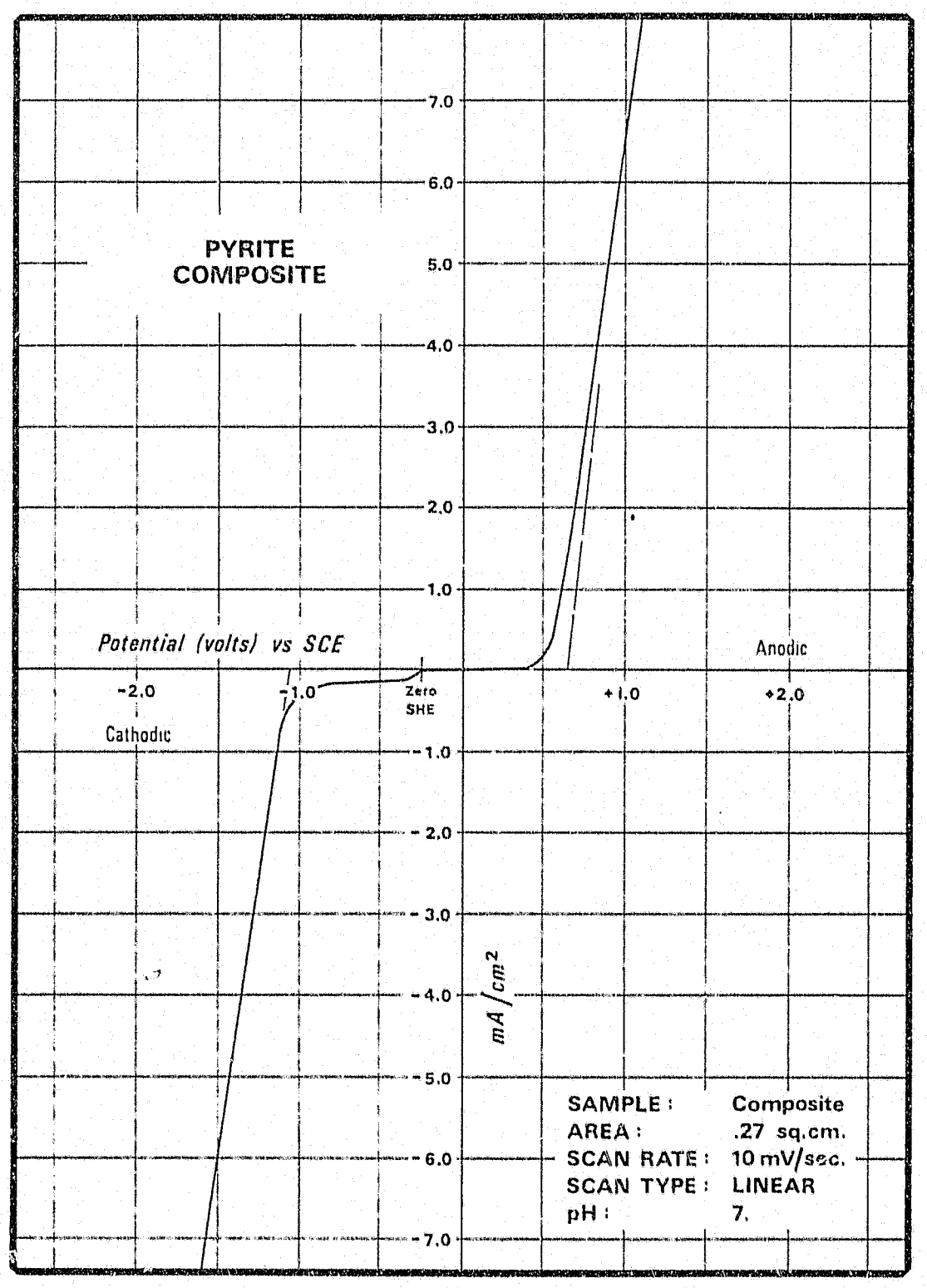


Fig. 3.2. Composite of the pyrite current-voltage curves. Area is given as the average area.

interest to this work are the two latter segments.

In a neutral electrolyte at pH 7, the open-circuit or rest potentials consistently occurred within the range observed by Sato (1960). It is interesting to note that, thermodynamically, pyrite should undergo anodic dissolution at the observed rest potentials (Hansuld, 1961). That this does not occur has been attributed to the development of an oxide film on the surface of the pyrite (Hansuld, ibid). This film develops immediately upon exposure to air after grinding or polishing or, in a natural state, due to the presence of dissolved oxygen in water. The surface states are drastically altered during cutting and polishing but the film develops regardless. The half-wave occurring at -250 mV can be attributed to either the reduction of the oxide film or a similar reduction of molecular oxygen to water. At more cathodic potentials the surface appears bright and clean (Klein, 1977) but a measurable cathodic current is always present. This half-wave potential is quite consistent for all the iron sulfides measured. Hansuld (ibid) indicates a two step stability field for pyrite, one being metastable and corresponding to the equilibrium curve segment, and the other being stable and corresponding to the observed cathodic half-wave. Accordingly, pyrite, as we know and observe it, exists in a metastable state, at least at its surface. The range of equilibrium was of primary concern for the impedance measurements but impedance measurements were made transgressing the half-wave potential.

A range of pH's were used on electrode py-d-05. This electrode seemed to be of the highest quality. The pH's

ranged from 2 to 10 and were created using Britton-Robinson buffers but the supporting electrolyte remained neutral. The results are shown in Fig 3.3. The cathodic reduction potentials monotonically decreased with pH however not as would be expected (i.e. linear in the log pH/linear Eh plane), but according to an odd powered exponential

$$E_c = 567mV \exp(0.09pH) \qquad 3.6$$

This is shown on Fig. 3.4. The change in anodic limiting potentials was minimal and too small to accurately measure although the extremes are plotted on Fig. 3.4.

3.5.2 Marcasite - FeS_2

Fig. 3.5 is a composite of the marcasite current-voltage curves. Similarity to pyrite would be expected as marcasite has the same composition and is an orthorhombic dimorph of pyrite. The anodic limiting reaction potential is +680 mV and the cathodic limiting reaction potential is -1080 mV. The range of equilibrium and apparent rate limited half-wave are virtually the same as pyrite. Due to the similarity of marcasite to pyrite, no impedance measurements were made on marcasite.

3.5.3 Pyrrhotite - FeS

Fig. 3.6 is a composite of the pyrrhotite current-voltage curves. Although pyrrhotite appears stoichiometric in formula and differs distinctly in habit from pyrite, the current-voltage curves were surprisingly similar. The anodic

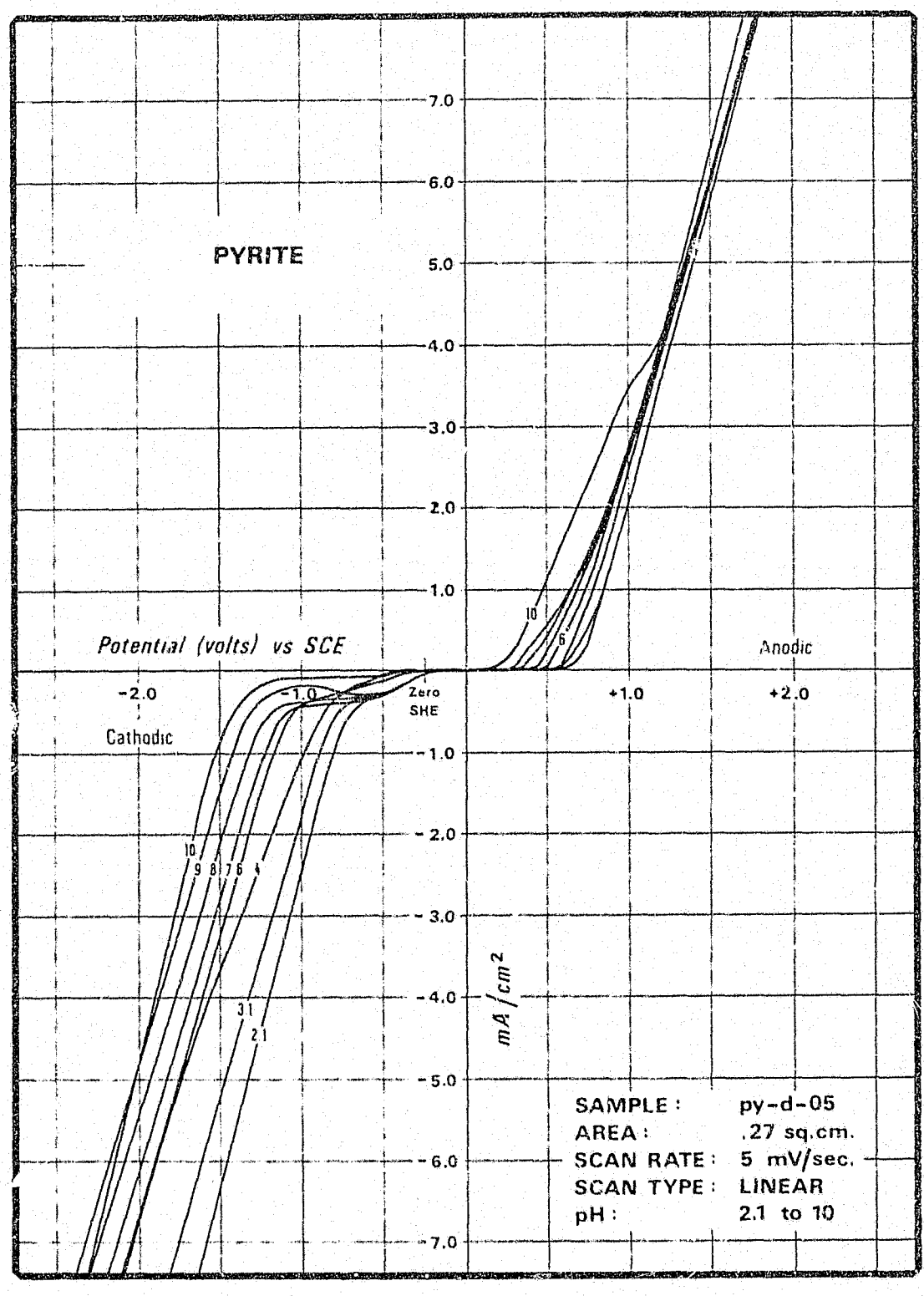


Fig. 3.3. Pyrite current-voltage curves for multiple pH's.

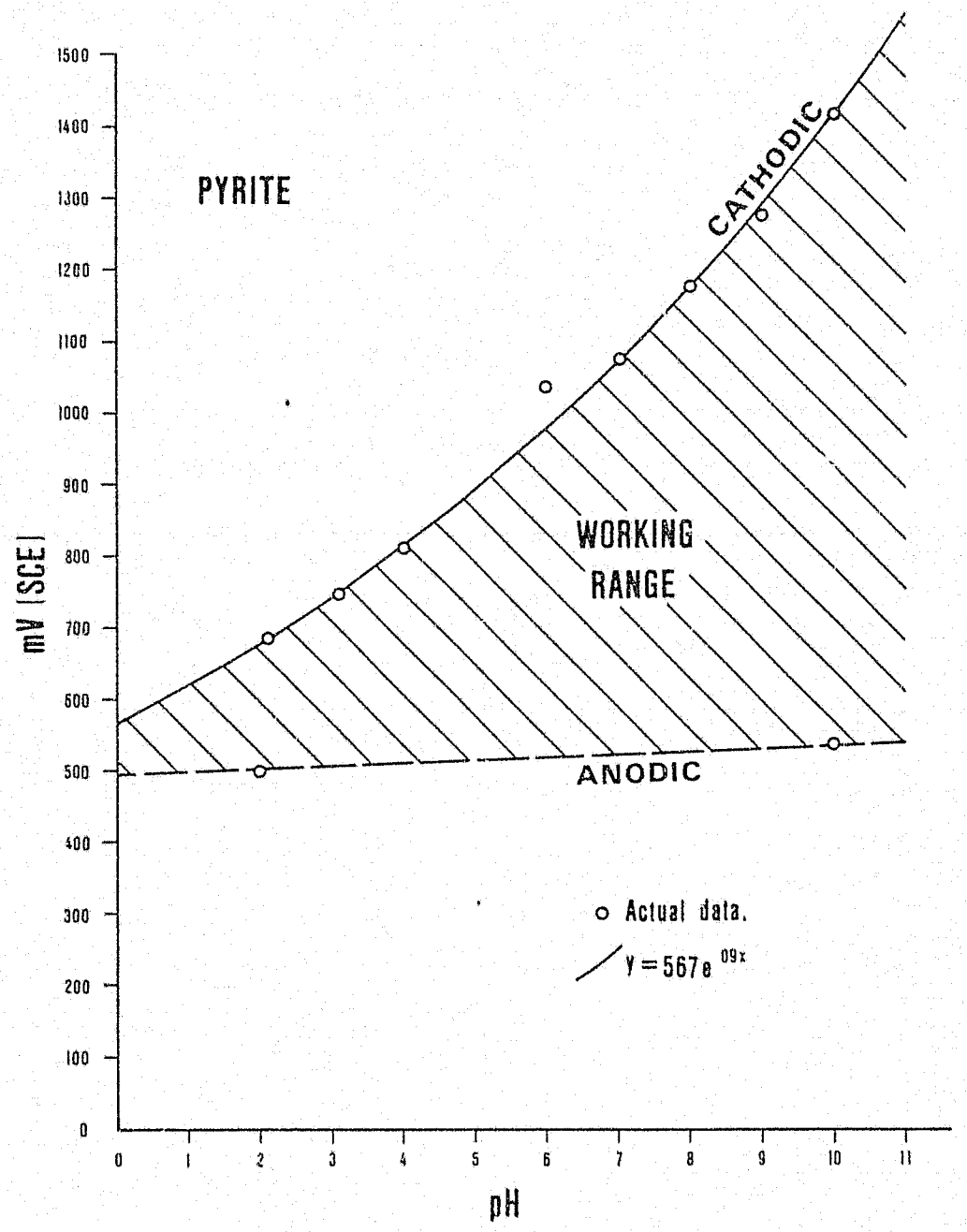


Fig. 3.4. Pl of anodic and cathodic limiting potentials for pyrite. Data are from Fig. 3.3.

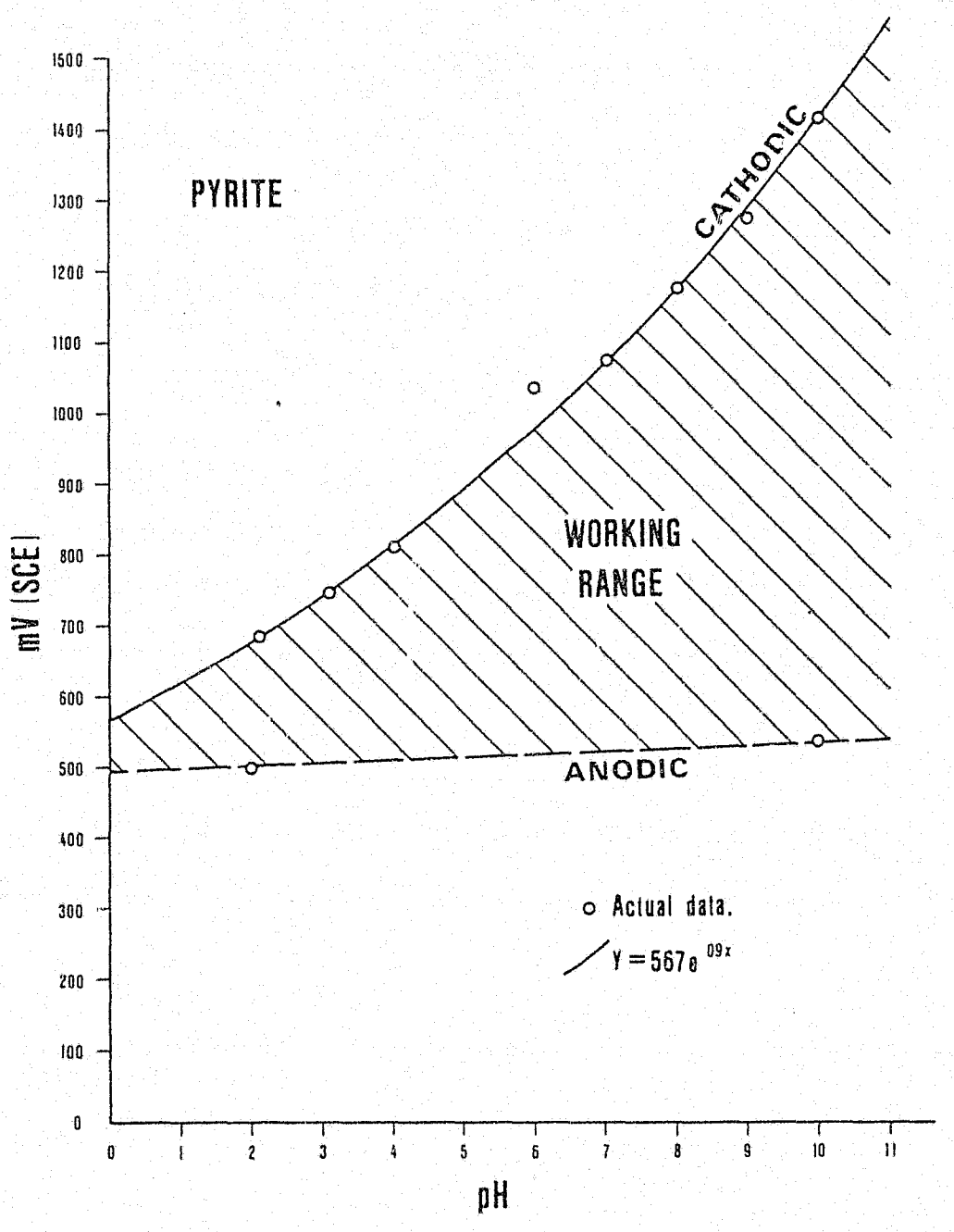


Fig. 3.4. Plot of anodic and cathodic limiting potentials for pyrite. Data are from Fig. 3.3.

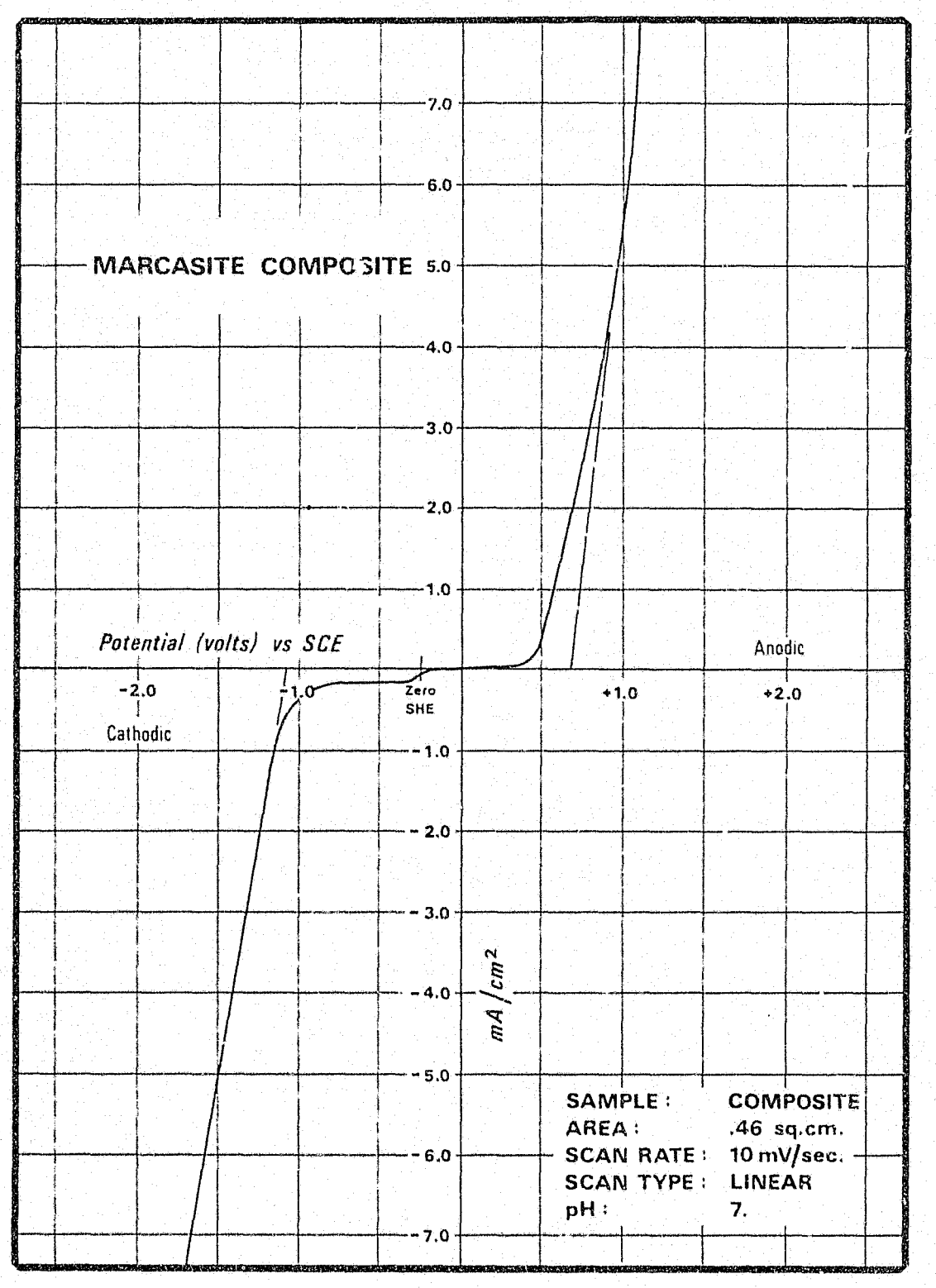


Fig. 3.5. Composite of the marcasite current-voltage curves. Area is given as the average area.

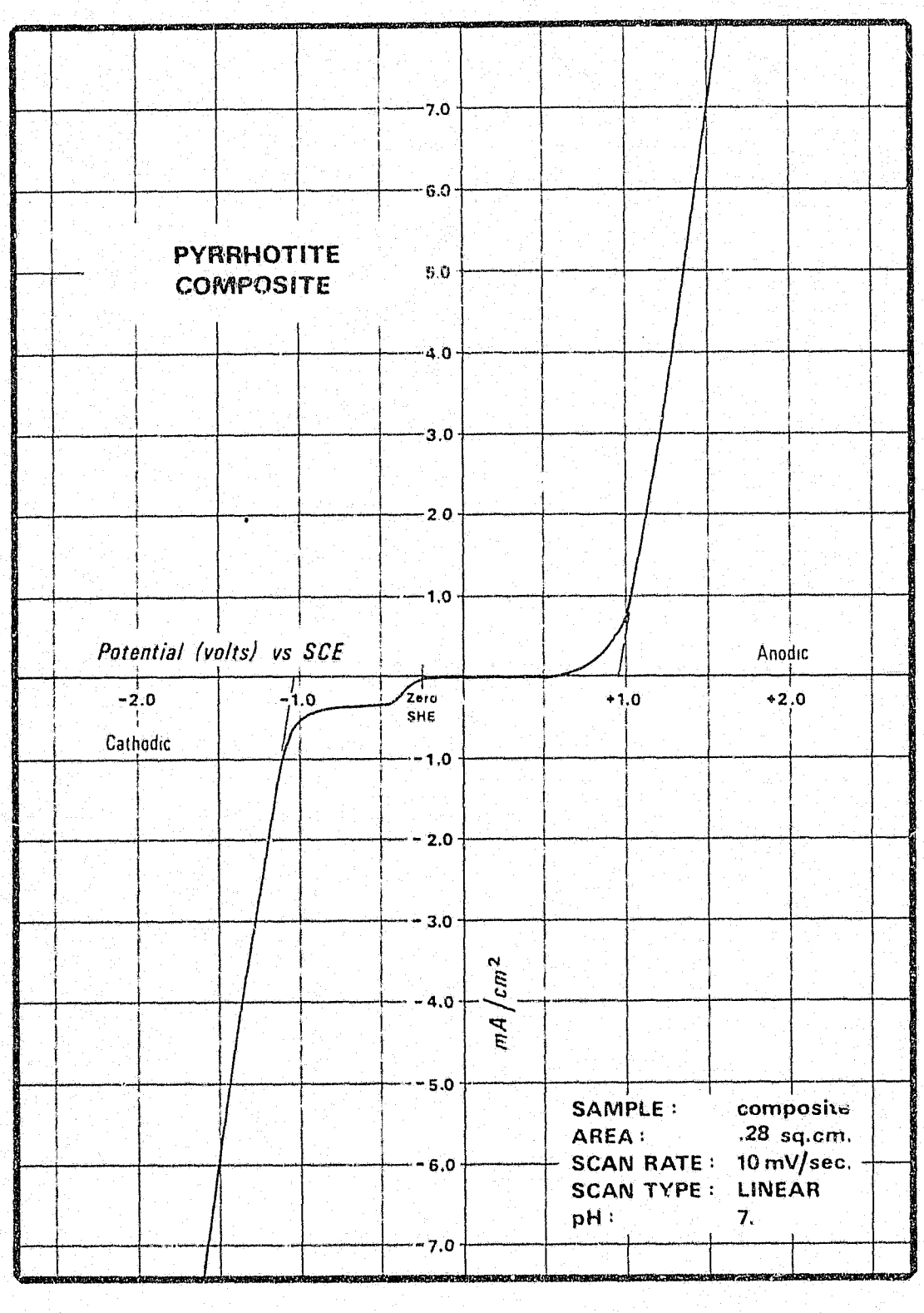


Fig. 3.6. Composite of the pyrrhotite current-voltage curves. Area is given as the average area.

dissolution potential is somewhat higher at +960 mV, the cathodic discharge potential is very similar at -1040 mV and a cathodic half-wave was observed at -350 mV.

The cathodic portions of the current-voltage curves for pyrite, marcasite and pyrrhotite are so similar that a single shape defines them all. The same situation nearly exists for the anodic portions except for the higher dissolution potential for pyrrhotite. These similarities suggest that the iron sulfides would be indistinguishable from each other in the quasi-linear region and in fact may indicate a common overall current-voltage response for iron sulfides in general (at least within the limitations of the current research).

3.5.4 Chalcopyrite - $CuFeS_2$

A great deal of electrochemical research has been done on chalcopyrite because of its significance as the primary copper ore mineral. However, since the interest has been towards solving metallurgical problems, it is not surprising that little of the work has been done at a pH of 7 in a neutral electrolyte. Fig. 3.7 is a composite of the chalcopyrite current-voltage curves. The composite curve is clearly of different character from those of the iron sulfides. A rate limited half-wave occurs on the anodic side at approximately +100 mV but the anodic dissolution potential of +960 mV is similar to that of pyrrhotite. The cathodic discharge potential at -1190 mV is higher than that of the iron sulfides. There is no well defined cathodic rate limited reaction although the transition to cathodic

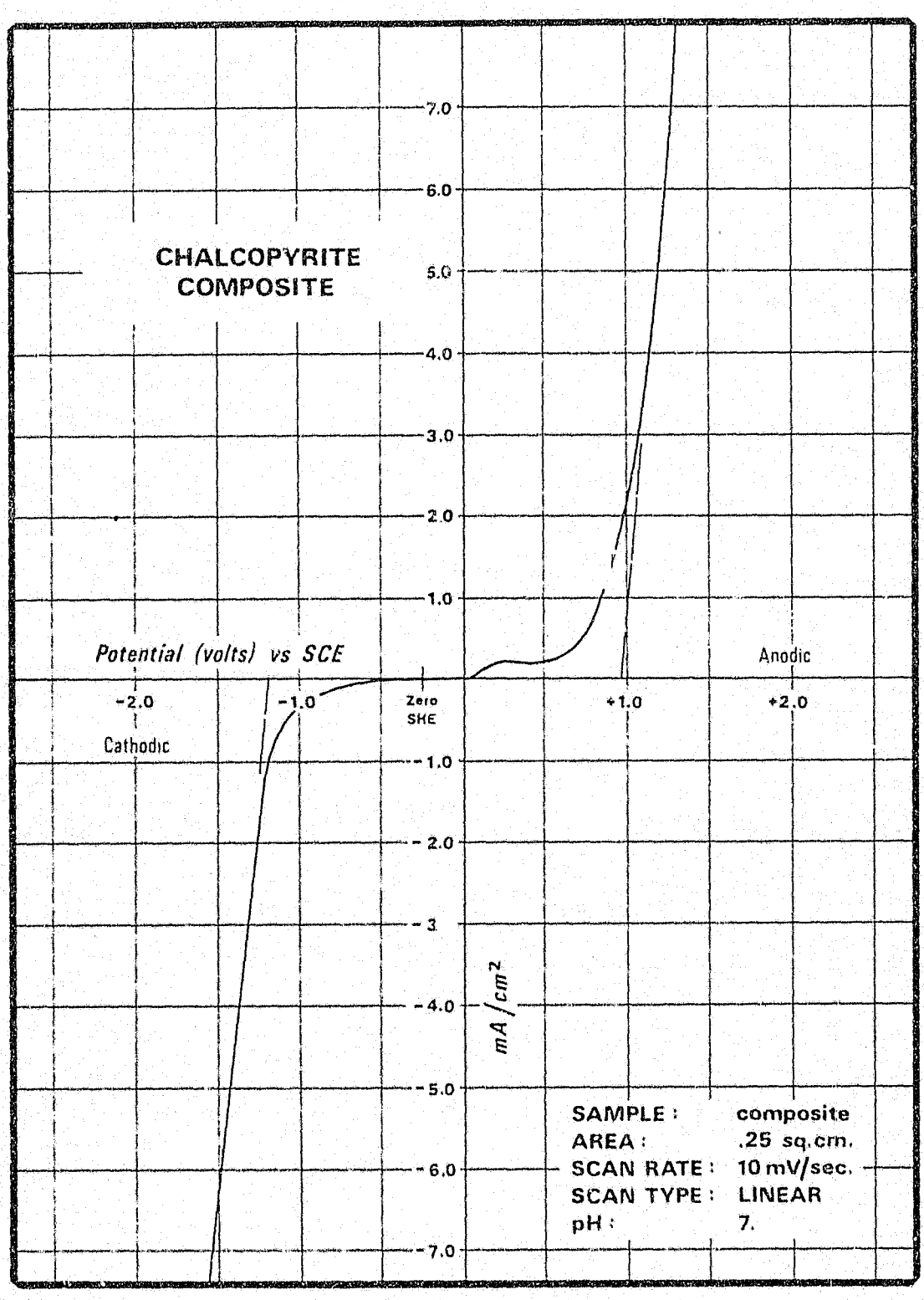


Fig. 3.7. Composite of the chalcopyrite current-voltage curves. Area is given as the average area.

discharge appears to start around -500 mV. This is likely due to intermediate reactions and indeed, some of the individual chalcopyrite samples had a well defined rate limited reaction occurring around -700 mV. The range of equilibrium appeared to occur between +100 mV and -500 mV. Impedance measurements were made in and beyond this range.

3.5.5 Chalcocite - Cu_2S

Fig. 3.8 is a composite of the chalcocite current-voltage curves. Although chalcocite is only a binary compound it has a current-voltage curve very similar and perhaps slightly more complex than chalcopyrite. An anodic half-wave occurs almost at zero potential, and is similar to that of chalcopyrite. The anodic dissolution potential is considerably greater at +1500 mV than that of chalcopyrite. The cathodic dissolution potential is also shifted to the right of chalcopyrite and occurs just beyond -500 mV and may be similar to that observed for some of the chalcopyrite samples although that of chalcocite is well defined.

The range of equilibrium was considered to be between -500 mV and zero. However, rest potentials generally occurred between zero and +300 mV. This put them well within the range of the anodic half-wave yet the observed current was usually less than 1 μA. This clearly illustrated that the approach used to measure the background polarisation curves had some shortcomings. Impedance measurements were made well into the anodic range.

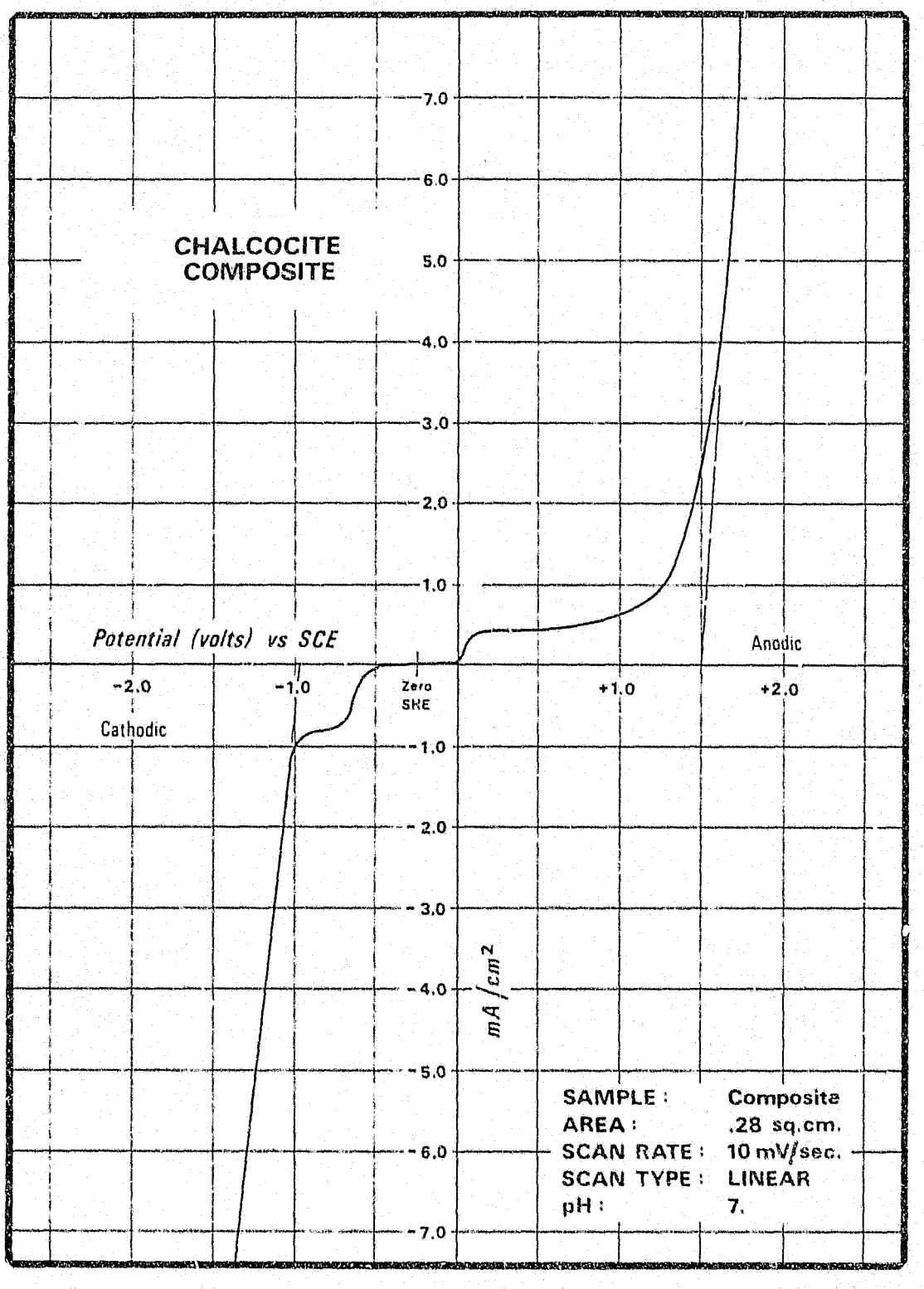


Fig. 3.8. Composite of the chalcocite current-voltage curves. Area is given as the average area.

3.6. Summary

The results of the voltammetric phase of the research demonstrate a definite difference in activation potentials for the various members measured of the Cu-Fe-S system. These differences relate to the constituents present but apparently not to their formula ratio. All electrodes produced characteristic current-voltage plots with three distinct properties. There were two nearly parallel linear portions of the plots representing the evolution of H_2 gas in the cathodic direction and surface corrosion of the electrode in the anodic direction. The portion of the plot between the limiting potential reactions can vary from being linear (similar to semiconductor current-voltage curves) to rather complex in appearance.

The more complex the curve generally the more reactions and rate limiting mechanisms are taking place. The types and rates of reactions observed are controlled by the activity and availability of ions in the electrode material and are primarily influenced by the surface states. The appearance of the different reactions and rate limiting mechanisms is controlled by the sweep rate. The approximate ranges of interest for impedance measurements were thus determined. It was within and slightly beyond these ranges that the impedance measurements were performed.

4 IMPEDANCE MEASUREMENTS

4.1 Introduction

Impedance measurements in electrochemistry are rapidly gaining in popularity. This is due, primarily, to automation and the increased precision with which measurements can be made over large dynamic ranges. Older methods involved bridge balancing or Lissajous figures and accordingly were much slower and less accurate. The technique is commonly known as the faradaic impedance method, or alternatively, the faradaic admittance method, the difference being only how the data are presented.

4.2 Faradaic Impedance

In the faradaic impedance method a periodic alternating voltage of low amplitude is applied to the electrode under study. The amplitude and phase shift of the resulting alternating current (ac) are measured. The ratio of the amplitude of the driving voltage to the amplitude of the resultant current is the impedance, Z^*, with dimensions of ohms. The phase angle, θ, is the phase shift of the resultant ac relative to the driving signal. Its dimensions are degrees or radians.

The electrode need not be at equilibrium (in fact, far more interesting and useful results are obtained if it is not), but the signal applied should be of sufficiently low

4 IMPEDANCE MEASUREMENTS

4.1 Introduction

Impedance measurements in electrochemistry are rapidly gaining in popularity. This is due, primarily, to automation and the increased precision with which measurements can be made over large dynamic ranges. Older methods involved bridge balancing or Lissajous figures and accordingly were much slower and less accurate. The technique is commonly known as the faradaic impedance method, or alternatively, the faradaic admittance method, the difference being only how the data are presented.

4.2 Faradaic Impedance

In the faradaic impedance method a periodic alternating voltage of low amplitude is applied to the electrode under study. The amplitude and phase shift of the resulting alternating current (ac) are measured. The ratio of the amplitude of the driving voltage to the amplitude of the resultant current is the impedance, Z^*, with dimensions of ohms. The phase angle, θ, is the phase shift of the resultant ac relative to the driving signal. Its dimensions are degrees or radians.

The electrode need not be at equilibrium (in fact, far more interesting and useful results are obtained if it is not), but the signal applied should be of sufficiently low

peak or rms amplitude (less than 10 mV) that the electrode is not driven for from the observing potential. If the current-voltage curve, in the region of the observing potential, is linear, the resulting alternating current will differ from the driving signal, in a linear sense, in magnitude and phase as dictated by the electrode/electrolyte interfacial parameters and any chemical reactions with respective rate limiting processes. It is through analysis of impedance measurements that meaningful conclusions about the interface can be drawn. There are two modes of current conduction across the interface; faradaic conduction and nonfaradaic conduction.

4.2.1 Faradaic Conduction

If the electrode/electrolyte interface behaves resistively, the resulting ac flow will be a result of charge transfer taking place with the corresponding oxidation or reduction of an electroactive species. This is termed faradaic conduction and can be observed at virtually all frequencies. In current flow of this type, charged particles existing either in the electrolyte or the electrode are transported to the interface by the gradient of the applied potential. At the interface they undergo a change in state (through oxidation or reduction) and in the new state can be either transported away from or remain at the interface. The potential necessary to drive a current across the interface is non-Ohmic and is dictated by the resistance of the charged particles to undergo a change in state. This resistance is termed the charge transfer resistance and in an

equivalent circuit would be represented by a resistor.

4.2.2 Nonfaradaic Conduction

If the electrode/electrolyte interface behaves capacitively, the resulting ac flow will be as a charging and discharging current (displacement current). This is termed nonfaradaic conduction and is generally observed at higher frequencies. In current flow of this type, the charged particles involved do not cross the interface and the electrical double layer acts as the capacitive barrier.

All electrode/electrolyte interfaces behave capacitively to some degree. The value and the potential dependence of the double layer capacitance are intrinsic properties of the electrode material. Differences in value observed due to pH, surface treatment or various electrolytes are ultimately due to a change in the surface potential and hence a change in the double layer capacitance.

If the double layer were purely capacitive (ideal case), the magnitude of the ac would very as the inverse of the frequency, the ac flow would be purely reactive and no current would flow at zero frequency. This double layer capacitance is usually represented by a capacitor in an equivalent circuit.

4.3 Warburg Impedance

When the charge transfer process at an interface is a combination of faradaic and nonfaradaic conduction, but the dominant and rate limiting process is mass transfer in the solution, the resulting impedance response is characteristic

and has been termed the Warburg impedance by Grahame (1952). Grahame is careful to limit the phenomenon to his class II species which undergo rapid vharge transfer at the interface but are limited in the rate at which they can diffuse through the solution to and from the interface. This diffusion is governed by Fick's second law from which Grahame analytically derives the Warburg impedance. He then demonstrates that the resultant impedance response would vary inversely as the square root of the driving frequency. Because of this peculiar response, it cannot be described by any simple combination of circuit elements. Hence, it was given a special symbol by Grahame



to indicate its presence and influence in an equivalent circuit. The Warburg impedance is also seen elsewhere as diffusion impedance, Z_d^* . Similar effects can be seen due to diffusion through solid material and along surfaces. From an observational point of view, diffusion in either case will appear the same and to separate them requires independent tests. However, it is solution diffusion Warburg impedance that Madden and Marshall (1959) claimed to be the underlying cause of the IP phenomenon. They did not perform independent tests to determine whether or not their observed diffusional effects were truly solution related. Consequently, this has been assumed to be the case. Until this research, the hypothesis has not been tested.

4.4 Complex Plane Analysis

Plotting impedance data in the complex plane can be extremely useful in that the rate limiting processes determining the impedance characteristics are often immediately apparent. Generally, one can determine the relative influence of the various interfacial phenomena simply from observing the shape of the plot. To appreciate why these phenomena are so characteristic in the complex plane, a graphical progression of the impedance response from simple to more complex equivalent circuits is presented. Fig.4.1 shows the relationship in the complex impedance plane between the magnitude (Z^*) and phase (ϕ) for a simple frequency (ω). The in-phase or real component (Z') is the abscissa and the out-of-phase or imaginary component (Z'') is the ordinate. Magnitude and phase are converted to orthogonal resistance and reactance components through the conventional polar to rectilinear transformation equations

$$Z' = Z^* \sin \phi \qquad \& \qquad Z'' = Z^* \cos \phi \qquad 4.1$$

4.4.1 Resistance Element

As mentioned, faradaic conduction can be represented by a resistor in an equivalent circuit. Ideally, the impedance of a resistor is independent of frequency and can be represented in the complex plane by a single point; the reactive component being equal to zero. This is represented by

$$Z' = R \qquad \& \qquad Z'' = 0 \qquad 4.2$$

and is shown in Fig.4.2.

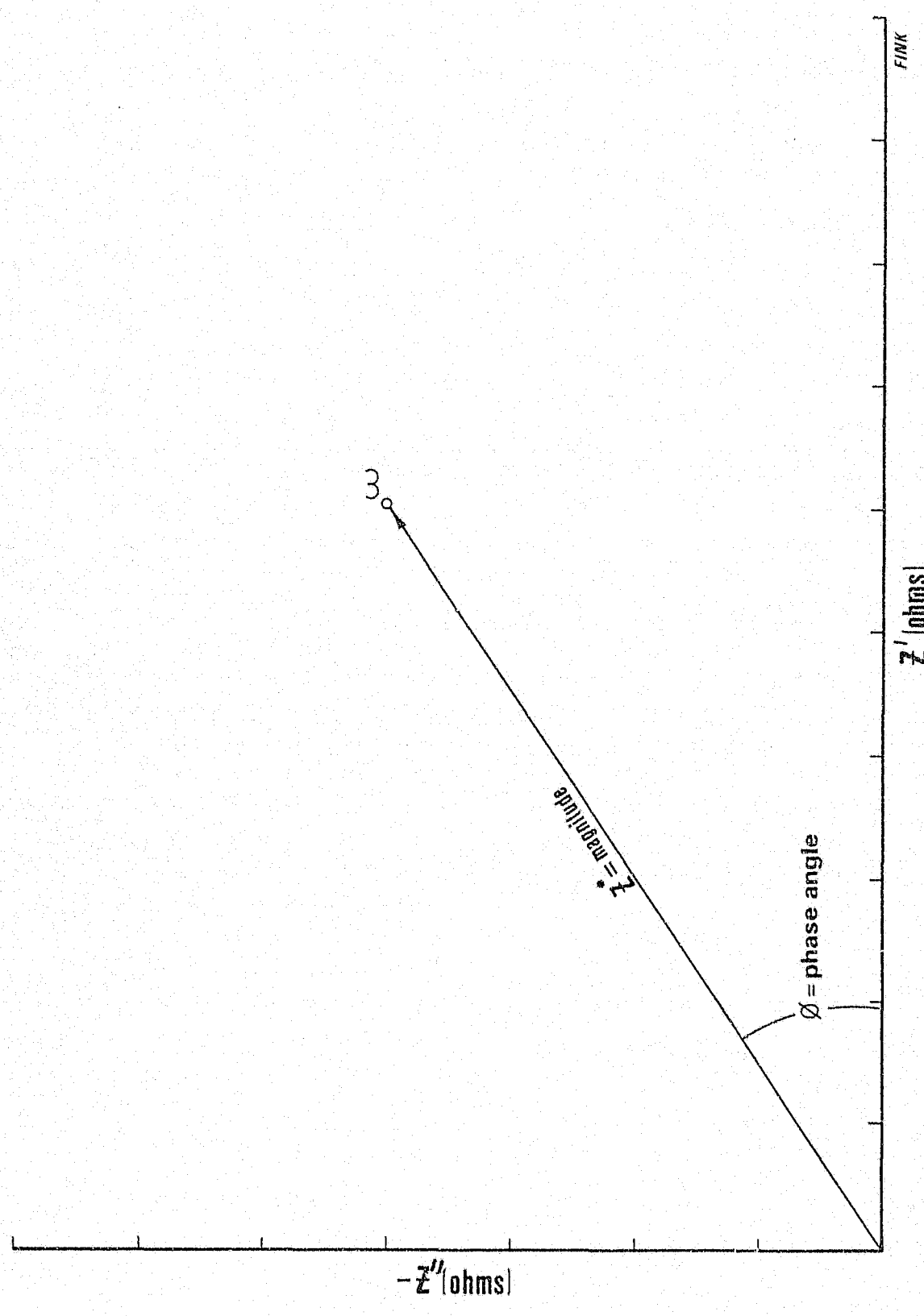


Fig. 4.1. Relationship between magnitude and phase in the complex plane.

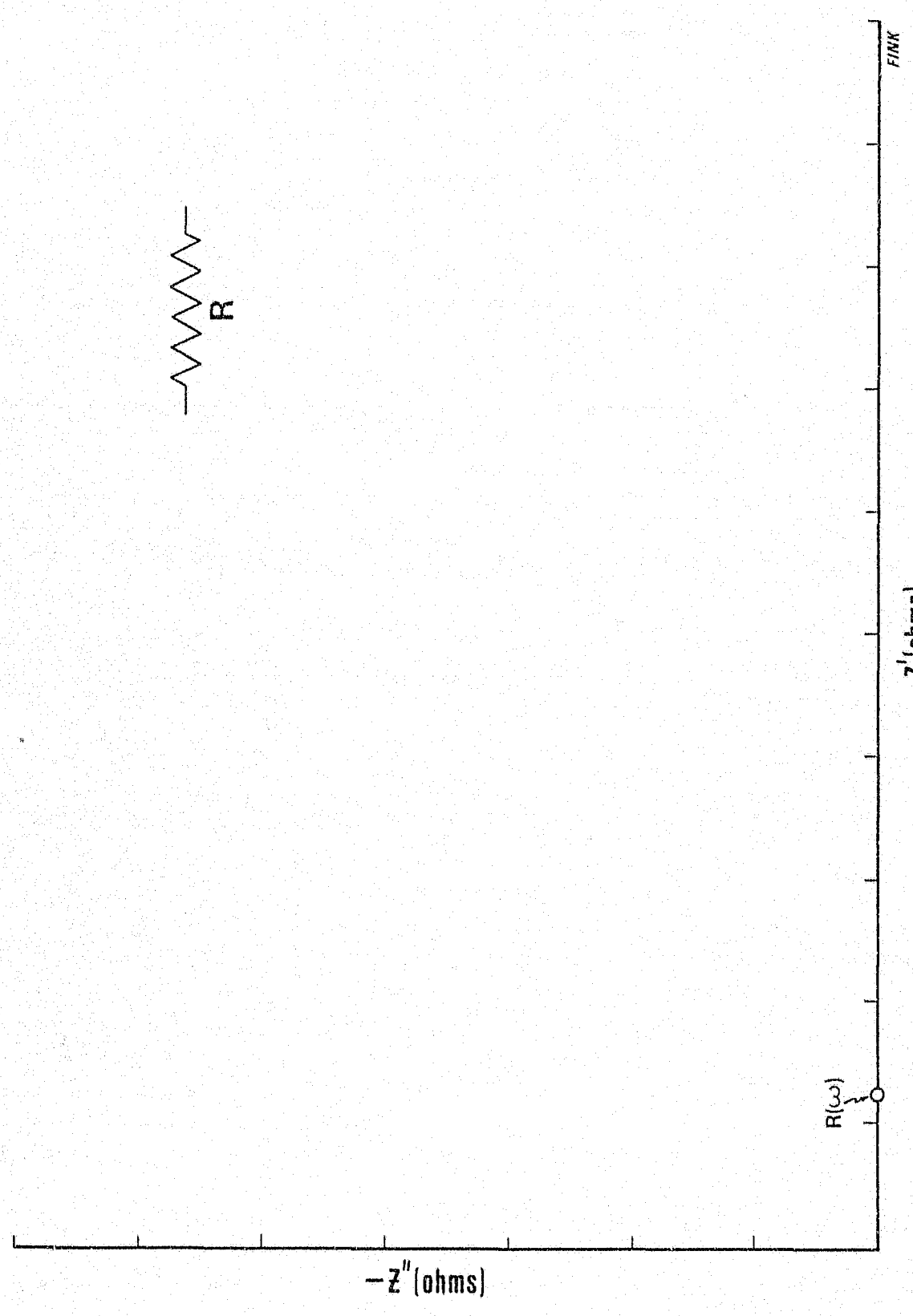


Fig. 4.2. Complex plane plot of an ideal resistance.

4.4.2 Capacitive Element

For an ideal capacitive element, the impedance is represented in the complex plane by a straight line coincident with the ordinate. This is represented by

$$Z' = 0 \qquad Z'' = -\frac{i}{\omega C} \tag{4.3}$$

and is shown in Fig.4.3.

4.4.3 Series RC Circuit

For a resistor and capacitor in series the resultant impedance is a straight capacitive line parallel to the ordinate but offset by a distance equal to the resistance. This is represented by

$$Z' = R \qquad Z'' = -\frac{i}{\omega C} \tag{4.4}$$

and is shown in Fig.4.4.

4.4.4 Parallel RC Circuit

For a parallel RC circuit, the resultant impedance plot in the complex plane is a semi-circle of diameter R. This is a more complex circuit since the in-phase and out-of-phase are both frequency dependent. It can be shown (Armstrong, et al) that

$$Z' = \frac{R}{1 + \omega^2 R^2 C^2} \tag{4.5}$$

and

$$Z'' = \frac{-i\omega R^2 C}{1 + \omega^2 R^2 C^2} \tag{4.6}$$

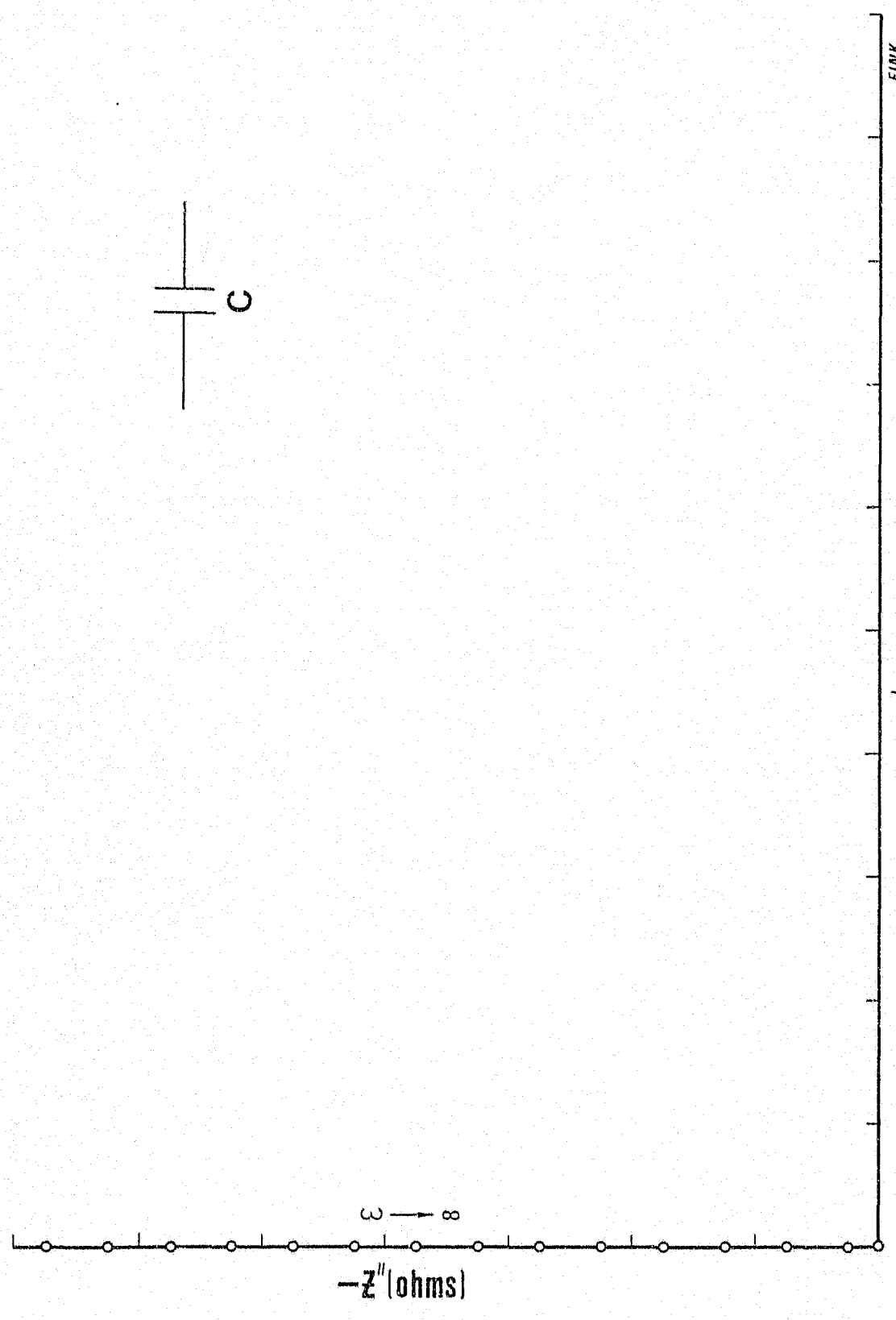


Fig. 4.3. Complex plane plot of an ideal capacitance.

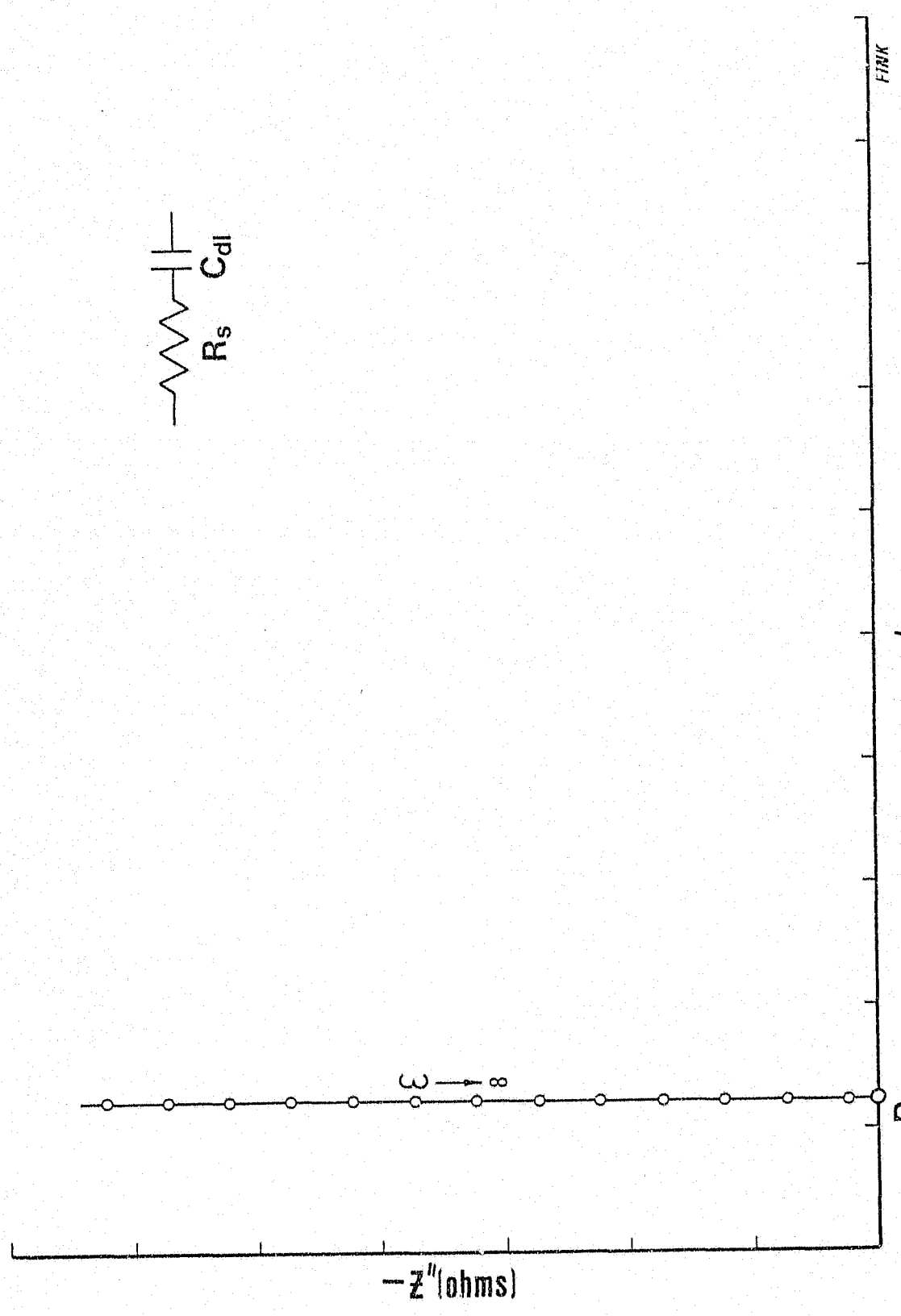


Fig. 4.4. Complex plane plot of an ideal r
l resistance and capacitance in series.

The impedance is plotted in Fig.4.5. It should be noted that the diameter of the semi-circle is equal to R and that C has no influence on the size of the circle. For a constant ω, changing C changes the location of the plot point on the semi-circle and the relative spacing between plot points, but does not alter the semi-circle size or location. In effect, for increasing C, the corresponding plot points, for each ω, simply slide along the semi-circle toward the high frequency end, or conversely for decreasing C, toward the low frequency end. The high frequency intercept with the abscissa (as $\omega \to \infty$) is zero and the low frequency intercept (as $\omega \to 0$) equals R. This parallel RC circuit is the basic approximation of an electrode/electrolyte interface where R is the charge transfer resistance R_{ct} and C is the double layer capacitance, C_{dl}. At this stage, no account has been made for solution and electrode resistance.

4.4.5 Parallel RC Circuit plus R_s

The solution resistance and electrode resistance are both in series with the charge transfer resistance and double layer capacitance. Hence, they can be lumped together in a single resistance, R_s. The effect on the impedance of the equivalent circuit is additive at all frequencies. The resultant complex plane plot, shown in Fig.4.6, is the same semi-circle simply shifted to the right by an amount equal to the resistance. This is represented by

$$Z' = R_s + \frac{R}{1 + \omega^2 R^2 C^2} \qquad 4.7$$

The impedance is plotted in Fig.4.5. It should be noted that the diameter of the semi-circle is equal to R and that C has no influence on the size of the circle. For a constant ω, changing C changes the location of the plot point on the semi-circle and the relative spacing between plot points, but does not alter the semi-circle size or location. In effect, for increasing C, the corresponding plot points, for each ω, simply slide along the semi-circle toward the high frequency end, or conversely for decreasing C, toward the low frequency end. The high frequency intercept with the abscissa (as $\omega \to \infty$) is zero and the low frequency intercept (as $\omega \to 0$) equals R. This parallel RC circuit is the basic approximation of an electrode/electrolyte interface where R is the charge transfer resistance R_{ct} and C is the double layer capacitance, C_{dl}. At this stage, no account has been made for solution and electrode resistance.

4.4.5 Parallel RC Circuit plus R_s

The solution resistance and electrode resistance are both in series with the charge transfer resistance and double layer capacitance. Hence, they can be lumped together in a single resistance, R_s. The effect on the impedance of the equivalent circuit is additive at all frequencies. The resultant complex plane plot, shown in Fig.4.6, is the same semi-circle simply shifted to the right by an amount equal to the resistance. This is represented by

$$Z' = R_s + \frac{R}{1 + \omega^2 R^2 C^2} \qquad 4.7$$

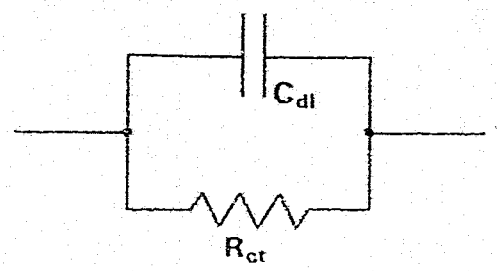


Fig. 4.5. Complex plane plot of a parallel RC circuit. The frequency occurring at the top of the semicircle is the resonant frequency for that circuit. The diameter of the circle is equal to R_{ct}.

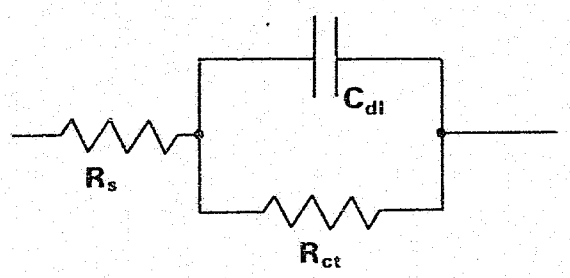


Fig. 4.6. Complex plane plot of a resistor in series with a parallel RC circuit. The semicircle of Fig. 4.5 is simply translated to the right by an amount equal to R_s.

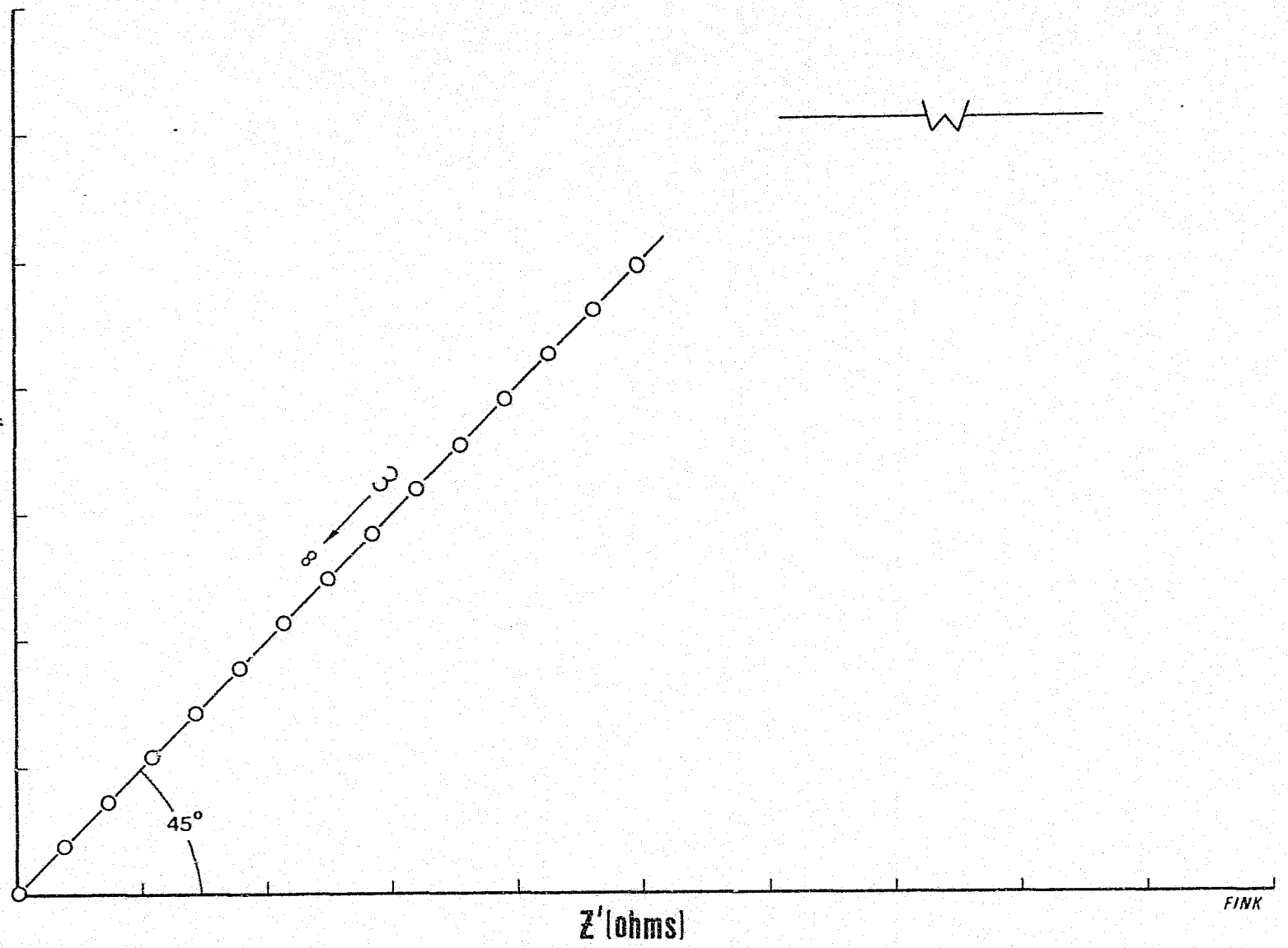


Fig. 4.7. Complex plane plot of the Warburg impedance when C_{dl}, R_{ct} and R_s equal zero.

and

$$Z'' = R_s + \frac{-i\omega R^2 C}{1 + \omega^2 R^2 C^2} \qquad 4.8$$

The resultant plot is shown in Fig.4.6.

4.4.5 Warburg Impedance

There is no analog equivalent circuit to adequately describe the Warburg impedance. However, for situations where R_s, R_{ct} and C_{dl} equal zero, the impedance response is mathematically defined (Grahame, 1952) as

$$Z' = \frac{\sigma}{\omega^{\frac{1}{2}}} \qquad 4.9$$

and

$$Z'' = \frac{-i\sigma}{\omega^{\frac{1}{2}}} \qquad 4.10$$

where is the Warburg coefficient and is derived from Fick's second law for both the oxidizing and reducing species in the Nernstian diffusion layer, and is given by Armstrong et al as

$$\sigma = \frac{RT}{n^2F^2\sqrt{2}}\left(\frac{1}{C_O D_O^{\frac{1}{2}}} + \frac{1}{C_O D_O^{\frac{1}{2}}}\right) \qquad 4.11$$

The resulting complex plane plot is shown in Fig.4.7.

4.4.6 Warburg plus R_s

As with the parallel RC equivalent circuit, the addition of R_s shifts the results in the complex plane along the abscissa. This is represented by

$$Z' = R_s + \frac{\sigma}{\omega^{\frac{1}{2}}} \qquad 4.12$$

and

$$Z'' = \frac{-i\sigma}{\omega^{\frac{1}{2}}} \qquad 4.13$$

The resulting complex plane plot and corresponding equivalent circuit are shown in Fig.4.8.

4.4.7 Warburg plus R_s plus small R_{ct}

If the charge transfer resistance is included but kept small compared to the influence of diffusion, the effect in the complex plane is a further shifting of the simple Warburg impedance line more positive on the abscissa as well as more negative on the ordinate. This is mathematically represented (DeRosa and Beard, 1977) by

$$Z' = R_s + R_{ct} + \frac{\sigma}{\omega^{\frac{1}{2}}} \qquad 4.15$$

and

$$Z'' = -i(\sigma/\omega^{\frac{1}{2}}) + -i(2\sigma^2 C_{dl}) \qquad 4.16$$

The equivalent circuit and resultant impedance plot are shown in Fig.4.9. It must be stressed that the Warburg impedance is very much greater than the charge transfer for such a plot to occur, as the equivalent circuit is identical to that of section 4.4.8.

Generally, for reactions where the diffision impedance is dominant, the straight line plot is representative. However, the thickness of the ac diffusion layer is seldom

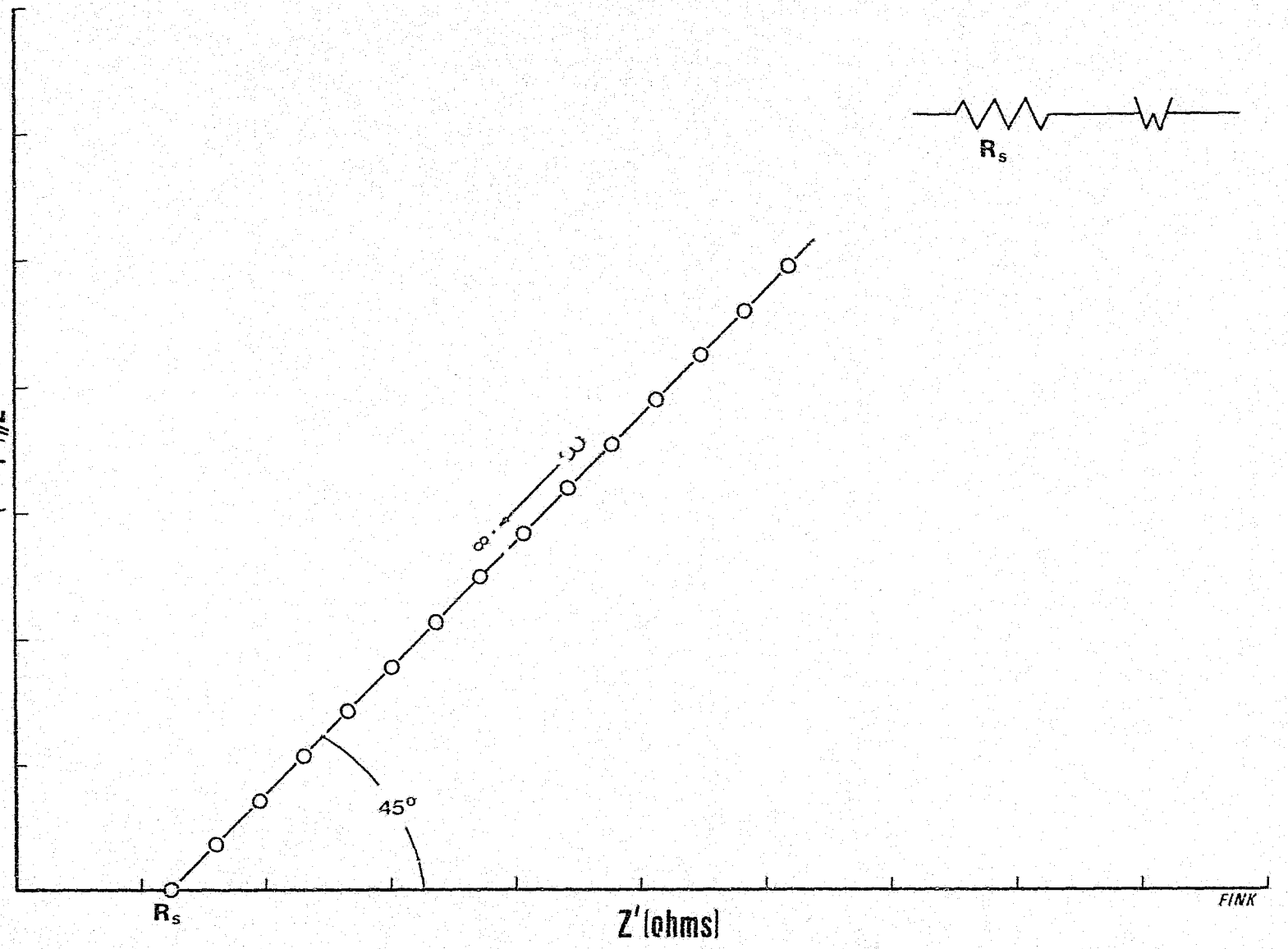


Fig. 4.8. Complex plane plot of a resistor in series with the Warburg impedance.

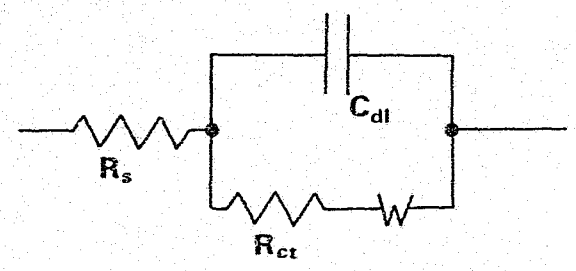


Fig. 4.9. Complex plane plot of a Randle's circuit where R_{ct} and C_{dl} are very small relative to the Warburg impedance.

taken into account. It is assumed to always be much smaller than the Nerstian diffusion layer. At high frequencies, this assumption is quite valid, but for low frequencies, the ac diffusion layer becomes larger, and can interact with the Nerstian diffusion layer. Armstrong et al (1978) have shown that the complex impedance for such a situation can be represented by

$$Z^* = \frac{\sigma_o}{\omega^{\frac{1}{2}}}(1-i)\tanh\left\{\delta_o(i\omega/D_o)^{\frac{1}{2}}\right\} + \frac{\sigma_r}{\omega^{\frac{1}{2}}}(1-i)\tanh\left\{\delta_r(i\omega/D_r)^{\frac{1}{2}}\right\} \quad 4.17$$

At high frequencies, this reduces to equations 4.15 and 4.16. At low frequencies, equation 4.17 reduces to

$$Z^* = R_s + R_{ct} + \sigma_o\delta_o(2/D_o)^{\frac{1}{2}} + \sigma_r\delta_r(2/D_r)^{\frac{1}{2}} \quad 4.18$$

The resultant impedance response is shown in Fig.4.10.

4.4.8 Randles' Circuit

The equivalent circuit presented in Figs.4.9 and 4.10 is the fundamental equivalent circuit analog for a solid electrode/electrolyte interface and was first presented by Randles (1947). The impedance responses of Figs.4.9 and 4.10 were derived from the Randles' circuit, however they were included in the previous section for the sake of continuity as the limiting cases described were dominated by Warburg impedance. When neither the charge transfer reaction nor the Warburg impedance is dominant, the resulting complex plane plot has an equal balance of both as seen in the bottom curve of Fig.4.11. This is represented by

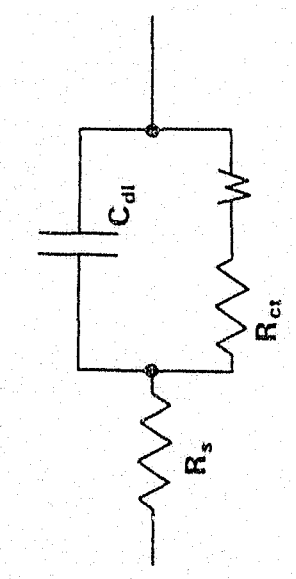


Fig. 4.10. Complex plane plot of a Randle's circuit where R_{ct} and C_{dl} are very small relative to the Warburg impedance and the ac diffusion layer interacts with the Warburg diffusion layer.

$$Z^* = R_s + \{1/i\omega C_{dl} + (1/R_{ct} + \sigma/\omega^{\frac{1}{2}} - i\sigma/\omega^{\frac{1}{2}})\} \quad 4.17$$

Sluyters (1960) showed the influence of changing the double layer capacity on the impedance response, while keeping the charge transfer resistance and Warburg coefficient at unity. The plots are presented in Fig.4.11.

Yet another possibility with the Randles' circuit is to include ac diffusion layer interaction in proportion to the charge transfer reaction. This can be seen in Fig.4.12 which is a plot of the impedance for the reduction of ferric ions to ferrous on a gold rotating disk electrode (Armstrong et al, 1976). The resonant peaks occur over three decades apart giving excellent definition to the aforementioned phenomena.

The past sections on equivalent circuits and their respective plots form the basis for the qualitative interpretation of the impedance data gathered in this research. It has been pointed out that most of the interfacial properties and their relative magnitudes can be determined directly from observing the complex impedance plane plots. This illustrates some of the advantages of complex plane analysis.

4.5 Procedures

The impedance measurements were performed at the National Institute for Metallurgy (NIM) in Randburg, South Africa under the guidance of Dr.Roger Paul of the Mineral and

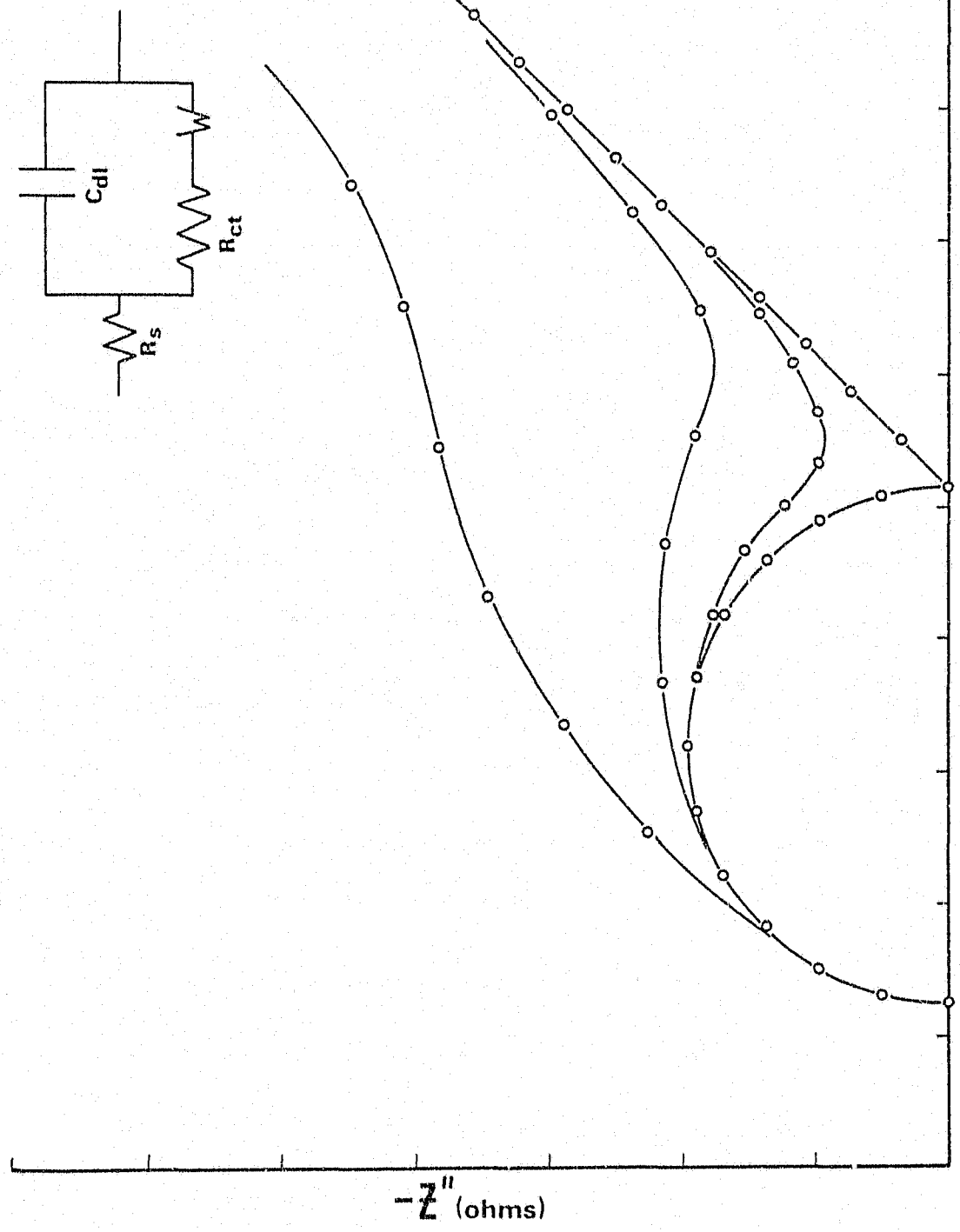


Fig. 4.11. Complex plane plot of a Randle's circuit where R_{ct} and the Warburg impedance are held at unity and C_{dl} is varied.

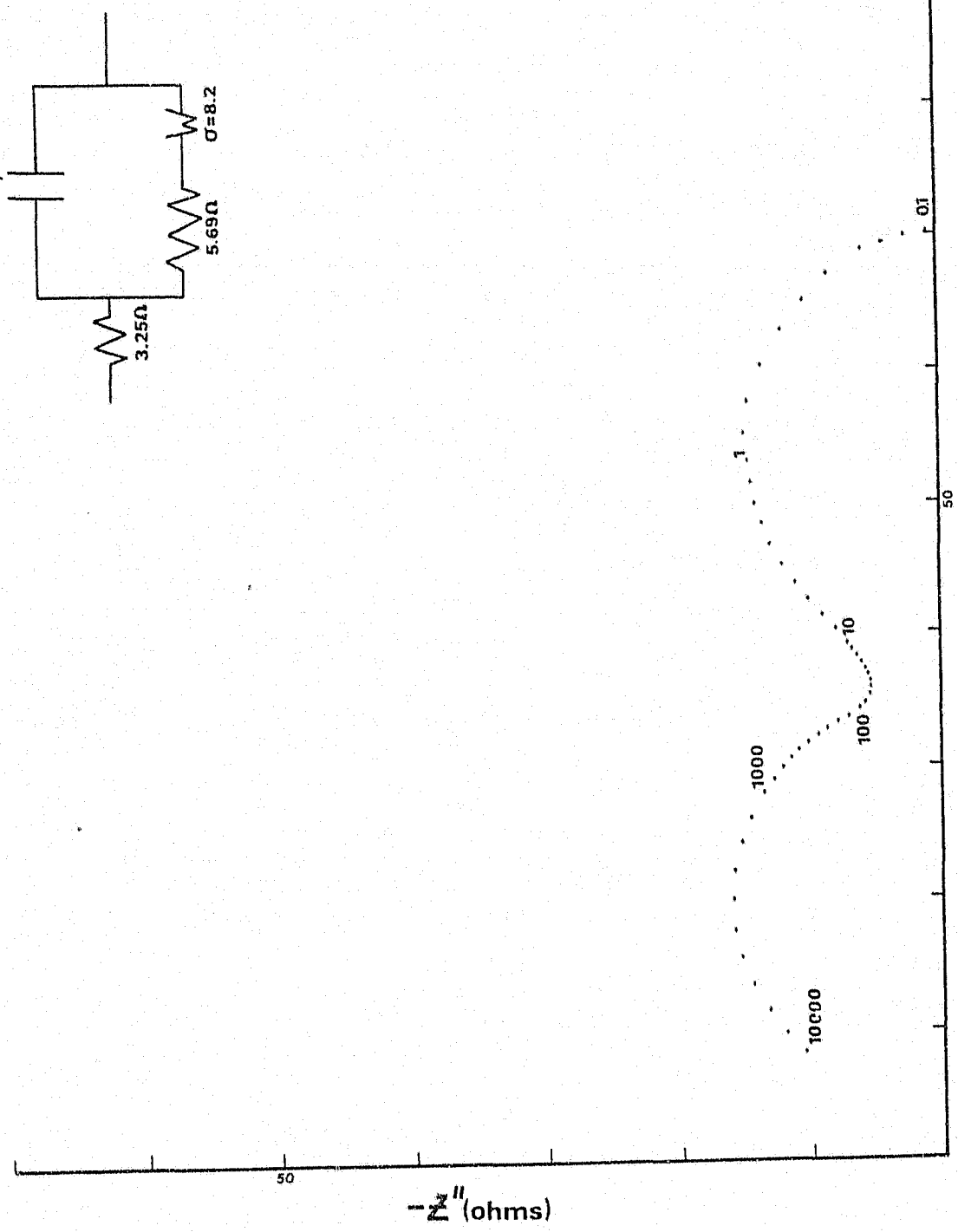


Fig. 4.12. Complex plane plot for the reduction of ferric ions to ferrous on a gold rotating disk electrode (from Armstrong et al, 1976).

Process Chemistry Division. The equipment used was a Solartron 1170 Frequency Response Analyser, a Solartron 1180 X-Y Plotter Interface, a NIM manufactured potentiostat and a Hewlett-Packard 7015B X-Y Plotter. The electrochemical cell is described in Appendix D.

Measurements were made primarily using a 10 mV rms (peak) square wave, although some measurements used a 10 mV rms sine wave for comparison purposes at low frequencies. The square wave was chosen over the normal sine wave in order to maintain a more similar situation to that utilized in conventional geophysical impedance measuring techniques. At higher frequencies, e.g. greater than 10 Hz, there is little if any difference. However, at frequencies less than 10 Hz, the electrochemical implications due to the difference in rise time between a square wave and a sine wave can be quite pronounced (especially in view of the fact that the Solartron 1170 could not put out a waveform of any lower amplitude than 10 mV).

To test the effects of diffusion on various impedances the cell was stirred by a magnetic stirrer. This usually created a noiser situation which was overcome with longer time averages. Generally, the measurements were made in an unstirred solution.

4.6 Results

For the sake of clarity, many of the impedance plots have been combined onto one plot. Although the high frequency data are very unclear due to the high density of data, it is the low frequency data that are of primary interest and

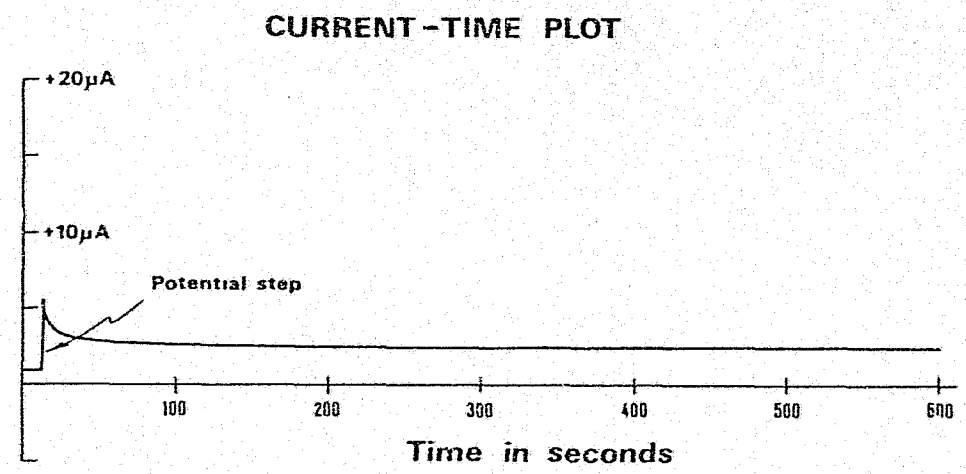
indicate the more dominant characteristics. The effort has been concentrated primarily on pyrite and chalcopyrite as they share the questionable prestige of being the most common non-ore and ore sulfides encountered, respectively. Several measurements have been made for a variety of bias potentials that bracket and include the range of rest potentials in a neutral solution of .25M NaCl at STP. Some combined electrode runs were performed in a solution of .1M $CuSO_4$ to test the electroactivity of the cupric ion.

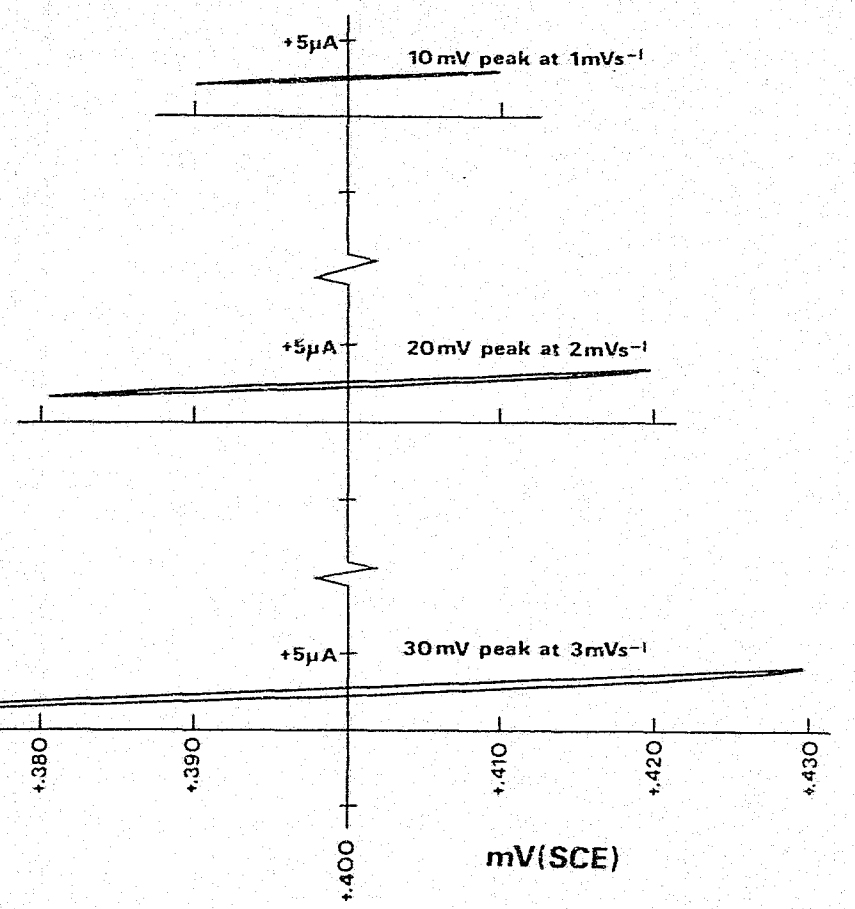
The impedance measurements consisted of letting the Solartron 1170 automatically run a sequence of frequencies from present front panel controls. The essential data from the front panel are as follows: 10 evenly spaced frequencies per decade (100, 80, 63, 50, 40, 32, 25, 20, 16, 13, 10), a square wave of 10 mV amplitude, starting frequency of either 10 kHz or 5 kHz descending to a terminating frequency ranging from 100 mHz down to 10 mHz, for all frequencies above 1 Hz a minimum sampling of 10 cycles was performed and below 1 Hz either 10 cycles or 1 cycle was used although on some overnight runs 10 cycle sampling was used down to 10 mHz. The data were automatically plotted in the complex impedance plane. All indicated potentials are referred to SCE.

The procedure for each spectral run consisted of inserting the freshly polished electrode and letting it reach equilibrium, then stepping the potential prior to each new measurement. This was monitored by making a current-time plot so that the equilibrium current could be readily determined to be constant. The current-time plot in

Fig.4.13 shows the current at the potential prior to increase. After the potential step, a logarithmic decay of the current to the new equilibrium value is seen. Once the current had stabilized (e.g.for any time beyond 300 seconds in this instance), the CV measurements were made. Fig.4.14 shows a plot of the stable portion of a current-voltage curve for pyrite. Each point was obtained after waiting until the current gradient was virtually zero. The CV measurements were made using a 10 mV peak waveform with a sweep rate of 1 mVs^{-1} to determine whether or not any net reactions could be observed. If none were observed, the peak voltage was increased to 20 mV, the sweep rate to 2 mVs^{-1} and another run made. If no reactions were observed, the peak voltage was increased to 30 mV, the sweep rate to 3 mVs^{-1} and a final run made. The CV measurements, as shown in Fig.4.1 graphically illustrated the presence or lack of linearity of the current-voltage curve in the vicinity of the potential examined. The CV plots also show the slope of the current-voltage curve, at the set potential. The amplitude and polarity of the equilibrium current can be obtained from the average intercept on the current axis. The four steps of monitoring the current versus time and making three CV measurements insured accurate knowledge of the condition of stability for the impedance measurements.

The impedance data were plotted directly and the digital information was not recorded. Critical or reference frequencies were marked on the plots as they were being plotted. This is apparent on the impedance plots as presented.





CHALCOPYRITE
ch-h-05
at +.400 mV(SCE)
unstirred
degassed
pH 7

Fig. 4.13. Current-time plot (on left) showing adjustment of current to a 50 mV increase in anodic potential from +350 to +400 mV. Plot on right is of CV measurements made after the current had stabilized. The slope of the CV plots indicates the slope of the current-voltage curve at the indicated potential. The plots are for several cycles and show no noticeable hysterisis effects.

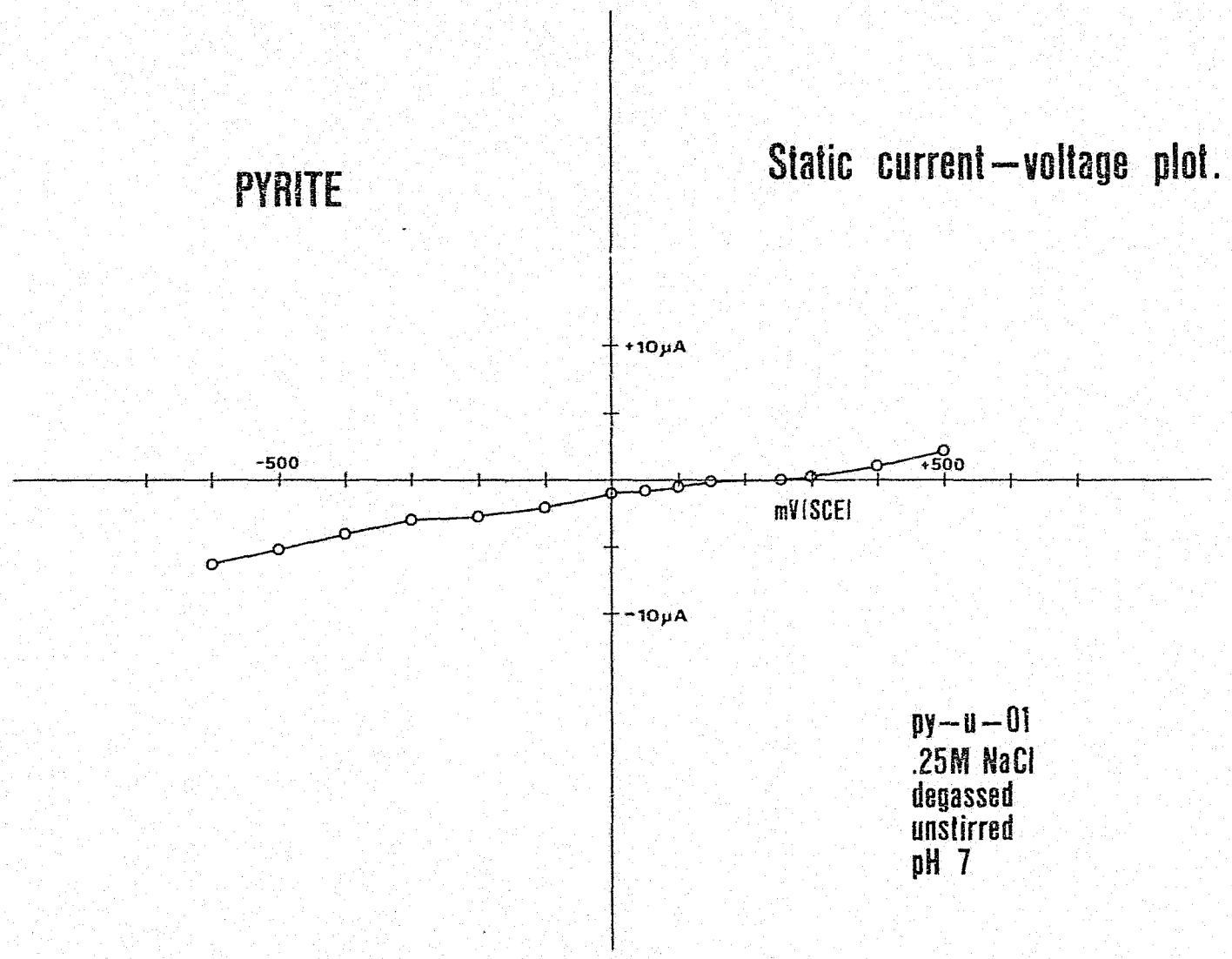


Fig. 4.14. Current-voltage plot of equilibrium currents for various potentials in the stability range for pyrite.

4.6.1 Pyrite

Two pyrite electrodes were selected for the pyrite impedance measurements. One specimen, py-d-05, from Balmat, New York, U.S.A., was a relatively pure and fairly resistive (approx. 700 ohms) specimen. It polished to a high sheen and produced some excellent spectra. The second specimen, py-u-01, from an unknown location in Arizona, was a more typical, lower resistivity (approx. 70 ohms) specimen that would likely be more representative of the type of pyrite generally found in porphyry copper environments. The spectra from the two pyrites were very similar with one notable exception. The angle beneath the abscissa on which the centres of the semicircles occurred was much greater for py-u-01 than for py-d-05. This tendency to flatten the spectra did not change with stirring so was attributed to be a solid state or surface effect.

4.6.1.1 Anodic Pyrite

Fig. 4.15 shows some anodic spectra for py-d-05. The abscissa is in kilohms and an R_s of approximately 700 ohms is quite clearly indicated. This 700 ohms is virtually all due to the resistance of the pyrite itself showing a minimal contribution form iR drop in the solution. The rest potential was approximately 250 mV. The 250 and 300 mV spectra are virtually identical and indicate a charge transfer rate limiting process with a very large C_{dl} and R_{ct}. As the potential was increased in 50 mV steps and the respective spectra measured, it was clear that the R_{ct} decreased, thereby making the resultant semicircles smaller. C_{dl}

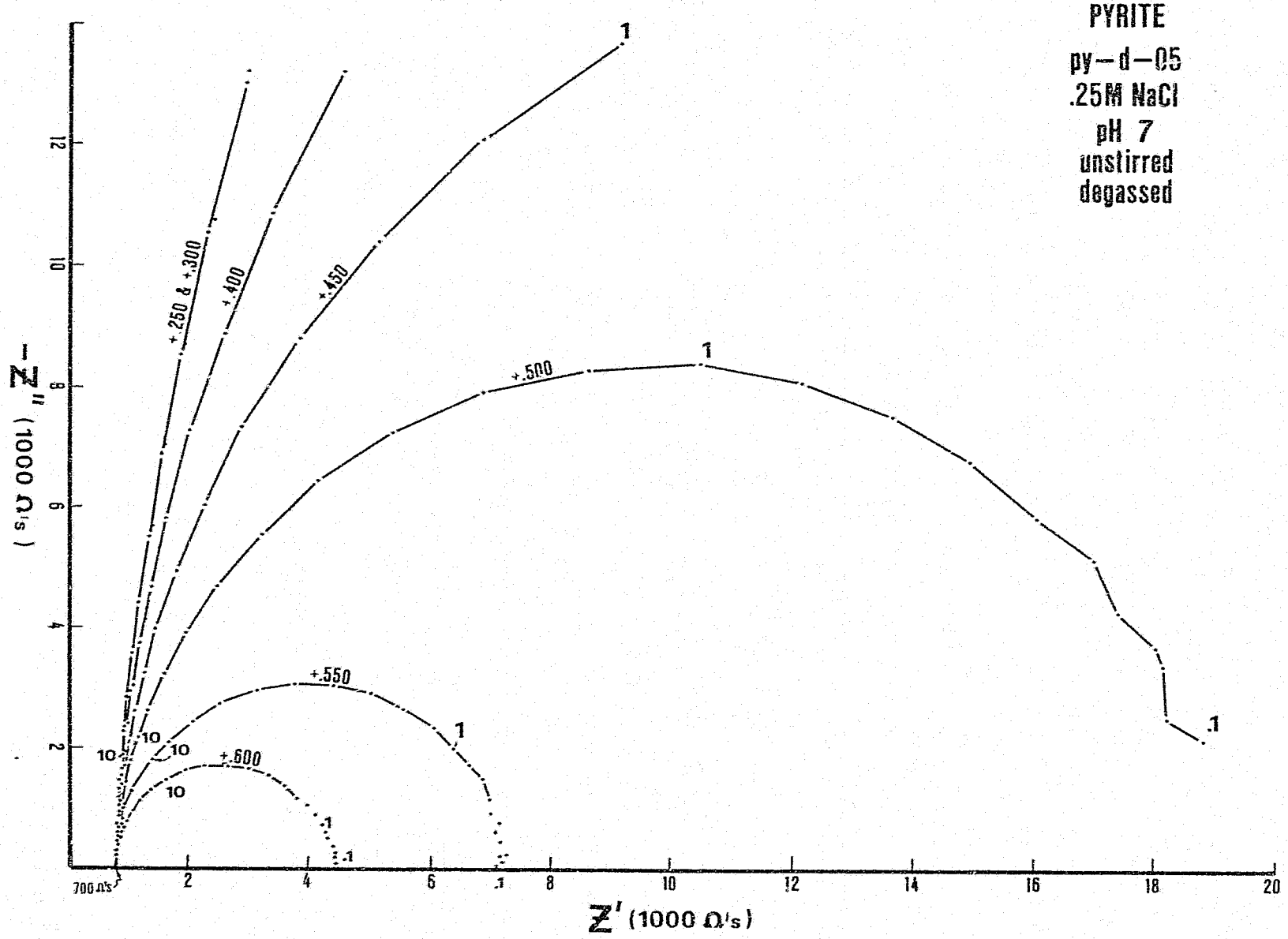


Fig. 4.15. Complex plane plot of anodic impedance spectra for pyrite.

appeared to remain constant at approximately 50 μF, as indicated by a semicircular occurrence of the 1 Hz values. The centres for the charge transfer semicircles do not lie on the abscissa but rather on a line 3.5° below the abscissa starting at the 700 ohm value. Another deviation from ideal charge transfer can be seen in the low frequency data of the +500, +550 and +600 mV plots. All three spectra in this potential range show slightly higher low frequency impedances than predicted for pure charge transfer. The possibility of the presence of solution diffusion was checked by stirring and rerunning the spectra. No significant changes, beyond the envelope of noise, were observed. Since the specimen is fairly resistive, which should indicate a relative degree of purity, the possibility of solid state or surface diffusion exists. But the effect is of second order compared to the charge transfer phenomenon and, in these spectra, of minimal importance. Overall, anodic pyrite in a neutral supporting electrolyte shows a well behaved charge transfer reaction with no indication of solution Warburg impedance.

4.6.1.2 Cathodic Pyrite

Cathodic impedance measurements on py-d-05, shown in Fig. 4.16, produced similar spectra to the anodic measurements, yet are noticeably different. Proceeding in a cathodic direction from 0 mV in -100 mV steps, the first salient feature is the -100 mV spectrum occurring to the left of the o mV spectrum. This is in obvious contrast with the spectra of the more cathodic potentials which occur in a logical sequence to the right. In fact, the 0 mV spectra

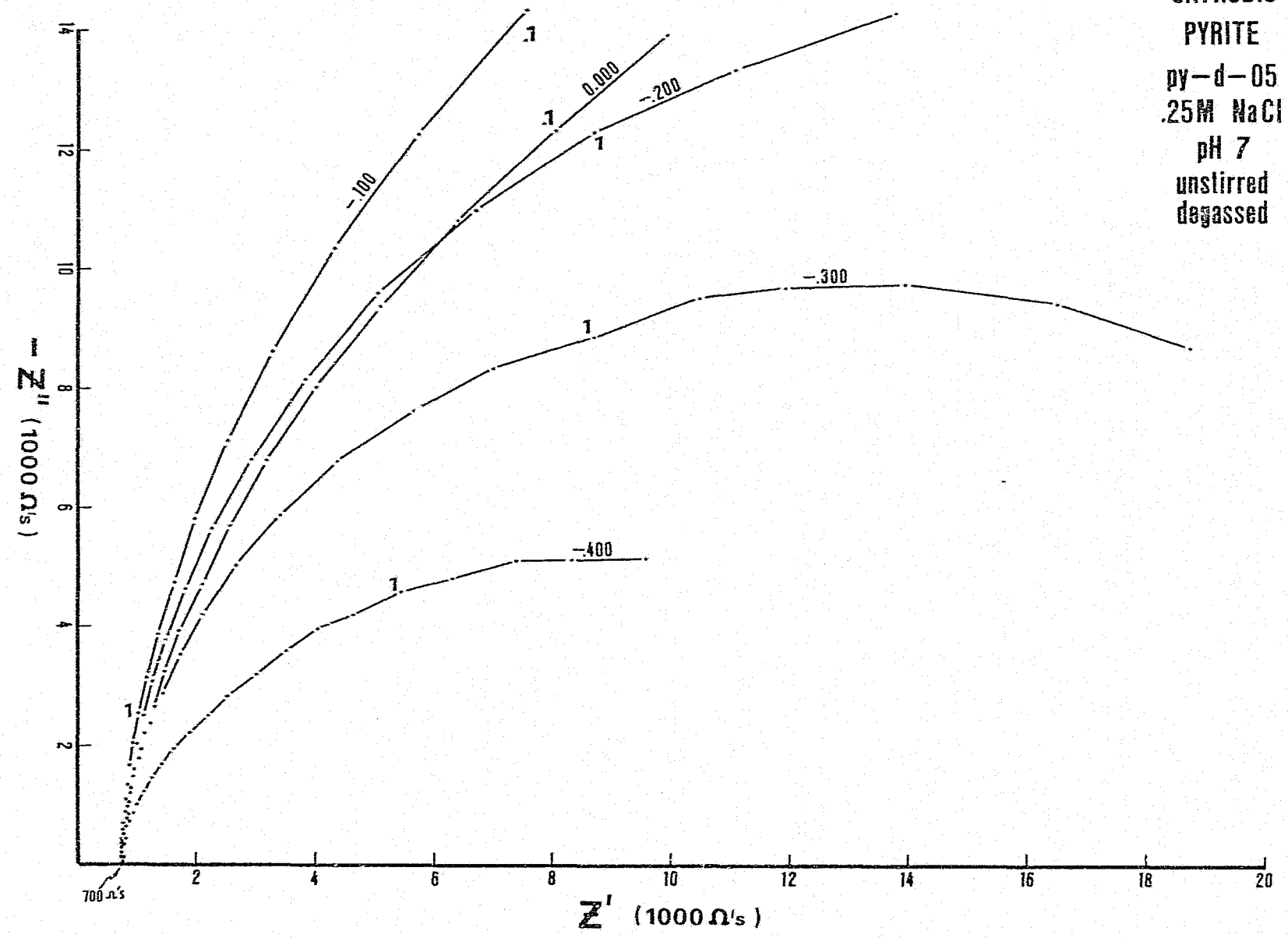


Fig. 4.16. Complex plane plot of cathodic impedance spectra for pyrite.

itself may be the anomalous one as the sequence from -100 to -400 mV appears normal. One possible explanation offered for this peculiarity is that the potentials of the more cathodic spectra transgress the range of the rate limiting step observed in the current-voltage plots. It is assumed the rate limiting process taking place at these potentials is charge transfer. This is indicated by two facts: 1. the plateau occurring in the current-voltage curves is present in spite of stirring, and 2. the shapes of the spectra are very nearly semicircular. Interestingly, the spectra are not as coincident with an ideal semicircle as were the anodic spectra. A distinct increase in impedance, relative to a higher frequency fitted semicircle, is indicated. This would normally suggest a diffusional process, but with no change due to stirring, solution diffusion is unlikely. Either a solid state or surfact diffusion phenomenon may be suggested to account for this anomalous impedance. With the exception of the low frequency impedance deviations, the anodic and cathodic pyrite spectra are reasonably similar. The point of primary importance is that the 0 mV and +250 mV spectra tend to establish a limit to the range of spectra observed for other pyrite electrodes measured at rest potential. Generally, for rest potentials occurring between zero and +250 mV, the spectra, at the scale shown in Figs. 4.15 and 4.16, varied from a nearly vertical capacitance plot or a slightly arcuate plot similar to that of anodic +250 mV. This steep portion of the plot is still semicircular but is a result of a very high R_{ct}. In no way can this steep rise be interpreted as a diffusional process for the reasons indicated.

A plot of the cathodic impedances for py-u-01 is shown in Fig. 4.17. Two semicircular trends in the data are evident and are indicated by A and B. The distance to their respective centres and the angle beneath the abscissa are also shown. The A semicircle represents the -100, -200, -600 and -1000 mV impedance runs. The B semicircle represents the -300 and -400 mV impedance runs. No explanation is made for the different semicircles but the observation was made. A plot of the 0.1 Hz impedances, shown in Fig. 4.18, for -300 to -1000 mV indicates a semicircle along which the frequency slides as a function of cathodic potential. This illustrates the aforementioned frequency sliding effect.

4.6.1.3 Data from Angoran

Data from Angoran (1975) replotted in the complex plane are shown in Figs. 4.19 and 4.20. The scales are different but the overall spectral character is clearly the same as that observed in this research. However, since Angoran fitted his data with an equivalent circuit model including a Warburg term, the Warburg coefficient appears to be far more influential than the other circuit parameters. There is good agreement with the C_{dl}, his being determined to be 44 and 49 μFcm^{-2}, but the Warburg coefficients of 8567 and 13360 $ohmcm^{-2}sec^{-\frac{1}{2}}$ versus charge transfer resistances of 89 and 102 $ohmcm^{-2}$ obviously cannot be justified. These values would produce a very small semi-circle on the real axis and a distinctly linear Warburg slope. The data show no small semi-circle, rather a portion of a very large one indicating a very large charge transfer resistance and a negligible Warburg coefficient. The equivalent circuit fitting procedure apparently has forced a very small charge transfer resistance to minimize the effect of the charge transfer reaction and taken the

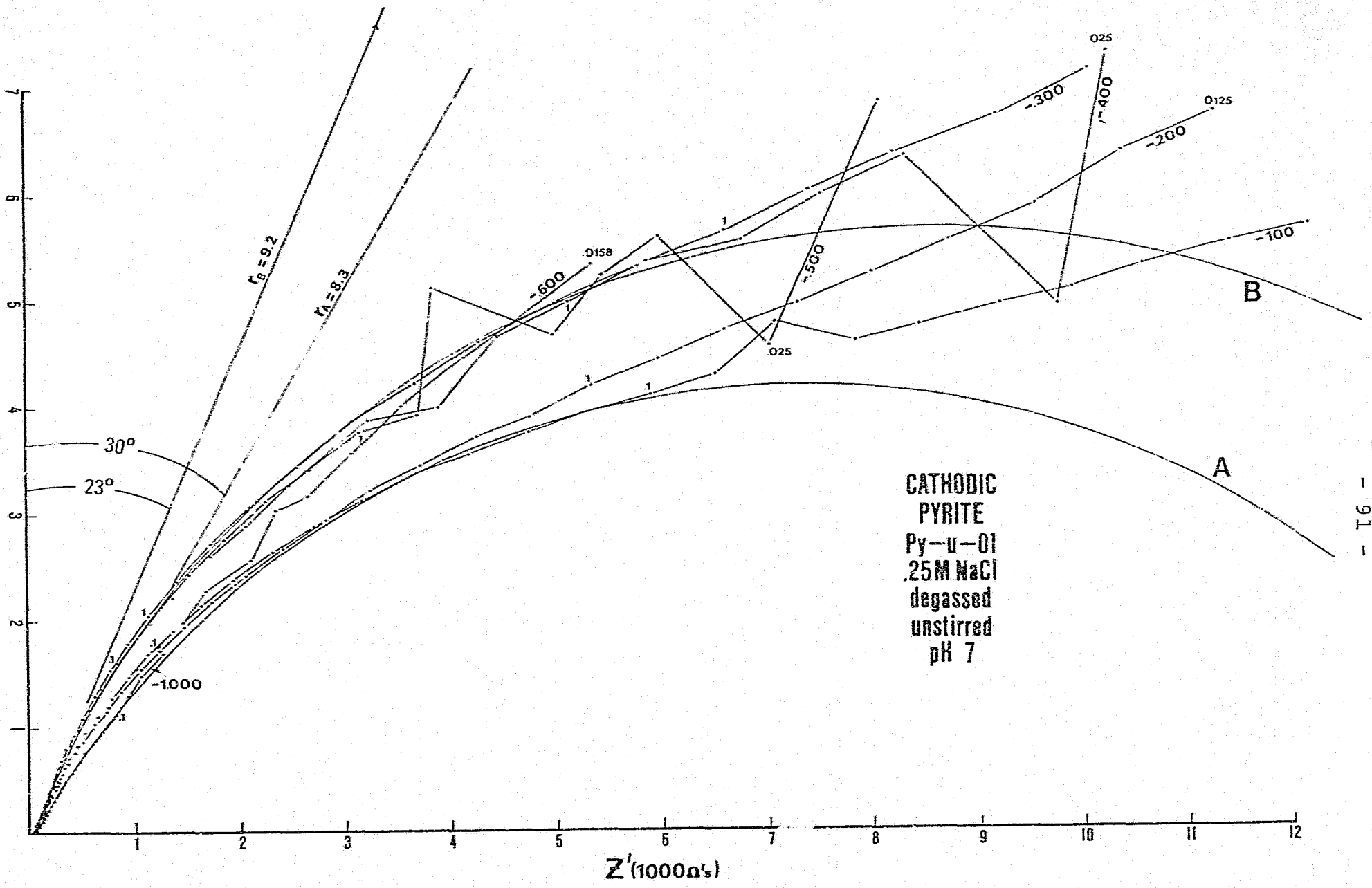


Fig. 4.17. Complex plane plot of cathodic impedances for py-u-01.

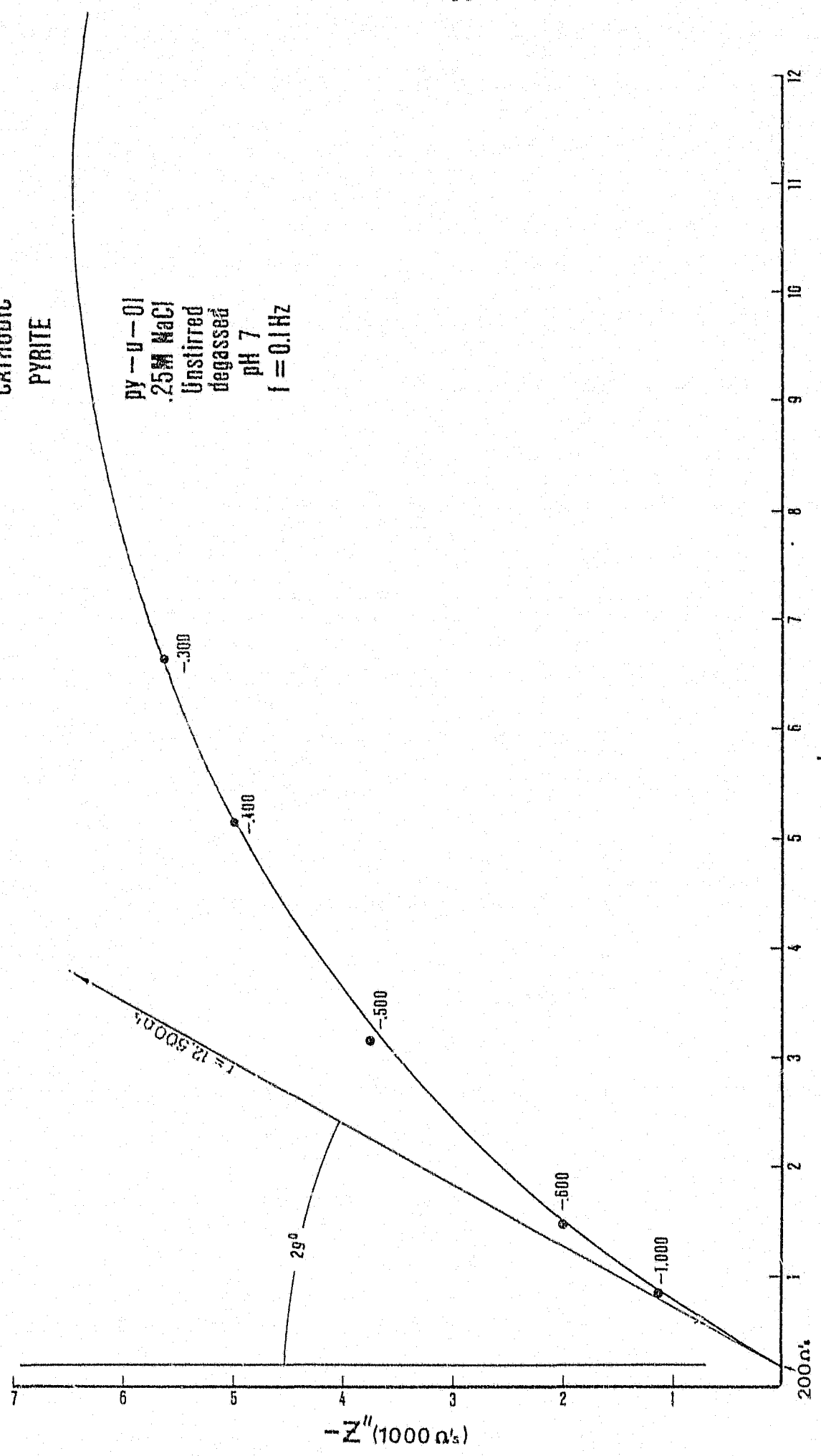


Fig. 4.18. Complex plane plot of cathodic impedances at 0.1 Hz for py-u-01.

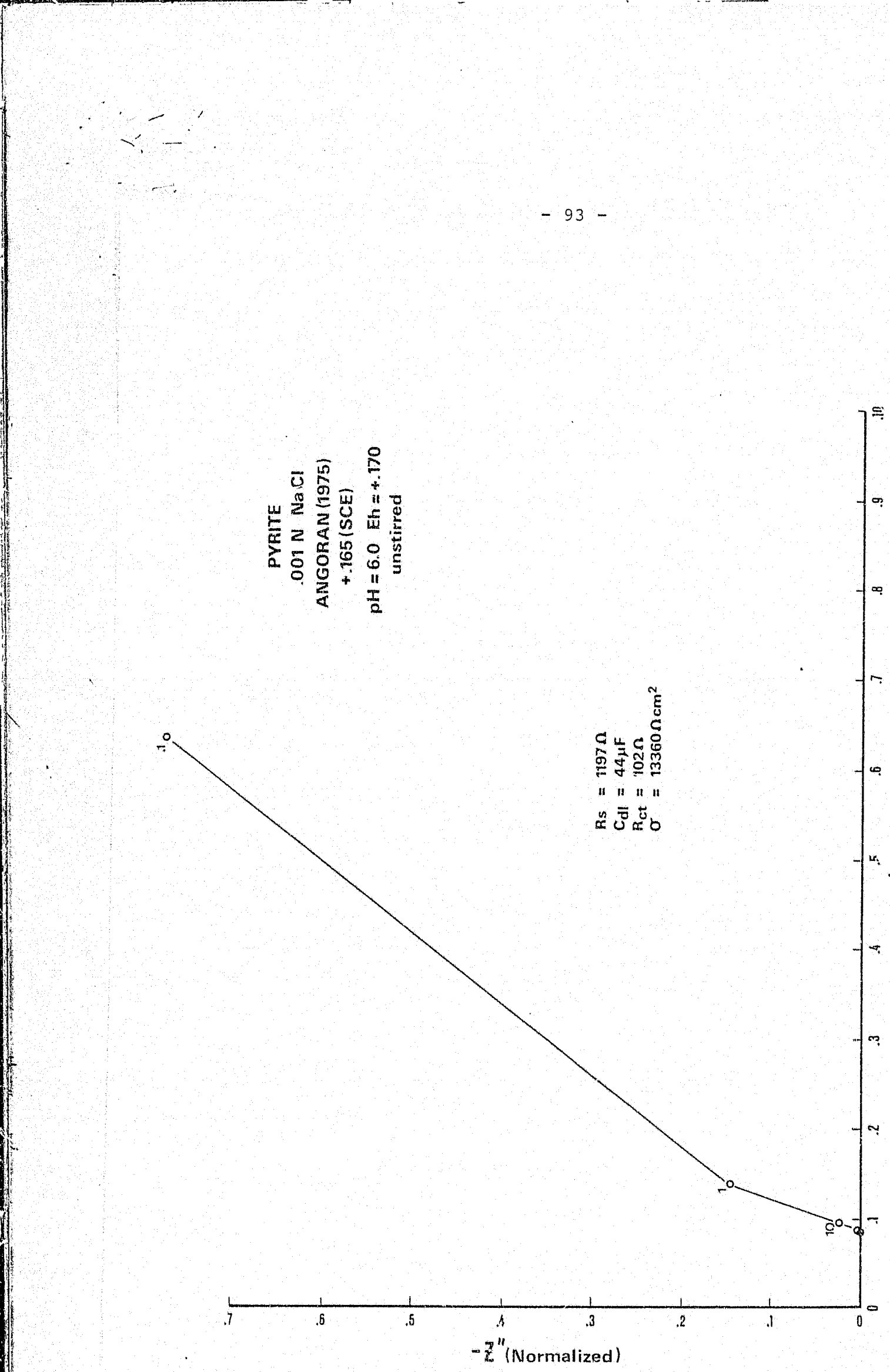


Fig. 4.19. Complex plane plot of pyrite impedances measured by Angoran (1975).

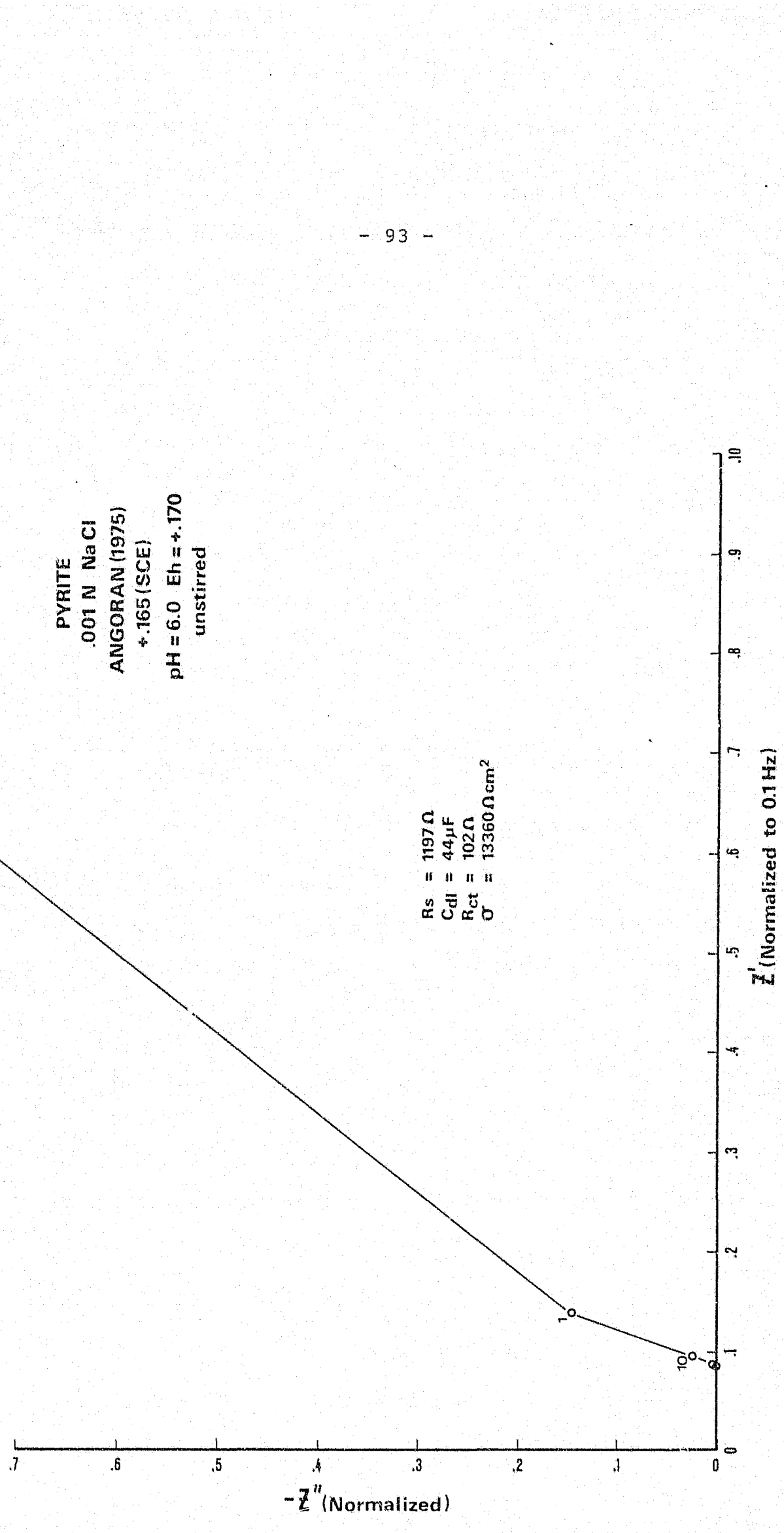


Fig. 4.19. Complex plane plot of pyrite impedances measured by Angoran (1975).

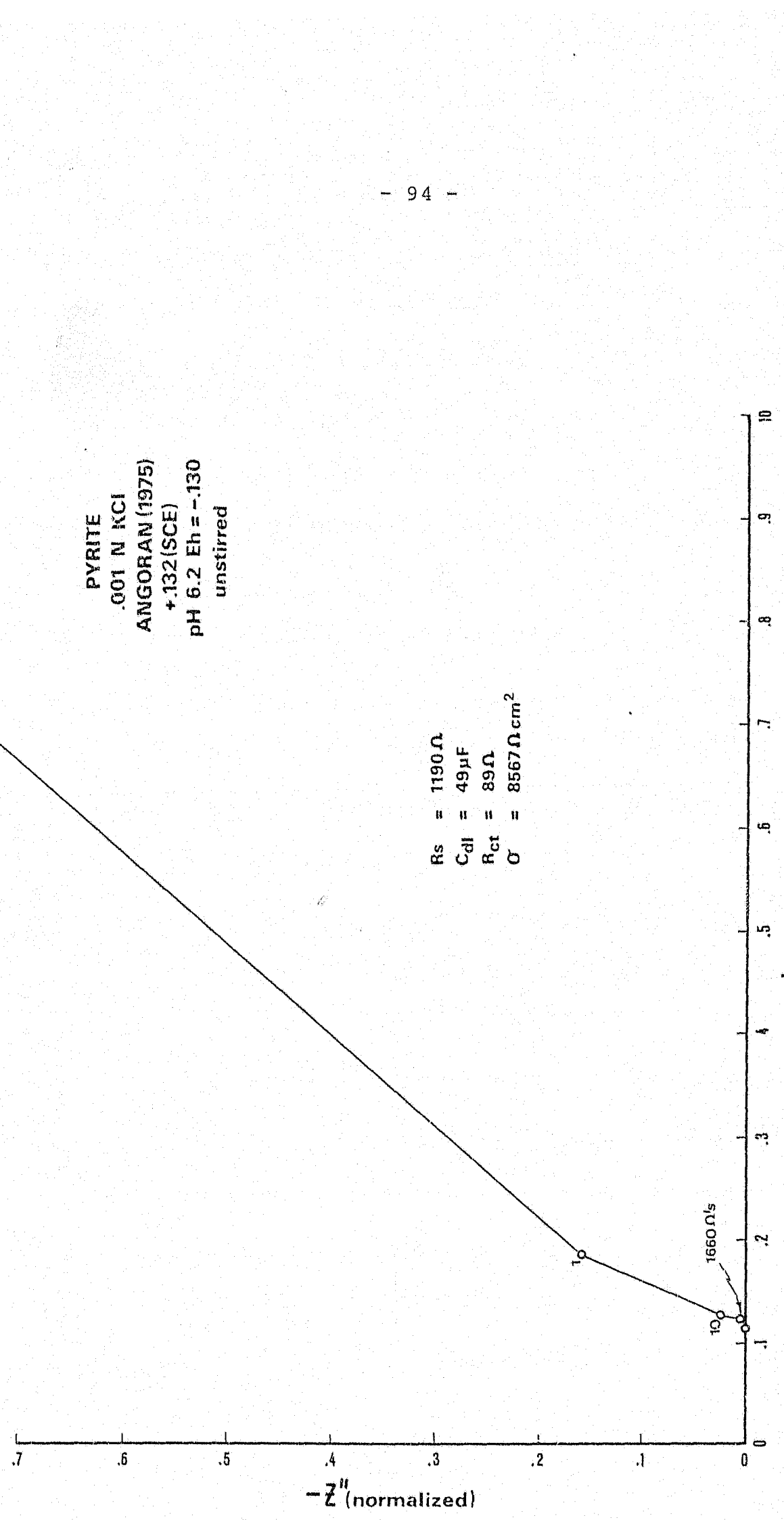


Fig. 4.20. Complex plane plot of pyrite impedances measured by Angoran (1975).

lower frequency values and attributed them purely to diffusion. The spectra measured in this research and shown in Figs. 4.15 and 4.16 clearly contradict Angoran's fitted circuit parameters for pyrite and illustrate that diffusional processes, whether solid state, surface or solution, play a negligible role in a neutral supporting electrolyte.

4.6.2 Chalcopyrite

A chalcopyrite specimen, ch-u-02, from an unknown location in Arizona, was used for most of the variable potential impedance measurements. The electrode had a bulk resistance of approximately 60 ohms. High frequency Z' values of $\pm$60 ohms indicate minimal iR drop due to supporting electrolyte. The impedances of several other chalcopyrite electrodes were measured at rest potentials and are compared to data from Angoran (1975).

4.6.2.1 Anodic chalcopyrite

Fig. 4.21 shows some anodic spectra for ch-u-02. The scale is the same as that of Fig. 4.15 for anodic pyrite. The most striking difference between pyrite and chalcopyrite is the large drop in the overall impedance seen for chalcopyrite. This is likely due to the unusual purity of py-d-05. A distinct difference in the character of the curves is also quite obvious. The chalcopyrite curves show a definite charge transfer type semicircular effect at frequencies greater than 10 Hz, as shown in Fig. 4.22, but at lower frequencies tend to be a fairly linear shape. This was initially considered to be a solution Warburg impedance effect but stirring of the solution while repeating the measurements produced no change. Hence, it is highly unlikely that

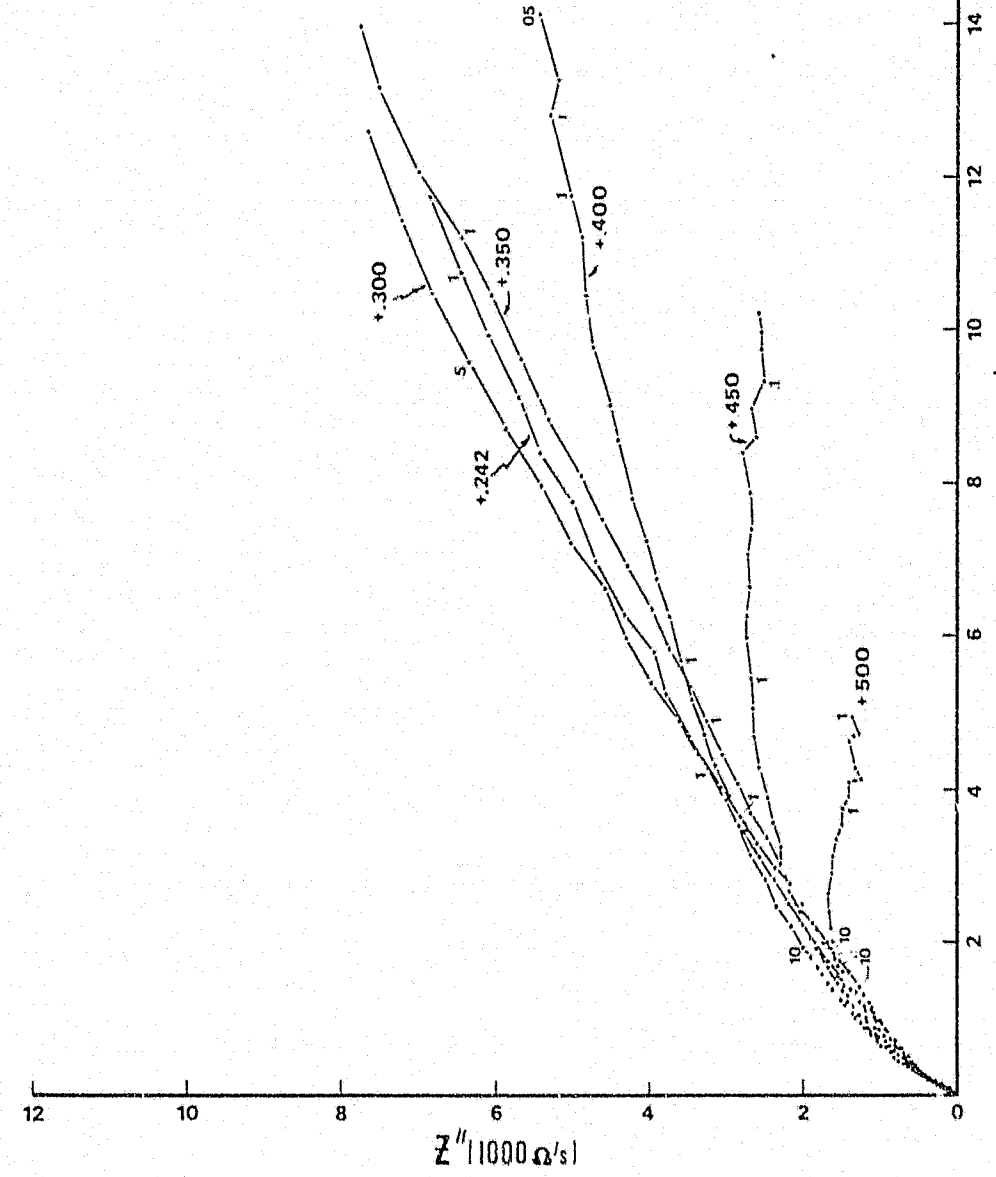


Fig. 4.21. Complex plane plot of anodic impedance spectra for chalcopyrite.

Author Fink J B
Name of thesis Interfacial phenomena between liquid electrolytes and semiconducting base metal sulfides 1979

PUBLISHER:
University of the Witwatersrand, Johannesburg
©2013

LEGAL NOTICES:

Copyright Notice: All materials on the University of the Witwatersrand, Johannesburg Library website are protected by South African copyright law and may not be distributed, transmitted, displayed, or otherwise published in any format, without the prior written permission of the copyright owner.

Disclaimer and Terms of Use: Provided that you maintain all copyright and other notices contained therein, you may download material (one machine readable copy and one print copy per page) for your personal and/or educational non-commercial use only.

The University of the Witwatersrand, Johannesburg, is not responsible for any errors or omissions and excludes any and all liability for any errors in or omissions from the information on the Library website.